FRUSTRATED ANTIFERROMAGNETS WITH EASY AXIS ANISOTROPY

A thesis submitted to
Tata Institute of Fundamental Research, Mumbai, India
for the degree of
Doctor of Philosophy
in
Physics

By
Arnab Sen
Department of Theoretical Physics
Tata Institute of Fundamental Research
Mumbai - 400 005, India

June 2009

Declaration

This thesis is a presentation of my original research work. Wherever contributions of others are involved, every effort is made to indicate this clearly, with due reference to the literature, and acknowledgement of collaborative research and discussions.

The work was done under the guidance of Professor Kedar Damle, at the Tata Institute of Fundamental Research, Mumbai.

(Arnab Sen)

In my capacity as the supervisor of the candidate's thesis, I certify that the above statements are true to the best of my knowledge.

(Kedar Damle)

Acknowledgments

First and foremost, I would like to thank my advisor Kedar Damle for all his guidance and support. It is also a pleasure to acknowledge Mustansir Barma, Chandan Dasgupta, Deepak Dhar, Gautam Mandal, Roderich Moessner, Shiraz Minwalla, H. R. Krishnamurthy, Sriram Ramaswamy, T. Senthil, Vijay Shennoy, Vikram Tripathi and Ashvin Vishwanath for the physics I have learnt from them. Among the students in TIFR, I thank Argha Banerjee, Debasish Banerjee, Kabir Ramola, R. Loganayagam, Partha Nag, Prasenjit Dutt and Shamik Gupta for the many physics discussions that I had with them. I thank the DTP office staff, Ajay Salve, Girish Ogale, Mohan Shinde, Rajan Pawar and Raju Bathija, for being extremely helpful at all times. Finally, I would like to thank my parents for always being extremely supportive to me.

Collaborators

This thesis is based on the work done in collaboration with Kedar Damle, Roderich Moessner, Ashvin Vishwanath and Fa Wang. In particular, Chapter 3 and Chapter 5 follow the papers by Sen, Wang, Damle and Moessner (2009) and Sen, Damle and Vishwanath (2008) respectively.

To My Parents

Contents

Synopsis

Introduction

Geometrically frustrated magnetic systems have been the object of many theoretical and experimental studies [1, 2, 3] for several decades now. These are systems in which all the spin interactions cannot be simultaneously satisfied because of the connectivity of the lattice. This opens up the possibility to have unconventional magnetic order or even novel spin liquid states without any long range spin order at low temperatures. The earliest theoretical model for geometric frustration was provided by Wannier [4] in 1950, who showed that the Ising antiferromagnet on the triangular lattice has very different behaviour compared to an antiferromagnet on a bipartite lattice (e.g. square lattice) in that there is no magnetic order down to zero temperature. On the triangular lattice, it is impossible to construct a spin configuration where each spin is anti-aligned with respect to its neighbours on any triangular unit. From the point of view of real materials, there are many examples [1, 2] in which the magnetic ions are arranged on non-bipartite lattices based on triangular units like the triangular, kagome and the pyrochlore lattices (see Fig 1).

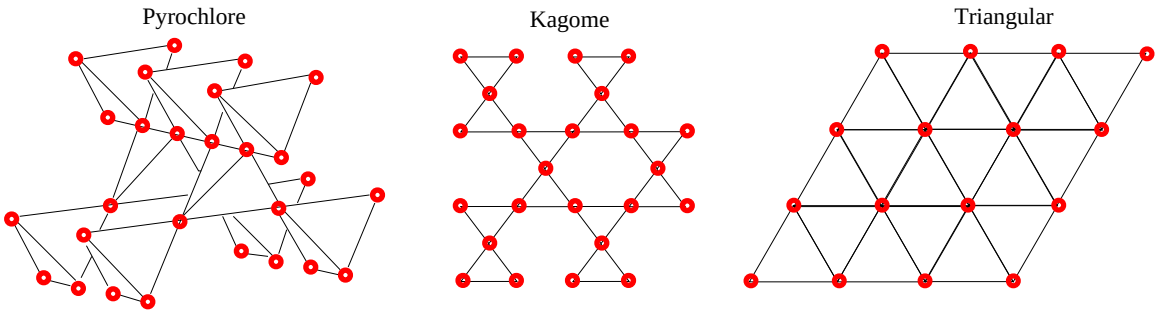

Figure 1: Examples of some lattices composed of triangular units where all exchange interactions cannot be simultaneously satisfied because of the connectivity of the lattice.

Geometrically frustrated systems often have many local minima in their classical energy landscape, or even a macroscopic number (i.e., number of ground states is exponential in the number of sites of the system) of classically inequivalent ground states [3]. For example, the triangular lattice Ising antiferromagnet has a residual entropy (at zero temperature) which is extensive [5] ($S/k_BN = 0.323$). Other examples are the Ising antiferromagnet on the kagome lattice and the Heisenberg antiferromagnet on the kagome and the pyrochlore lattice. On the other hand, XY and Heisenberg antiferromagnets on the triangular lattice have a unique ground state, the 120° Neel state (see Fig 2), even though not all bonds are fully satisfied.

Such *highly frustrated* systems, where the residual entropy is extensive, are very susceptible to the effects of perturbations [3]. The reason is the following: Different ground states are not related to each other by any symmetry of the Hamiltonian, and the degeneracy is purely *accidental*. Thus, a perturbation would, in general, lift this degeneracy since it is not protected. Various physical mechanisms like single-ion anisotropies, further neighbour interactions and lattice distortions are present as perturbations in any realistic experimental situation. The interplay of these perturbations in the ground state manifold of the nearest neighbour interaction Hamiltonian can give rise to complex magnetic phases at low temperatures in geometrically frustrated magnets. For example, in the Ni^{2+} ($S = 1$) based kagome antiferromagnet $Ni_3V_2O_8$ [6], first and second neighbour exchange interactions compete with smaller anisotropic terms to give rise to a rich phase diagram consisting of different incommensurate and commensurate phases in the presence of a magnetic field.

Even in the simplified nearest-neighbour Heisenberg antiferromagnet on such frustrated lattices, it is very interesting to ask how much of the classical picture at $S \to \infty$ survives quantum fluctuations when considering low spin like $S = 1/2, 1, 3/2$ etc. On bipartite lattices, the classical ground state remains a good caricature of the true quantum ground state for small spin length S. In the classical limit, the ground state for the antiferromagnetic Heisenberg Hamiltonian on bipartite lattices (like the square lattice in 2D and the cubic lattice in 3D) is the Neel state with $\vec{S} = S\hat{n}$ on one sublattice and $\vec{S} = -S\hat{n}$ on the other. The staggered magnetization acts as the order parameter for this state which breaks spin rotation symmetry. Neel order indeed survives even for small spin $S = 1/2$ [7] on the square and the cubic lattice.

However, for highly frustrated systems, since the classical energetics fails to pick up a unique ground state, the answer is far from obvious. The true quantum ground state can turn out to be any linear combination of the classical ground states and might lead to unusual magnetically ordered states. A controlled way to analyze quantum fluctuations is to do a $1/S$ expansion, which amounts to a semiclassical

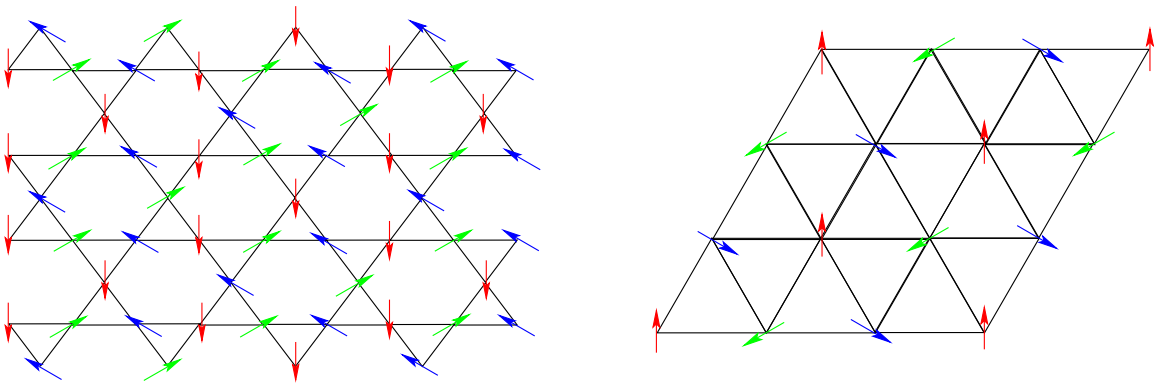

Figure 2: The $\sqrt{3} \times \sqrt{3}$ state on the kagome lattice which is stabilized at large-S and the 120° Neel state on the triangular lattice.

treatment of the full problem. Another exciting possibility is to see a spin liquid state in such models when the spin length becomes small. Quantum fluctuations might then become so strong that they destabilize any order present in the large S version. There is good numerical evidence on the triangular lattice [8] that the 120° Neel order (see Fig 2) survives the effects of quantum fluctuations down to $S = 1/2$, albeit with the order parameter reduced by about 59% from its classical value. Less is known with certainty for the kagome lattice for small values of S. Within the semiclassical treatment, it has been shown [9] that quantum fluctuations select coplanar states at leading order. These are still massively degenerate, and this degeneracy is lifted [10] at the next order to give the $\sqrt{3} \times \sqrt{3}$ state (see Fig 2) as the large-S ground state. There have been many studies of the kagome antiferromagnet [11, 12, 13, 14] aimed at understanding the extreme quantum limit of $S = 1/2$ but there is still no definite answer, even though there have been proposals of spin liquid states [15, 16] and valence bond crystal states [17, 18, 19] as the candidate ground state.

In this thesis, we study $S \geq 3/2$ kagome and triangular lattice antiferromagnets with the following spin Hamiltonian

$$\mathcal{H} = J \sum_{\langle ij \rangle} \vec{S}_i \cdot \vec{S}_j - D \sum_i (S_i^z)^2 - B \sum_i S_i^z \tag{1}$$

where J is the antiferromagnetic Heisenberg exchange and D is a single-ion uniaxial anisotropy of the easy axis type. B is an external magnetic field applied along the easy axis. This type of anisotropy is induced by local crystal fields through spin-orbit coupling, and is a perturbation which is present in kagome and triangular magnets because of the layered nature of materials. We consider the case where the uniaxial

anisotropy D dominates over the Heisenberg exchange J. For the pure Heisenberg model on the two lattices, the ground states typically involve coplanar arrangement of spins. However, collinear spin arrangements are preferred in the presence of a strong unaxial single-ion anisotropy. There are examples amongst rare earth magnets where uniaxial anisotropy is the dominant term. The pyrochlore spin ice compound $Ho_2Ti_2O_7$ is one such example [20] where $D \sim 50K$ while (ferromagnetic) $J \sim 1K$. The kagome antiferromagnet Nd-langasite ($Nd_3Ga_5SiO_{14}$) is another example [21] with $D \sim 10K$ and $J \sim 1.5K$. The classical ground states of such collinear spins are extensively degenerate, but in contrast to the isotropic case ($D = 0$), the effects of quantum fluctuations in selecting the low temperature state can be studied in a much more controlled way, and this is the focus of the work presented in this thesis.

In the following I shall describe the methodology used to tackle the problem and the main results.

Basic Approach

Effective Hamiltonian: When D dominates over J, the system prefers collinear spin configurations with $S_i^z = \sigma_i S$ (with $\sigma = \pm 1$). Due to the frustrated nature of J, the anisotropy D need not be *very large* to induce collinearity. In the classical ($S \to \infty$) limit, the system prefers a collinear state for $D > J$ on the kagome lattice and $D > 3J/2$ on the triangular lattice. In this regime, we expect an analysis based on the smallness of J/D to give reliable results. Quantum fluctuations are absent in the limit $J/D \to 0$, and can be studied in a controlled fashion for small J/D. We therefore use J/D as the expansion parameter in a systematic perturbative approach that allows us to calculate the effective low-energy Hamiltonian and the resulting low-temperature phases. We split up the Hamiltonian H as $H_0 + H_1$ where

$$\begin{aligned} H_0 &= -D \sum_i (S_i^z)^2 \\ H_1 &= J \sum_{\langle ij \rangle} S_i^z S_j^z + \frac{J}{2} \sum_{\langle ij \rangle} (S_i^+ S_j^- + h.c.) - B \sum_i S_i^z \end{aligned} \tag{2}$$

We then use standard degenerate perturbation theory [22] to obtain the effective Hamiltonian that encodes the splitting of the Ising subspace to each order in J/D. In the effective Hamiltonian approach, *real* quantum fluctuations (i.e., tunnelings between classical ground states) can be studied on an equal footing with virtual quantum fluctuations. The real quantum fluctuations are difficult to treat in a $1/S$ ex-

pansion (another controlled way to study quantum fluctuations) because they appear as non-perturbative events in a large-S expansion.

We show that while quantum transitions between different classical ground states is the dominant mechanism for degeneracy splitting below a critical spin length $S_c = 3/2$, the situation for all $S > S_c$ is entirely different. Here, virtual quantum transitions dominate the energetics, leading to 'potential energy' differences between different classical ground states. Because of the *classical* nature of the leading term of the effective Hamiltonian, it is simpler to deal with both analytically and numerically than the full quantum problem.

Dimer model simulations: When $T \ll JS^2$ (but above the scale introduced by quantum fluctuations), the collinear spin configurations which control the physics have a constraint in terms of spins on each triangle of the lattice. Such states can be represented as dimer coverings of classical close-packed dimer models on different lattices depending on the lattice on which the spins reside (kagome or triangular). Dimer models are defined by a phase space consisting of dimer coverings, in which dimers occupy a certain fraction of bonds on the lattice, and satisfy some given constraint on each site of the lattice. The energy difference induced between different classical states due to virtual quantum fluctuations can be conveniently written as a potential energy in this dimer subspace, so that different dimer coverings are now weighted according to this energy. For such dimer models, there are highly efficient Monte-Carlo algorithms [23, 24] based on non-local updates and we use these algorithms to perform numerical simulations to complement the analytics.

Kagome antiferromagnet in field

Low spin ($S = 1/2, 1$) isotropic Heisenberg model on the kagome lattice has been analyzed in the presence of an external field and there is good evidence from exact diagonalization studies [25] for the existence of a $M/M_{sat} = 1/3$ magnetization plateau which survives in the thermodynamic limit. The plateau state seems to be a collinear UUD spin liquid –meaning that it is a quantum superposition of states composed of $\uparrow\uparrow\downarrow$ spin tilings on each triangle of the kagome lattice. Note that quantum fluctuations play a crucial role in stabilizing the plateau at $T = 0$ as the magnetization plateau disappears in the classical limit.

In our work, we consider the case when anisotropy D dominates over the Heisenberg exchange J. In this case, a $M/M_{sat} = 1/3$ magnetization plateau exists even at a classical level when collinear states are preferred due to an anisotropy D. When $D \gg J$, the $m = 1/3$ magnetization plateau exists over a range of field $0 < B < 4JS$.

The $m = 1/3$ plateau is characterized by a 2:1 constraint that requires two spins on each triangle to be maximally polarized along the field, and one *minority* spin on each triangle to be maximally polarized anti-parallel to the field. States that satisfy this 2:1 constraint on each triangle are still macroscopically large in number. The $m = 1/3$ ensemble can be conveniently represented by encoding the presence of a minority spin by placing a dimer on the corresponding bond of the underlying honeycomb lattice (see Fig 3). The local $\uparrow\uparrow\downarrow$ constraint on each triangle implies that each site of the honeycomb lattice has a dimer coming out of it, and that no two dimers touch each other. The low temperature physics on the plateau is then determined by the leading order effective Hamiltonian that acts within this dimer subspace.

Because of the strong $2:1$ constraint, the first term that breaks the degeneracy (for any $S \geq 3/2$) of states in the dimer subspace is a *diagonal* term that occurs at $\mathcal{O}(J^6/D^5)$ due to virtual quantum fluctuations. In contrast, the leading *off-diagonal* term in the effective Hamiltonian due to real quantum fluctuations is at $\mathcal{O}(J^{6S-2}/D^{6S-3})$. Thus, the only case where off-diagonal terms dominate the low energy physics is the $S = 1$ case. It was recently shown that a one-third magnetization ($m = 1/3$) plateau with $\sqrt{3} \times \sqrt{3}$ collinear order is obtained in the presence of a magnetic field directed along the easy axis [26] in the $S = 1$ case. As we show in Ref [27], the case for all spin $S \geq 3/2$ is entirely different.

The effective Hamiltonian for $S = 3/2$ takes the following form [27]

$$\mathcal{H} = +c_1 \frac{J^6}{D^5} \sum_{\hexagon} \left(\frac{1}{6} |\hexagon_1\rangle\langle\hexagon_1| \right) - c_2 \frac{J^7}{D^6} \sum_{\hexagon} \left(|\hexagon_{3A}\rangle\langle\hexagon_{3B}| + h.c. \right) \tag{3}$$

where $\hexagon_m$ ($m = 0, 1, 2, 3$) denote hexagonal plaquettes with m dimers and $\hexagon_{3A}, \hexagon_{3B}$ represent the two flippable dimer configurations with three alternating dimers on a hexagonal plaquette. The values of the coefficients are $c_1 = \frac{2187}{16384} \approx 0.1335$ and $c_2 = \frac{27}{8192} \approx 3.3 \times 10^{-3}$. The potential energy $V(S) \equiv c_1(S) J^6/6D^5$ has been calculated for general S, and the result is $V(S) = (2S)^6 J^6/1024(2S-1)^5 D^5$. We have also used the semiclassical large-S expansion procedure of Ref [28] and calculated the semiclassical effective Hamiltonian in the large-S limit: The leading $\mathcal{O}(J^6/D^5)$ term obtained by expanding the semiclassical result in powers of J/D agrees precisely with the large-S limit of the perturbative result obtained above for arbitrary S.

The low temperature physics is thus well-described by a classical dimer model with weights associated with the potential energy term in the effective Hamiltonian. This classical potential energy is minimized by any configuration with no hexagon having precisely one dimer on it. As there are a large number of such configurations, a more

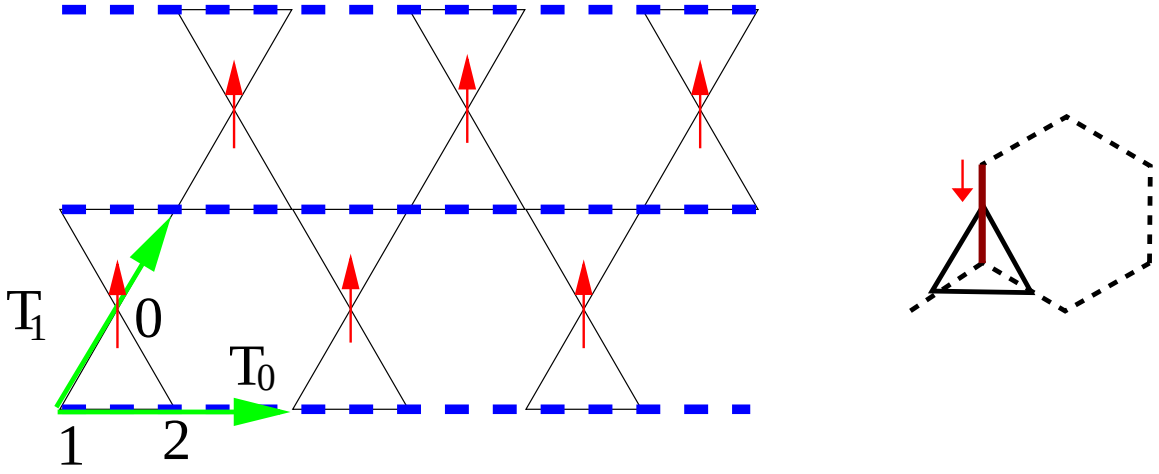

Figure 3: Sublattice rotation symmetry breaking on the $m = 1/3$ plateau: Dotted lines denote alternating arrangement of spins with average moment zero; up arrows correspond to $S_z = +S$. Dimer representation of low energy $m = 1/3$ configurations is also shown.

detailed analysis is needed to elucidate the nature of the low temperature state. For doing this, we have employed a generalization of the procedure of Refs [23, 24] to efficiently simulate an interacting classical dimer model with this potential energy term—our algorithm employs non-local loop updates but preserves detailed balance in order to generate the correct equilibrium Gibbs distribution at temperature T.

As the temperature is lowered to below $T_c \approx 0.23V(S)$, we find that the system undergoes a transition to a state with (sublattice) rotation symmetry breaking as shown in Fig 3: In this simplest schematic of the ordered state, one spontaneously chosen sub-lattice of spins acquires the maximal polarization $+S$ along the field. In order to satisfy the strong $2:1$ constraint on each triangle, the spin moments on the other two sub-lattice sites then alternate $+S,\ -S\ldots$ in one of the two possible alternating arrangements along a stripe. This ordering can be conveniently characterized using a Z_3 sublattice order parameter $\Phi = \sum_p m_p e^{2p\pi i/3}$, where m_p denotes the sublattice magnetization of the p^{th} sublattice (Fig 3). Note that the $U(1)$ spin rotation symmetry of the Hamiltonian stays unbroken for collinear states. A very similar ordering was suggested earlier for an isotropic kagome antiferromagnet in field in the semiclassical limit [29].

This system also provides us with an interesting example of glassy physics without the presence of disorder. Although the fully equilibriated system only breaks rotation symmetry by forming *disordered* stripes, this equilibriation is achieved in our numerics because the algorithm incorporates non-local loop updates that can flip a macroscopic number of spins in one move. In the experimental system, the dynamics is of course

purely local. Such local spin flips cost significant potential energy, and the system needs to change the internal state of an entire stripe to avoid this potential energy penalty. Systems with very similar potential energy landscapes have been the subject of earlier studies which demonstrate that the time-scale for changing the internal state of a stripe diverges rapidly with system size if the dynamics is local [30]. It is thus clear that the low temperature phase displays glassy freezing of the stripes.

We have also numerically studied the behaviour of the system for $T_c \lesssim T$ with purely local two-spin exchange dynamics satisfying detailed balance, and monitored the temperature dependence of the single-spin autocorrelation function for a range of moderately large values for the ratio $JS^2/V(S)$. In these simulations, the magnetic field B is fixed to its nominally optimal value $B = 2JS$ which places the system close to the center of the $m = 1/3$ plateau. Note that the ratio $JS^2/V(S)$ is kept finite as we wish to explore the higher temperature dynamics, and configurations outside the 'dimer subspace' are *allowed* but *exponentially unlikely* (as opposed to forbidden). We find that the single spin autocorrelation time τ increases very rapidly as we lower the temperature. Indeed, $\tau(T)$ can be fit well by an activated functional form of the Vogel-Fulcher type $\tau(T) = \exp(\Delta/(T - T_f(L)))$, thus extending further the analogy to other models of glass-formers [30].

To summarize, we have predicted an unusual sublattice ordered $m = 1/3$ magnetization plateau at low temperature in $S \geq 3/2$ kagome antiferromagnets with strong easy axis anisotropy that breaks sublattice rotation symmetry but not translational symmetry. This is also an interesting example of slow glassy dynamics in a spin system without any disorder.

Kagome and triangular antiferromagnets in zero field

The kagome and triangular lattice Ising antiferromagnets do not show any magnetic order down to $T = 0$ [5]. In both the cases, the $T = 0$ ground state is obtained by requiring that there is exactly one frustrated bond (connecting a pair of aligned spins) on each triangle. This 'minimally frustrated' ensemble of states has a residual entropy of $0.502k_B$ ($0.32k_B$) per site in the kagome (triangular) case. This macroscopic entropy ensemble of ground states can be conveniently represented by dimer coverings on the dice (honeycomb) lattice dual to the kagome (triangular) lattice, wherein a dimer is placed on every link of the dual lattice that intersects a frustrated bond of the original spin configuration. In the kagome case, spin correlators averaged over this ensemble yield spin correlators that are very short ranged. In the triangular case, the spin correlators are not long range ordered, but correlations at the three-sublattice

wavevector rapidly builds up with decreasing temperature.

When $D \gg J$, the low energy states selected by the anisotropy map on to the configurations of the corresponding classical Ising antiferromagnet. However, as we show [31], quantum dynamics arising due to the transverse spin components leads to a multi-spin interaction which makes the low temperature behaviour very different from the classical Ising case in both the kagome and the triangular lattices. When D dominates over J, the leading D term picks collinear spin states. The low energy physics in this collinear regime, which can be described by Ising pseudo-spin variables σ:$S_i^z = \sigma_i S$ with $\sigma_i = \pm 1$, is then best described in terms of an effective Hamiltonian $\mathcal{H}$ that encodes the splitting of this degenerate Ising subspace.

For any $S > 3/2$ [31], the effective Hamiltonian takes the following form (to $\mathcal{O}(J^3/D^2)$):

$$\mathcal{H} = J_1 \sum_{\langle ij \rangle} \sigma_i \sigma_j - J_2 \sum_{\langle ij \rangle} \frac{1 - \sigma_i \sigma_j}{2} (\sigma_i H_i + \sigma_j H_j) \tag{4}$$

where $J_1 = JS^2$, $J_2 = \frac{S^3 J^3}{4D^2(2S-1)^2}$, and the *exchange field* $H_i \equiv \Gamma_{ij}\sigma_j$ with $\Gamma_{ij} = 1$ for nearest neighbours and zero otherwise. In the above, the first term corresponds to the leading effect of the z component of the spin exchange, while the second term arises from the effects of *virtual* quantum transitions of pairs of anti-aligned spins out of the low energy Ising subspace. An additional $\mathcal{O}(J^{2S}/D^{2S-1})$ pseudo-spin exchange term, representing real quantum transitions, is subdominant for $S > 3/2$.

When $J_2 \ll T \ll J_1$, the physics is controlled by the ground states of the corresponding Ising antiferromagnet. In these ground states each triangle has exactly one frustrated bond connecting a pair of aligned spins. This ensemble of ground states can be conveniently represented by dimer coverings on the dual dice lattice in the kagome case and the dual honeycomb lattice in the triangular case. A dimer is placed on every link of the dual lattice that intersects a frustrated bond on the direct lattice. This defines a hard-core dimer model on the honeycomb lattice (dual to the triangular lattice) where no two dimers touch each other. On the dice lattice (dual to kagome lattice), a hard dimer constraint is operative only on the 3-coordinated dice lattice sites, while the 6-coordinated sites have a soft constraint that an even number of dimers touch them.

Quantum fluctuations make their presence felt once the temperature is comparable or below the scale J_2. To understand the behaviour at such low temperature, we analyze the effects of the multispin interaction term J_2 projected in the minimally frustrated Ising subspace. We show that the *complicated* looking J_2 term can be

written in the following compact form [31] in dimer language by using the constraint that all spin configurations in this subspace have exactly one frustrated bond per triangle:

$$H_D = 2J_2 \sum_P n^2 |nP\rangle\langle nP| \tag{5}$$

where $|nP\rangle$ denotes elementary plaquettes with n dimers on their perimeter.

Kagome lattice: It is shown that this potential energy H_D is minimized [31] for the dice lattice when elementary plaquettes with no dimers on their perimeter are disallowed. In spin language, it implies that *no spin should be the minority spin of both the triangles to which it belongs.* We find [31] that it is possible to construct a large subset of states with macroscopic entropy satisfying the rule, and all related to each other by local spin flips.

We perform detailed Monte-Carlo simulations of H_D to further investigate the effects of the J_2 term. In order to obtain reliable numerical results, we have developed a new loop algorithm [32] that can handle the non-trivial Boltzmann weight associated with H_D as well as keep track of the different constraints on the 3- and 6-coordinated sites. We see no evidence at all of any phase transition as we lower the temperature to access the $T \to 0$ limit. Although there is no transition, we find that the liquid state at low temperature is quite different from the intermediate temperature Ising paramagnet. A clear signature of this crossover to the semiclassical spin liquid regime can be obtained by monitoring the spin structure factor (that can be probed in neutron scattering experiments) $S(\vec{q}) = |S_0(\vec{q}) \exp(iq_y/2) + S_1(\vec{q}) + S_2(\vec{q}) \exp(iq_x/2)|^2$ where $S_\alpha(\vec{q})$ is the Fourier transform of the spin density on sublattice α of the Kagome lattice and q_x (q_y) refers to the projection of $\vec{q}$ on to lattice direction T_0 (T_1) measured in units of inverse Bravais lattice spacing (Fig 3). The spin structure factor ($S(\vec{q})$) evolves continuously (see Fig 4) from being quite featureless in the classical cooperative Ising regime $T^* \ll T \ll J_1$ to developing characteristic crescents of high intensity diffuse scattering in the low temperature semiclassical spin liquid regime $T \ll T^*$ where $T^* \sim 1.3J_2$. Precursors of these features are already present at a temperature scale $T \sim 2T^*$. This is in sharp contrast to the $S = 1$ case where the quantum dynamics connects different classical ground states and induces spin nematic order [26].

Experiments on Nd-langasite: Recent experiments on the spin-9/2 easy axis Kagome antiferromagnet Nd-Langasite have seen a liquid-like state with fluctuating moments and no long range order down to $50mK$. From the estimated values [22] of the isotropic exchange interaction and the single-ion anisotropy ($J \sim 1.5K$, $D \sim 10K$), the crossover from a classical cooperative Ising paramagnet to a semiclassical spin

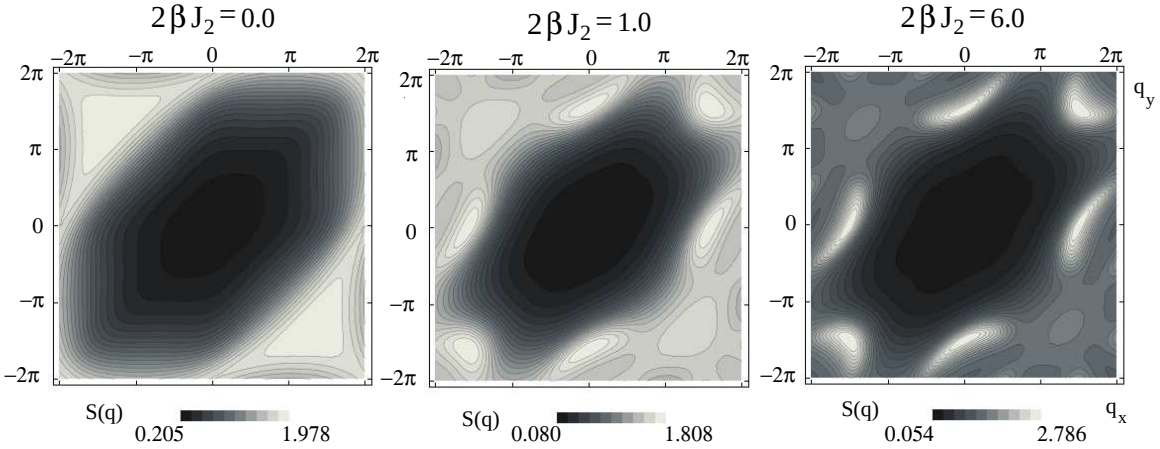

Figure 4: Spin structure factor $S(\vec{q})$ shown for three different temperatures, showing crossover to semiclassical spin liquid regime for the easy axis kagome antiferromagnet. Here $q_x(q_y)$ refers to the projection of $\vec{q}$ on to the lattice direction $T_0(T_1)$ (see Fig 3) measured in units of inverse Bravais lattice spacing.

liquid only occurs for temperatures significantly below $50mK$ ($T^* \approx 16mK$) in this model with an isotropic exchange and a simple single-ion anisotropy term (which is expected [22] to be a good starting point for Nd-Langasite).

We therefore expect a simple classical Ising description to work fairly well for the bulk of the temperature range studied in the recent low temperature experiments. Since correlations in the cooperative Ising paramagnet are extremely short-ranged and featureless, this is consistent with the fact that data from recent neutron scattering experiments (which probe the spin structure factor) show nearly featureless diffuse scattering that can be fit quite well to a model [33, 34] of spin correlations in which nearest neighbour spins are correlated, but there are no correlations of spins further away from each other.

Triangular lattice:

On the honeycomb lattice (dual to triangular lattice), H_D is minimized [31] by requiring that all hexagons have precisely two dimers on their perimeter. It can be shown that the entropy of such states is sub-extensive. All such dimer configurations only include dimers of at most two different orientations on the honeycomb lattice (in which all nearest neighbour bonds have one of the three possible orientations) and the bonds of the remaining orientation have no dimers on them. This suggests a breaking of rotational symmetry. From numerics, we indeed find [31] that below a critical temperature $T_c \approx 1.67J_2$, the system orders into a orientationally ordered state (Fig 5) in which the mean Ising exchange energy on a link of the triangular lattice depends on its orientation, but not its position. A Z_3 order parameter to characterize this symmetry breaking can be written down as $\Phi = \sum_p -B_p \exp(2p\pi i/3)$, where

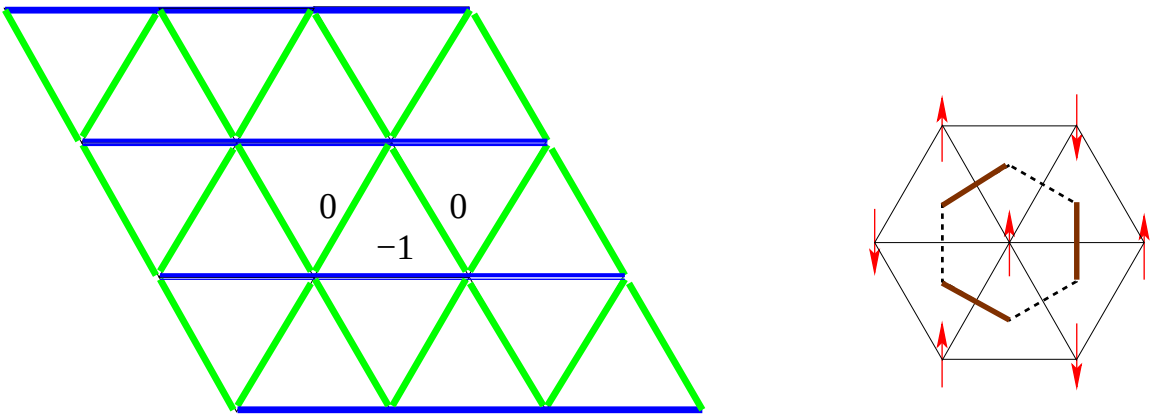

Figure 5: Orientationally ordered state on the triangular lattice. The average Ising exchange energy of the blue (dark) bonds is lower than that of the green (light) bonds. The representation of the triangular lattice spin configuration in terms of dimers (dark bonds) on the dual honeycomb net is also shown.

B_p denotes the average of the Ising exchange energy $\sigma_i\sigma_j$ on all links $\langle ij\rangle$ of the p^{th} orientation ($p = 0, 1, 2$) on the triangular lattice. In this ordered state, the Ising pseudospins are antiferromagnetically arranged in parallel rows oriented along one spontaneously chosen principle direction of the triangular lattice. This is in sharp contrast to the $S = 1$ case [26] which has coexisting three-sublattice spin-density wave order for the z component of the spin, as well as spin-nematic order in the transverse components of the spins because of the leading quantum dynamics.

Since each such row can be in one of two internal states corresponding to the two antiferromagnetic arrangements of the spins on that row, this ordered state does not break any translational symmetry. This implies the absence of any Bragg peak at some particular wave vector in the structure factor of the pseudospins σ(which corresponds to leading zz component in J/D of the structure factor of the physical spins) . However, there are Bragg lines with an enhanced signal due to the quasi-1D degeneracy of the system.

In the orientationally ordered state, the total easy axis magnetization and the corresponding susceptibility go as $\mathcal{O}(\exp(-J_2(S)/T))$ since perfect orientational order implies zero magnetization for each individual antiferromagnetic row of spins, and defects cost energy of order $J_2(S)$. As this ordered phase is stable to small magnetic fields at which corresponding Zeeman energy is small compared to the multispin interaction term J_2, this implies the presence of a low temperature *zero magnetization plateau* that extends for a range of magnetic fields $0 < |B| < B_c \sim J^3/D^2$.

To summarize, we have predicted that for $S > 3/2$, the kagome antiferromagnet with strong easy axis anisotropy goes into a semiclassical spin liquid state with dis-

tinctive and unusual short-ranged correlations below a crossover temperature $T^* \approx 0.08 J^3 S/D^2$, while the triangular magnet with strong easy axis anisotropy undergoes a first order transition at $T_c \approx 0.1 J^3 S/D^2$ to an orientationally ordered collinear state that gives rise to a zero-magnetization plateau for small magnetic fields along the easy axis.

Bibliography

[1] A. P. Ramirez, "*Strongly geometrically frustrated magnets*," Annu. Rev. Mat. Sci. **24**, 453 (1994).

[2] P. Schiffer and A. P. Ramirez, "*Recent experimental progress in the study of geometrical magnetic frustration*," Comments Cond. Mat. Phys. **18**, 21 (1996).

[3] R. Moessner, "*Magnets with strong geometric frustration*," Can. J. Phys. **79**, 1283 (2001).

[4] G. H. Wannier, "*Antiferromagnetism. The triangular Ising net*," Phys. Rev. **79**, 357 (1950).

[5] R. Liebmann, *Statistical Mechanics of Periodic Frustrated Ising Systems* Springer, Berlin (1986).

[6] G. Lawes *et al.*, "*Competing magnetic phases on a kagome staircase*," Phys. Rev. Lett. **93**, 247201 (2004).

[7] J. D. Reger and A. P. Young, "*Monte Carlo simulations of the spin*-1/2 *Heisenberg antiferromagnet on a square lattice*," Phys. Rev. B **37**, 5978 (1988).

[8] L. Capriotti, A. E. Trumper and S. Sorella, "*Long-Range Neel order in the triangular Heisenberg model*," Phys. Rev. Lett. **82**, 3899 (1999).

[9] J. T. Chalker, P. C. W. Holdsworth and E. F. Shender, "*Hidden order in a frustrated system: Properties of the Heisenberg kagome antiferromagnet*," Phys. Rev. Lett. **68**, 855 (1992).

[10] A. Chubukov, "*Order from disorder in a kagome antiferromagnet*," Phys. Rev. Lett. **69**, 832 (1992).

[11] R. R. P. Singh and D. A. Huse, "*Three-sublattice order in triangular and kagome lattice spin-half antiferromagnets*," Phys. Rev. Lett. **68**, 1766 (1992).

[12] P. W. Leung and V. Elser, "*Numerical studies of a 36-site kagome antiferromagnet*," Phys. Rev. B **47**, 5459 (1993).

[13] F. Mila, "*Low-Energy sector of the $S = 1/2$ kagome antiferromagnet*," Phys. Rev. Lett. **81**, 2356 (1998).

[14] G. Misguich and B. Bernu, "*Specific heat of the $S = 1/2$ Heisenberg model on the kagome lattice: High-temperature series expansion analysis*," Phys. Rev. B **71**, 014417 (2005).

[15] M. Hermele, T. Senthil and M. P. A. Fisher, "*Algebraic spin liquid as the mother of many competing orders*," Phys. Rev. B **72**, 104404 (2005).

[16] Y. Ran, M. Hermele, P. A. Lee and X. G. Wen, "*Projected-Wave-Function study of the spin-1/2 Heisenberg model on the kagome lattice*," Phys. Rev. Lett. **98**, 117205 (2007).

[17] A. V. Syromyatnikov and S. V. Meleyev, "*Hidden long-range order in kagome Heisenberg antiferromagnets*," Phys. Rev. B **66**, 132408 (2002).

[18] P. Nikolic and T. Senthil, "*Physics of low-energy singlet states of the kagome lattice quantum Heisenberg antiferromagnet*," Phys. Rev. B **68**, 214415 (2003).

[19] R. Budnik and A. Auerbach, "*Low-Energy Singlets in the Heisenberg Antiferromagnet on the Kagome Lattice*," Phys. Rev. Lett. **93**, 187205 (2004).

[20] M. J. Harris *et al.*, "*Geometrical frustration in the ferromagnetic pyrochlore $Ho_2 Ti_2 O_7$*," Phys. Rev. Lett. **79**, 2554 (1997).

[21] A. Zorko *et al.*, "*Easy-Axis kagome antiferromagnet: Local-Probe study of $Nd_3 Ga_5 SiO_{14}$*," Phys. Rev. Lett. **100**, 147201 (2008).

[22] H. Primas, "*Generalized perturbation theory in operator form*," Rev. Mod. Phys. **35**, 710 (1963).

[23] A. W. Sandvik and R. Moessner, "*Correlations and confinement in nonplanar two-dimensional dimer models*," Phys. Rev. B **73**, 144504 (2006).

[24] F. Alet *et al.*, "*Interacting classical dimers on the square lattice*," Phys. Rev. Lett. **94**, 235702 (2005).

[25] D. C. Cabra, M. D. Grynberg, P. C. W. Holdsworth and P. Pujol, "*From classical to quantum kagome antiferromagnet in a magnetic field*," Phys. Rev. B **65**, 094418 (2002).

[26] K. Damle and T. Senthil, "*Spin nematics and magnetization plateau transition in anisotropic kagome magnets*," Phys. Rev. Lett. **97**, 067202 (2006).

[27] A. Sen, K. Damle and A. Vishwanath, "*Magnetization plateaus and sublattice ordering in easy-axis kagome lattice antiferromagnets*," Phys. Rev. Lett. **100**, 097202 (2008).

[28] U. Hizi and C. Henley, "*Effective hamiltonian for the pyrochlore antiferromagnet: semiclassical derivation and degeneracy*," Phys. Rev. B **73**, 054403 (2006).

[29] S. R. Hassan and R. Moessner, "*Semiclassical degeneracies and ordering for highly frustrated magnets in a field*," Phys. Rev. B **73**, 094443 (2006).

[30] D. Das, J. Kondev, and B. Chakraborty, "*Activated dynamics at a non-disordered critical point*," Europhys. Lett. **61**, 506 (2003).

[31] A. Sen, F. Wang, K. Damle and R. Moessner, "*Triangular and kagome antiferromagnets with a strong easy-axis anisotropy*," Phys. Rev. Lett. **102**, 227001 (2009).

[32] A. Sen, K. Damle and R. Moessner (unpublished).

[33] J. Robert *et al.*, "*Spin-Liquid correlations in the Nd-Langasite anisotropic kagome antiferromagnet*," Phys. Rev. Lett. **96**, 197205 (2006).

[34] H. D. Zhou *et al.*, "*Partial field-induced magnetic order in the spin-liquid kagome* $Nd_3Ga_5SiO_{14}$," Phys. Rev. Lett. **99**, 236401 (2007).

Publications

- Arnab Sen, Kedar Damle and T. Senthil, "*Superfluid insulator transitions of hard-core bosons on the checkerboard lattice*," Phys. Rev. B **76**, 235107 (2007), arXiv:cond-mat/0701476v2.

- Arnab Sen, Kedar Damle and Ashvin Vishwanath, "*Magnetization plateaus and sublattice ordering in easy-axis kagome lattice antiferromagnets*," Phys. Rev. Lett. **100**, 097202 (2008), arXiv:0706.2362v2.

- Arnab Sen, Prasenjit Dutt, Kedar Damle and Roderich Moessner, "*Variational Wave-function study of the triangular lattice supersolid*," Phys. Rev. Lett. **100**, 147204 (2008), arXiv:0801.0791v2.

- Arnab Sen, Fa Wang, Kedar Damle and Roderich Moessner, "*Triangular and kagome antiferromagnets with a strong easy-axis anisotropy*," Phys. Rev. Lett. **102**, 227001 (2009), based on arXiv:0805.2658v1 (2008) and arXiv:0807.1163v1 (2008).

Chapter 1

Introduction

In many ionic insulators, some of the ions have well formed moments ('spins') due to the presence of incomplete shells in their ground state. Electron-electron Coulomb interactions, together with the Pauli exclusion principle, give rise to 'exchange' interactions between these magnetic moments which decay rapidly with increasing distance between the ions. Frequently, such interactions can be well described [1] by a Heisenberg Hamiltonian of the form

$$H = \sum_{i,j} J_{ij} \vec{S}_i \cdot \vec{S}_j \tag{1.1}$$

where the spin operator $\vec{S}$ for each ion denotes its *total* angular momentum which, in general, has both a spin and an orbital part. Closely related models are the XY and Ising models, where the number of spin components is $n = 2$ and $n = 1$ respectively .

Such interactions often lead to magnetically ordered states at low enough temperatures. In *unfrustrated* magnets, where all the interactions can be simultaneously minimized, the nature of the magnetic ordering can be usually understood in terms of the minimum of the classical exchange energy ($S \to \infty$ corresponds to the classical limit) even for small spin length S. For example, consider the classical ground state of the nearest neighbour antiferromagnetic ($J > 0$) Heisenberg Hamiltonian on a bipartite lattice like the simple cubic lattice. It is a two-sublattice ordered *Neel* state with $\vec{S} = S\hat{n}$ on one sublattice and $\vec{S} = -S\hat{n}$ on the other (where $\hat{n}$ is some arbitrary direction) which minimizes all the exchange interactions at the same time. This state breaks spin rotation symmetry and a Neel order parameter $\vec{N} = \frac{1}{N}\sum_i \epsilon_i \vec{S}_i$ (where $\epsilon_i = +1$ on one sublattice and -1 on the other sublattice of the bipartite lattice and N denotes the number of sites) can be defined to characterize the symmetry breaking. Within mean field theory, there is a finite temperature phase transition at

the transition temperature $k_B\Theta_{CW} = \frac{zS(S+1)J}{3}$ (where z is the coordination number) below which the system breaks spin rotation symmetry spontaneously. However, the Neel order parameter does not commute with the Hamiltonian H, and quantum fluctuations play an important role for finite S. It has been rigorously shown [2] that for the nearest neighbour Heisenberg antiferromagnet on a hypercubic lattice, the ground state has Neel order even in the extreme quantum limit of $S = 1/2$.

1.1 Geometric Frustration

Frustrated magnets have very different physics compared to their unfrustrated counterparts [3, 4, 5]. Frustrated systems have competing interactions which cannot be simultaneously minimized. Geometrically frustrated magnets are systems in which all the spin interactions cannot be satisfied together due to the connectivity of the lattice. Geometric frustration provides a route to destabilize the Neel order that is obtained at low temperatures for antiferromagnets on bipartite lattices. The frustration can lead to unconventional magnetic order or even novel spin liquid states without long range spin order at asymptotically low temperatures. Let us consider a very simple example to illustrate geometric frustration. Consider three Ising spins ($\sigma_i = \pm 1$) which lie on the vertices of a triangle and interact antiferromagnetically with each other. To minimize the energy on a bond, the Ising spins should be opposite to each other, i.e. their product should be -1. However, it is impossible to minimize the bond energies on all the three bonds and the best that can be done is to leave one bond *frustrated* (where the product of the spins is $+1$) and the other two *unfrustrated* (the product of spins being -1). Similarly, the energy cannot be minimized at all the bonds for XY or Heisenberg spins on a triangle. There are many ionic insulators in which the magnetic ions are arranged on non-bipartite lattices [3, 4] based on triangular units. Examples include the pyrochlore, kagome and the triangular lattices (Fig 1.1) which provide experimental realizations of geometric frustration.

It is particularly interesting to look at systems which are *highly frustrated* in the classical limit, where the number of inequivalent ground states (not related by some global symmetry of the Hamiltonian) scales exponentially with system size. For example, the triangular lattice Ising antiferromagnet has a residual entropy [6] (at zero temperature) which is extensive ($S/k_BN = 0.323$). Other examples are the Ising antiferromagnet on the kagome lattice and the Heisenberg antiferromagnet on the kagome and the pyrochlore lattice. On the other hand, XY and Heisenberg antiferromagnets on the triangular lattice have a unique ground state, the 120° Neel state (see Fig 1.2), even though all the bonds are not fully satisfied.

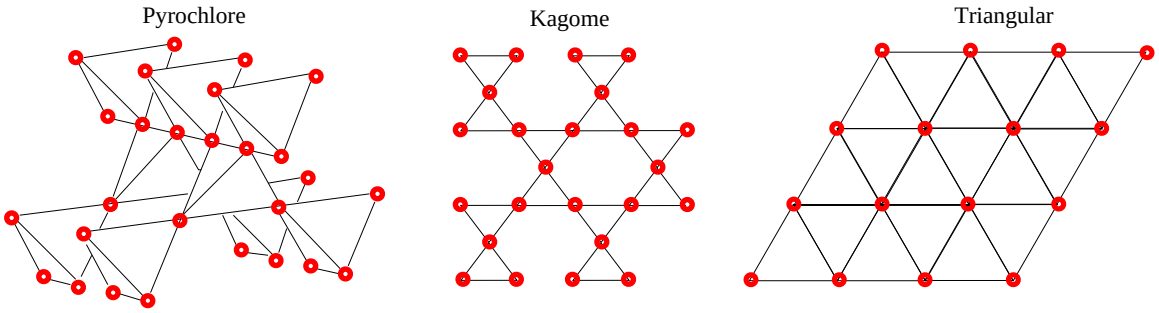

Figure 1.1: Examples of some lattices composed of triangular units where all exchange interactions cannot be simultaneously satisfied because of the connectivity of the lattice.

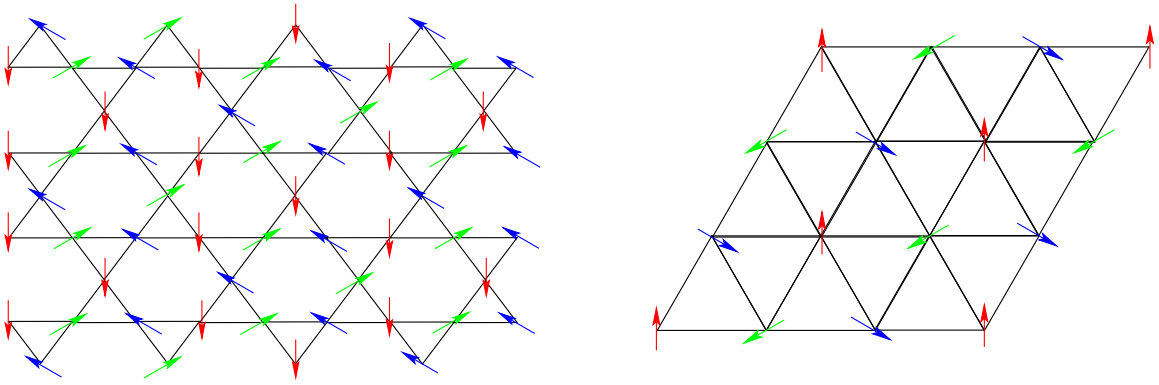

Figure 1.2: The $\sqrt{3} \times \sqrt{3}$ state on the kagome lattice which is stabilized at large-S and the 120° Neel state on the triangular lattice.

Highly frustrated magnetic systems have a characteristic [3] magnetic susceptibility behaviour (Fig 1.3) which is very different from unfrustrated magnets. Their inverse susceptibility χ^{-1} follows the Curie-Weiss law down to temperatures well below the expected mean field ordering temperature Θ_{CW}. There is a transition to some magnetically ordered or glassy state only at some low temperature $T_f \ll \Theta_{CW}$. In the intermediate temperature regime, $T_f < T < \Theta_{CW}$, a cooperative paramagnetic regime is obtained. Ramirez [3] has defined the "frustration index" $f \equiv |\Theta_{CW}|/T_f$, where a large value of f indicates strong frustration. The fate of the system below T_f often depends strongly on the additional perturbations that are present in the system.

Highly frustrated systems are very susceptible to the effects of perturbations [5]. Different types of perturbations lead to different ground state(s) being chosen at $T \to 0$ from the extensive ground state manifold of the leading interactions. Various physical mechanisms like magnetic anisotropies, further neighbour interactions, lattice distortions and non-magnetic defects are always present as perturbations in any realistic experimental situation. The interplay of these perturbations in the ground state manifold of the leading exchange interaction Hamiltonian can give rise to rich behaviour which is sensitive to their relative importance.

Another effect that is potentially important at $T \ll |\Theta_{CW}|$ in such systems is fluctuations due to the quantum nature of the spins. Even in the simplified nearest neighbour Heisenberg antiferromagnet on such frustrated lattices, it is very interesting to ask how much (if at all) of the classical picture at $S \to \infty$ survives quantum fluctuations when considering low spin like $S = 1/2, 1, 3/2, \cdots$. Since the classical energetics fails to pick up a unique ground state, the answer is far from obvious. The true ground state can turn out to be any linear combination of the classical ground states and might lead to unconventional ordered states or spin liquids. A controlled way to analyze quantum fluctuations is to perform a $1/S$ expansion. It is possible that quantum fluctuations become so strong that they destabilize any order present in the large-S problem when the extreme quantum limit of $S = 1/2$ is approached to give a spin liquid state.

Much of the theoretical work has focussed on the challenging case of spin 1/2 moments with Heisenberg exchange interactions [7]. There is good numerical evidence on the triangular lattice [8] that the 120° Neel order survives down to $S = 1/2$, albeit with the order parameter reduced by about 59% from its classical value. Less is known with certainty for the kagome lattice for small values of S. Quantum fluctuations can be included in a perturbative manner by doing a semi-classical $1/S$ expansion about the classical solution. Within the $1/S$ treatment, it has been shown that quantum

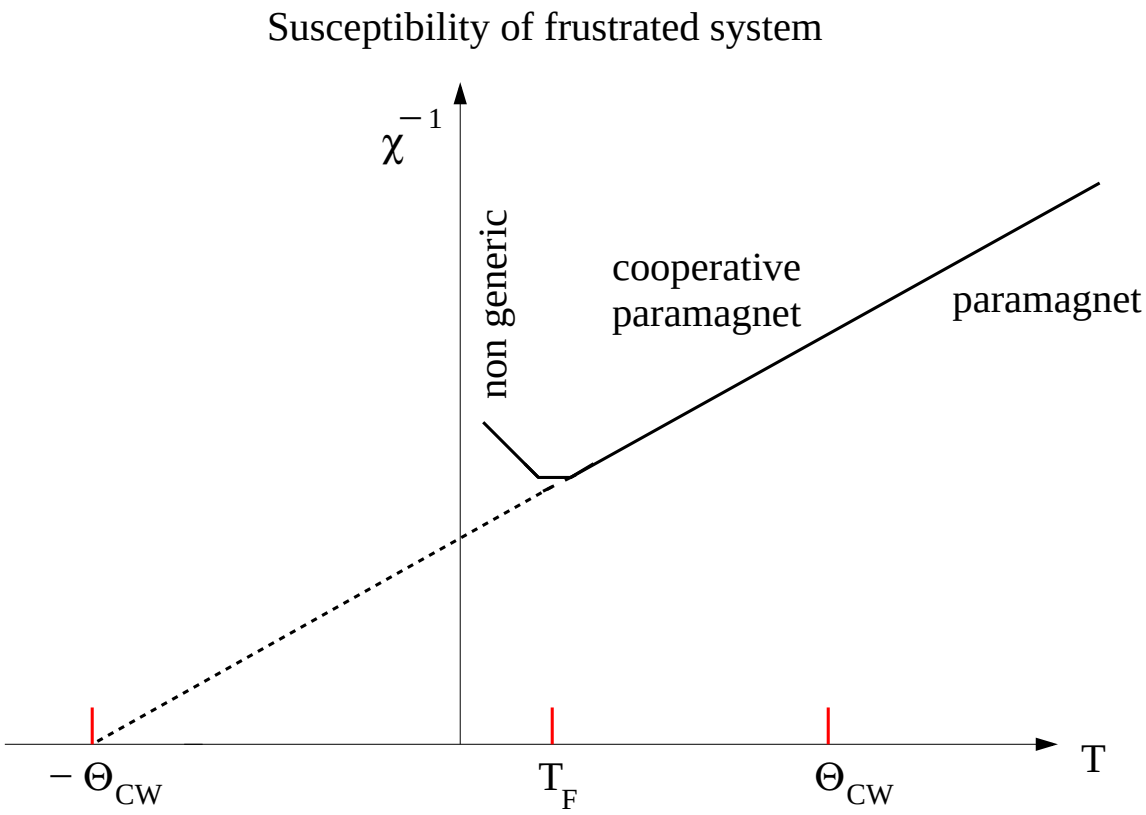

Figure 1.3: Schematic illustration of characteristic susceptibility behaviour of highly frustrated systems. The susceptibility follows a Curie-Weiss law much below the mean field ordering temperature Θ_{CW}.

fluctuations select coplanar states [9] at leading order for the kagome antiferromagnet. However, these are still massively degenerate, and this degeneracy is lifted at the next order [10] to give the $\sqrt{3} \times \sqrt{3}$ state as the large-S ground state (Fig 1.2). However, the $\sqrt{3} \times \sqrt{3}$ state does not survive in the strong quantum limit of $S = 1/2$. There have been many studies [11, 12, 13, 14] of the kagome antiferromagnet aimed at understanding the extreme quantum limit of $S = 1/2$ but there is still no definite answer, even though there have been proposals of spin liquid states [15, 16] and valence bond crystal states [17, 18, 19] as candidate ground states.

1.2 Strong easy axis anisotropy

In the opposite Ising limit, there are no quantum fluctuations. These frustrated Ising models on the kagome and the triangular lattices have been of interest in statistical mechanics for over half a century now [20], and are known to have a macroscopic degeneracy of inequivalent classical ground states. The residual entropy of the ground state ensemble equals $0.502k_B$ ($0.323k_B$) per spin in the kagome (triangular) lattice case [6]. It is known that the Ising model on both the lattices do not display any spin order down to zero temperature [6], unlike the square lattice Ising antiferromagnet which shows a finite temperature phase transition into the Neel phase.

Such "Ising spins" can and do actually arise in experiments when the spins have a strong easy-axis anisotropy in addition to the usual isotropic exchange coupling J in their magnetic Hamiltonian. In this thesis, we study $S \geq 3/2$ kagome and triangular lattice antiferromagnets with the following spin Hamiltonian

$$H = J \sum_{\langle ij \rangle} \vec{S}_i \cdot \vec{S}_j - D \sum_i (S_i^z)^2 - B \sum_i S_i^z \tag{1.2}$$

where J is the antiferromagnetic Heisenberg exchange between nearest neighbour spins, D is a single-ion uniaxial anisotropy of the easy axis type and B is an external magnetic field applied along the easy axis. This type of anisotropy is induced by local crystal fields through spin-orbit coupling [1]. There are known examples in rare earth magnets where the uniaxial anisotropy D is the dominant term. The pyrochlore spin ice compound $Ho_2Ti_2O_7$ is one such example where $D \sim 50K$ and (ferromagnetic) $J \sim 1K$ [21]. The quasi two-dimensional kagome antiferromagnet Nd-langasite ($Nd_3Ga_5SiO_{14}$) is another example [22] with $D \sim 10K$ and $J \sim 1.5K$.

We consider the situation where the uniaxial anisotropy D dominates over the Heisenberg exchange J, and collinear spin configurations dominate at low tempera-

tures (a collinear spin configuration can be labelled as $S_i^z = \sigma_i S$ where $\sigma_i = \pm 1$). For the pure Heisenberg model ($D = 0$) on the two lattices, the ground state typically involves coplanar arrangement of spins (Fig 1.2). Due to the frustrated nature of J, the anisotropy D need not be very large to induce collinear ground states. It can be shown that the system prefers a collinear state for $D > J$ on the kagome lattice and $D > 3J/2$ on the triangular lattice in the classical limit. Note that the physics in this (collinear) regime is different from that of the intermediate anisotropy regime [23, 24], in which non-collinear spin configurations dominate at low temperatures and magnetic fields, leading to a sequence of non-collinear phases in the classical problem.

In the collinear regime, we expect an analysis based on the smallness of J/D to give reliable results. Quantum fluctuations are absent in the limit $J/D \to 0$ and can be studied in a controlled manner for small J/D. When $D \gg J$, collinear spin states (that can be described by Ising pseudo-spin variables $\sigma : S_i^z = \sigma_i S$) have the minimum energy and all non-collinear states have an energy gap of at least $D(2S-1)$ (ignoring $O(J)$ corrections). The low energy physics (when $T \ll D(2S-1)$) in this regime is then best described in terms of an effective Hamiltonian, written in terms of these Ising pseudo-spins, that encodes the splitting of this degenerate Ising subspace to each order in J/D due to quantum corrections. We find that multi-spin interactions arising from the presence of exchange coupling between the transverse spin components make the low temperature behaviour very different from the well known classical Ising case.

1.3 Outline

The rest of this thesis is organized as follows. In Chapter 2, we derive the effective Hamiltonian at zero field for the kagome and triangular lattices in a J/D expansion and show that for any $S > 3/2$, $O(J^3 S/D^2)$ terms change the behaviour from the classical Ising model at low temperatures. We also evaluate the effective Hamiltonian within the semiclassical large-S expansion and show that the large-S limit of the perturbative result obtained for arbitrary S matches precisely with the semiclassical analysis.

In Chapter 3, we derive the physical consequences of quantum fluctuations on the low energy properties of the kagome and triangular lattice systems in zero field for $S > 3/2$. We show that multi-spin interactions at $O(J^3 S/D^2)$, which arise due to the quantum nature of the spins, changes the physics at low temperature from the pure Ising case. The kagome magnet goes into a spin liquid state with distinctive

and unusual short-ranged correlations, while the triangular magnet undergoes a first order phase transition to an orientationally ordered collinear state.

In chapter 4, we consider the kagome lattice in a finite magnetic field along the easy axis, where the magnetic field is chosen to induce a 1/3 magnetization plateau. The magnetization plateau is characterized by a strong $2:1$ constraint that requires two spins on each triangle to be maximally polarized along the field and one, minority, spin in each triangle to be maximally polarized antiparallel to the field. We derive the effective Hamiltonian in a perturbative expansion in J/D and show that the first term (for any $S \geq 3/2$) the breaks the degeneracy of these $2:1$ states occurs only at $O(J^6/D^5)$. We calculate the term explicitly for a general S and show that it matches the semiclassical effective Hamiltonian in the large-S limit.

In chapter 5, we analyze the physical consequences of the effective Hamiltonian for the kagome problem at finite field (in the 1/3 magnetization plateau) for $S \geq 3/2$. The system on this plateau develops an unusual order at low temperature that breaks sublattice rotation symmetry but not translational symmetry. We also discuss the extremely slow dynamics associated with this ordering that leads to glassy freezing of the system in the absence of any disorder.

The conclusions are given in chapter 6. Most of the results presented in this thesis have been published earlier in Refs [25, 26].

References

[1] K. Yosida. Theory of Magnetism. *Springer*, (1996).

[2] T. Kennedy, E. H. Lieb and B. S. Shastry. Existence of Neel order in some spin-1/2 Heisenberg antiferromagnets. *J. Stat. Phys.* **53**, 1019 (1988).

[3] A. P. Ramirez. Strongly geometrically frustrated magnets. *Annu. Rev. Mater. Sci.* **24**, 453 (1994).

[4] P. Schiffer and A. P. Ramirez. Recent experimental progress in the study of geometrical magnetic frustration. *Comments Condens. Matter Phys.* **18**, 21 (1996).

[5] R. Moessner. Magnets with strong geometric frustration. *Can. J. Phys.* **79**, 1283 (2001).

[6] R. Liebmann. Statistical Mechanics of periodic frustrated Ising systems. *Springer*, Berlin (1986).

[7] G. Misguich and C. Lhuillier. Two dimensional quantum antiferromagnets. Review chapter in *Frustrated Spin Systems*, edited by H.T. Diep (World Scientific, Singapore, 2005).

[8] L. Capriotti, A. E. Trumper and S. Sorella. Long-range Neel order in the triangular Heisenberg model. *Phys. Rev. Lett.* **82**, 3899 (1999).

[9] J. T. Chalker, P. C. W. Holdsworth and E. F. Shender. Hidden order in a frustrated system: properties of the Heisenberg kagome antiferromagnet. *Phys. Rev. Lett.* **68**, 855 (1992).

[10] A. Chubukov. Order from disorder in a kagome antiferromagnet. *Phys. Rev. Lett.* **69**, 832 (1992).

[11] R. R. P. Singh and D. A. Huse. Three-sublattice order in triangular and kagome lattice spin-half antiferromagnets. *Phys. Rev. Lett.* **68**, 1766 (1992).

[12] P. W. Leung and V. Elser. Numerical studies of a 36-site kagome antiferromagnet. *Phys. Rev. B* **47**, 5459 (1993).

[13] F. Mila. Low-energy sector of the $S = 1/2$ kagome antiferromagnet. *Phys. Rev. Lett.* **81**, 2356 (1998).

[14] G. Misguich and B. Bernu. Specific heat of the $S = 1/2$ Heisenberg model on the kagome lattice: High-temperature series expansion analysis. *Phys. Rev. B* **71**, 014417 (2005).

[15] M. Hermele, T. Senthil and M. P. A. Fisher. Algebraic spin liquid as the mother of many competing orders. *Phys. Rev. B* **72**, 104404 (2005).

[16] Y. Ran, M. Hermele, P. A. Lee and X. G. Wen. Projected wave-function study of the spin-1/2 Heisenberg model on the kagome lattice. *Phys. Rev. Lett.* **98**, 117205 (2007).

[17] A. V. Syromyatnikov and S. V. Meleyev. Hidden long-range order in kagome Heisenberg antiferromagnets. *Phys. Rev. B* **66**, 132408 (2002).

[18] P. Nikolik and T. Senthil. Physics of low-energy singlet states of the kagome lattice quantum Heisenberg antiferromagnet. *Phys. Rev. B* **68**, 214415 (2003).

[19] R. Budnik and A. Auerbach. Low-energy singlets in the Heisenberg antiferromagnet on the kagome lattice. *Phys. Rev. Lett.* **93**, 187205 (2004).

[20] G. H. Wannier. Antiferromagnetism. The triangular Ising net. *Phys. Rev.* **79**, 357 (1950).

[21] M. J. Harris *et al.* Geometric frustration in the ferromagnetic pyrochlore $Ho_2Ti_2O_7$. *Phys. Rev. Lett.* **79**, 2554 (1997).

[22] A. Zorko *et al.* Easy-axis kagome antiferromagnet: local-probe study of $Nd_3Ga_5SiO_{14}$. *Phys. Rev. Lett.* **100**, 147201 (2008).

[23] S. Miyashita Magnetic properties of Ising-like Heisenberg antiferromagnets on the triangular lattice. *J. Phys. Soc. Jpn.* **55**, 3605 (1986).

[24] P. E. Melchy and M. E. Zhitomirsky. Interplay of anisotropy and frustration: triple transitions in a triangular-lattice antiferromagnet. *preprint* axXiv:0812.3574 (2008).

[25] A. Sen, F. Wang, K. Damle and R. Moessner. Triangular and kagome antiferromagnets with a strong easy-axis anisotropy. *Phys. Rev. Lett.* **102**, 227001 (2009).

[26] A. Sen, K. Damle and A. Vishwanath. Magnetization plateaus and sublattice ordering in easy-axis kagome lattice antiferromagnets. *Phys. Rev. Lett.* **100**, 097202 (2008).

Chapter 2

Effective Hamiltonian in zero field

In this chapter, we derive the effective Hamiltonian for $S > 3/2$ moments on the kagome and triangular lattices, where the spins interact with a nearest neighbour antiferromagnetic Heisenberg exchange $J > 0$ in the presence of a single-ion anisotropy $D > 0$ that picks out a common easy axis z:

$$H = J \sum_{\langle ij \rangle} \vec{S}_i \cdot \vec{S}_j - D \sum_i (S_i^z)^2 \tag{2.1}$$

Let us first consider the problem in the classical limit, where we take $\vec{S}_i$ to be vectors of fixed length S, so that $\vec{S} = S\hat{n}$ where $\hat{n}$ is a unit vector. Consider the case where the system consists of only three spins on a single triangle. Then a collinear ground state is induced for any $D > J/2$ (Fig 2.1). The ground state is simply the spin configurations where the spins are maximally polarized parallel or anti-parallel to the z axis, and the triangle has only one frustrated bond connecting a pair of aligned spins. From this it is easy to see that if $D > J$ on the kagome lattice and $D > 3J/2$ on the triangular lattice [1, 2], any spin configuration where the spins are maximally polarized parallel or anti-parallel to the z axis and there is exactly

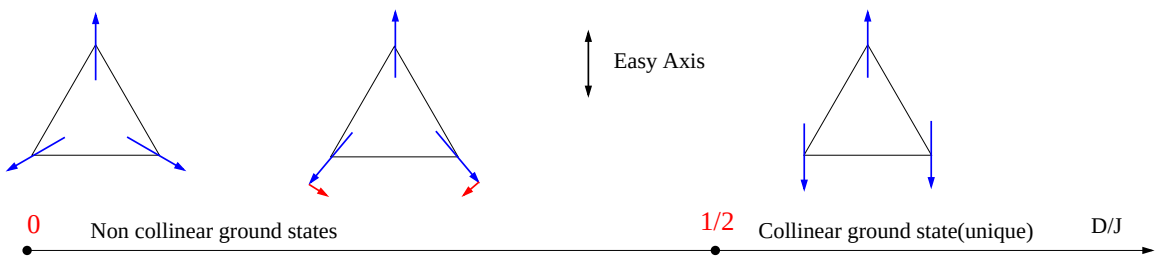

Figure 2.1: Evolution of the classical ground state on a single triangle for different values of D/J. The ground state becomes collinear once $D > J/2$.

one frustrated bond on every triangle of the lattice is a ground state of the classical problem. Thus, due to the frustrated nature of J, collinear regime where the low energy physics is dominated by such states, is reached for relatively small values of D/J. In this collinear regime, we expect an analysis based on the smallness of J/D to give reliable results. With this in mind, we use J/D as the small parameter in a systematic perturbative approach that allows us to calculate the effective low-energy Hamiltonian and the resulting low-temperature phases.

2.1 Effective Hamiltonian

When D dominates over J, the leading D term picks collinear spin states that can be described by Ising pseudospin variables σ: $S_i^z = \sigma_i S$ with $\sigma_i = \pm 1$. The low energy physics in this regime (when $T \ll D(2S-1)$) is then best described in terms of an effective Hamiltonian $\mathcal{H}$ that encodes the splitting of this degenerate Ising subspace. We split up the Hamiltonian as $H = H_0 + V$, where

$$\begin{aligned} H_0 &= -D\sum_i (S_i^z)^2 \\ V &= V_d + V_o = (J\sum_{\langle ij\rangle} S_i^z S_j^z - \mathcal{E}_0) + \frac{\lambda J}{2}\sum_{\langle ij\rangle}(S_i^+ S_j^- + S_i^- S_j^+) \end{aligned} \tag{2.2}$$

We have added a constant $-\mathcal{E}_0$ to the potential term where $\mathcal{E}_0$ is the ground state energy of any collinear spin configuration which has exactly one frustrated bond in each triangle. λ is introduced as a book-keeping device and is set to one at the end of the calculation. H_0 is diagonal in the S_i^z basis and V can be written as the sum of a diagonal (V_d) and an off-diagonal (V_o) operator in this basis.

We then use standard degenerate perturbation theory (assuming $J \ll D$) to derive the effective Hamiltonian $\mathcal{H}$ that lives in the reduced Hilbert space of collinear states. We use the Van Vleck method of unitary transformations [3] to do this and the method is explained in Appendix B. For each energy eigenvalue of H_0 in Eq 2.2, there is a huge degeneracy of eigenstates. To set up notation, we denote a state by $|i,\alpha\rangle$ where α stands for the energy eigenvalue and i is the state index. $E_{i,\alpha}$ denotes the energy (with respect to H_0) of the state. Writing $\mathcal{H} = \mathcal{H}_1 + \mathcal{H}_2 + \mathcal{H}_3 + \cdots$ where $\mathcal{H}_n$ is the contribution to the effective Hamiltonian at $O(J^n/D^{n-1})$, the following expressions

are obtained for $n = 1, 2, 3$ using the Van Vleck formalism:

$$\begin{aligned}
\langle j,\alpha_g|\mathcal{H}_1|i,\alpha_g\rangle &= \langle j,\alpha_g|V|i,\alpha_g\rangle \\
\langle j,\alpha_g|\mathcal{H}_2|i,\alpha_g\rangle &= \sum_{\gamma\neq g}\frac{\langle j,\alpha_g|V|k,\gamma\rangle\langle k,\gamma|V|i,\alpha_g\rangle}{E_g-E_{k,\gamma}} \\
\langle j,\alpha_g|\mathcal{H}_3|i,\alpha_g\rangle &= \sum_{\gamma_1\neq g,\gamma_2\neq g}\frac{\langle j,\alpha_g|V|k_2,\gamma_2\rangle\langle k_2,\gamma_2|V|k_1,\gamma_1\rangle\langle k_1,\gamma_1 V|i,\alpha_g\rangle}{(E_g-E_{k_1,\gamma_1})(E_g-E_{k_2,\gamma_2})} \\
&- \frac{1}{2}\sum_{\gamma_1\neq g,\gamma_2\neq\gamma_1}\frac{\langle j,\alpha_g|V|k_2,\gamma_2\rangle\langle k_2,\gamma_2|V|k_1,\gamma_1\rangle\langle k_1,\gamma_1 V|i,\alpha_g\rangle}{(E_g-E_{k_1,\gamma_1})(E_{k_2,\gamma_2}-E_{k_1,\gamma_1})} \\
&+ \frac{1}{2}\sum_{\gamma_1\neq\gamma_2,\gamma_2\neq g}\frac{\langle j,\alpha_g|V|k_2,\gamma_2\rangle\langle k_2,\gamma_2|V|k_1,\gamma_1\rangle\langle k_1,\gamma_1 V|i,\alpha_g\rangle}{(E_g-E_{k_2,\gamma_2})(E_{k_2,\gamma_2}-E_{k_1,\gamma_1})} \\
&- \frac{1}{2}\sum_{\gamma_1\neq\gamma_2,\gamma_1\neq g,\gamma_2\neq g}\frac{\langle j,\alpha_g|V|k_2,\gamma_2\rangle\langle k_2,\gamma_2|V|k_1,\gamma_1\rangle\langle k_1,\gamma_1 V|i,\alpha_g\rangle}{(E_g-E_{k_1,\gamma_1})(E_g-E_{k_2,\gamma_2})}
\end{aligned} \tag{2.3}$$

Here α_g stands for the ground state manifold of H_0 and E_g denotes the ground state energy of H_0. The terms determining $\langle j,\alpha_g|\mathcal{H}_n|i,\alpha_g\rangle$ can be thought of as processes in which a state i in the ground state manifold of H_0 makes transitions to states $|k_1,\gamma_1\rangle,\cdots,|k_{n-1},\gamma_{n-1}\rangle$ due to the action of V and comes back to a state j in the ground state manifold (which can be different from i) at the n^{th} application of V. At $O(J)$, the term $\mathcal{H}_1 = J_1(S)\sum_{\langle ij\rangle}\sigma_i\sigma_j - \mathcal{E}_0$ is generated where $J_1(S) = JS^2$. When the temperature is low enough such that $T \ll J_1(S)$, the important low energy states are further restricted to the collinear states where each triangle has only one frustrated bond due to this $O(J)$ term.

These are just the ground states of the corresponding classical Ising antiferromagnet on the kagome and the triangular lattices. As mentioned earlier, this "minimally frustrated" ensemble of states has a residual entropy [4] of $0.502k_B$ ($0.323k_B$) per spin in the kagome (triangular) lattice case. Is this macroscopic degeneracy lifted at higher orders in J/D? At $O(J^2/D)$, the only possible diagonal process (where $i = j$ in $\langle j,\alpha_g|\mathcal{H}_n|i,\alpha_g\rangle$) is when V_o acts on an unfrustrated bond to move the system to a virtual excited state, and then acts on the same bond to make the system return to the "minimally frustrated" ground state manifold. However, since there are two unfrustrated bonds in each triangle, the number of such processes is independent of the particular state in the ensemble and no further degeneracy is lifted at $O(J^2/D)$.

However, the degeneracy is lifted by diagonal processes at $O(J^3/D^2)$. The relevant process is when V_o, V_d and V_o act on an unfrustrated bond in the given order. The only term that contributes when calculating $\langle i,\alpha_g|\mathcal{H}_3|i,\alpha_g\rangle$ is the first term in Eq

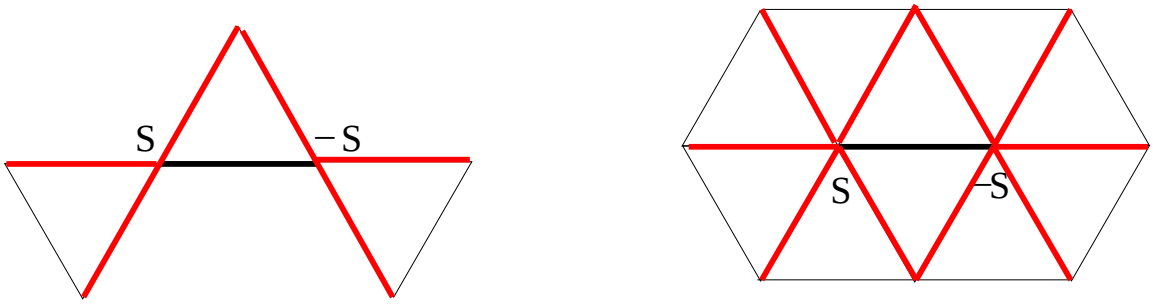

Figure 2.2: When V_o acts on an unfrustrated bond (shown as thick black bond) in the lattice (kagome or triangular), the exchange energy changes on that bond itself and on other bonds, shown in red, which share a site with that bond.

2.3. It can be immediately seen that $E_g - E_{k_1,\gamma_1} = -2D(2S-1)$ and $E_g - E_{k_2,\gamma_2} = -2D(2S-1)$. Similarly, $\langle i,\alpha_g|V_o|k_2,\gamma_2\rangle = \langle k_1,\gamma_1|V|i,\alpha_g\rangle = \lambda JS$. We need to then evaluate $\langle k_2,\gamma_2|V_d|k_1,\gamma_1\rangle$. For this, we note that since $V_d = (J\sum_{\langle ij\rangle} S_i^z S_j^z - \mathcal{E}_0)$, it equals the change in exchange energy when the spin $S_i^z = S$ is changed to $S_i^z = S-1$ and the other spin $S_j^z = -S$ is changed to $S_j^z = -S+1$ on an unfrustrated bond $\langle ij\rangle$ by an application of V_o. The exchange energy change equals $-JS(\sigma_i H_i + \sigma_j H_j) - J(2S-1)$ where the *exchange field* is defined as $H_i \equiv \sum_j \Gamma_{ij}\sigma_j$ with $\Gamma_{ij} = 1$ for nearest neighbours and zero otherwise (see Fig 2.2). From this, $\mathcal{H}_3$ can be calculated explictly and (ignoring a constant term) we obtain [5]

$$\mathcal{H}_3 = -\lambda^2 J_2(S) \sum_{\langle ij\rangle} \frac{1-\sigma_i\sigma_j}{2}(\sigma_i H_i + \sigma_j H_j) \tag{2.4}$$

where $J_2(S) = \frac{S^3J^3}{4D^2(2S-1)^2}$. There is another diagonal process that is possible at $O(J^3/D^2)$. Consider three bonds which lie on a single triangle. Then, for each triangle, there are 2 possible processes at third order where V_o acts on each of the three bonds once and gives the same state back at the end of the process (Fig 2.3). These processes do not, however, lift the degeneracy of minimally frustrated states since the total number of triangles with two $+S$ and one $-S$ or two $-S$ and one $+S$ is the same for any minimally frustrated state.

What about off-diagonal processes where we start from one minimally frustrated ground state and finally go into another? The most basic of such processes is when an unfrustrated bond with spins $+S$ and $-S$ is acted upon repeatedly with V_o to give $-S$ and $+S$ on that bond. The minimum order at which such off-diagonal processes contribute to the effective Hamiltonian is $O(J^{2S}/D^{2S-1})$, since a minimum of $2S$ applications of V_o is necessary for such a process. Also, such a process causes a transition from one minimally frustrated configuration to another only when the

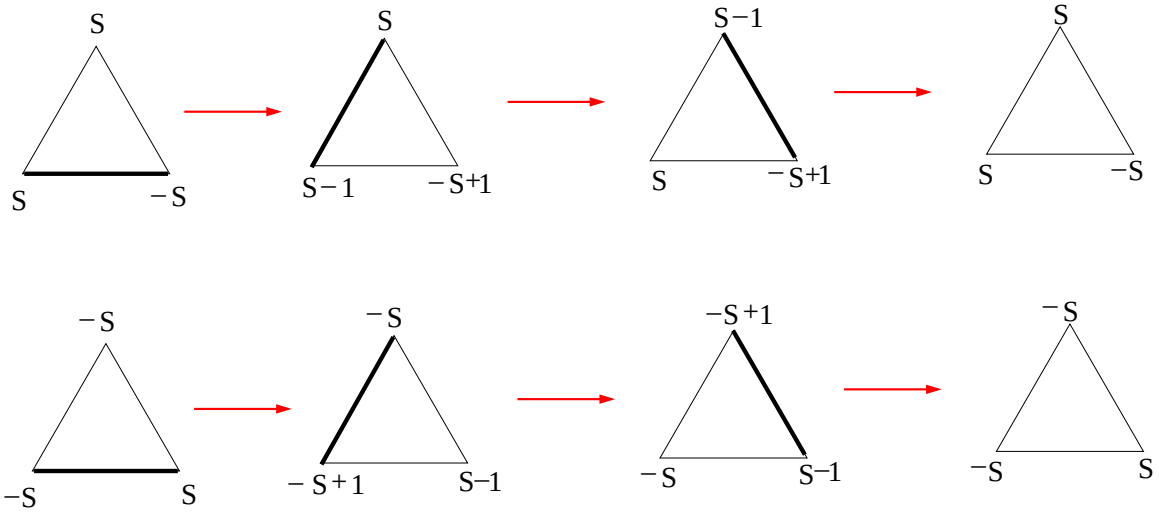

Figure 2.3: A three bond process on a triangle where the thick black line indicates the bond on which V_o acts. Such processes occur at $O(J^3/D^2)$ but do not lift any degeneracy.

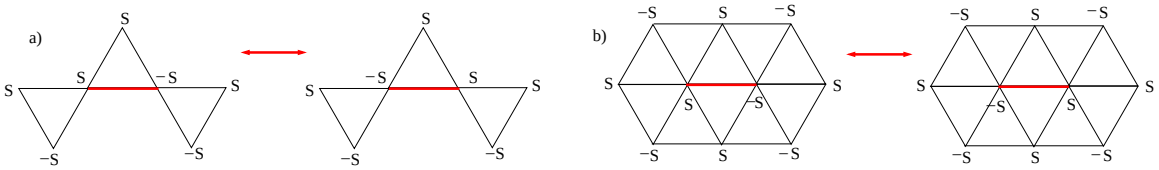

Figure 2.4: Basic off-diagonal processes where the spins on the unfrustrated bond (marked in red) are "flipped". The minimum order of such processes is $O(J^{2S}/D^{2S-1})$.

unfrustrated bond has a certain pattern of surrounding spins. On the kagome lattice, both the spins on the triangles connected to the unfrustrated bond and not belonging to the sites of that bond itself should be anti-aligned (Fig 2.4). On the triangular lattice, the 8 sites connected to the sites of the unfrustrated bonds should be anti-aligned with respect to each other (Fig 2.4). Thus, the off-diagonal processes are sub-dominant for any $S > 3/2$.

For any $S > 3/2$, to (leading) $O(J^3/D^2)$, the effective Hamiltonian (ignoring unimportant terms) is given by [5]:

$$\mathcal{H} = J_1(S) \sum_{\langle ij \rangle} \sigma_i \sigma_j - J_2(S) \sum_{\langle ij \rangle} \frac{1 - \sigma_i \sigma_j}{2} (\sigma_i H_i + \sigma_j H_j) \tag{2.5}$$

where $J_1(S) = JS^2$ and $J_2(S) = \frac{S^3 J^3}{4D^2(2S-1)^2}$.

For $S = 3/2$ the $J_2(S)$ and the off-diagonal term in the effective Hamiltonian $\mathcal{H}$ are both at $O(J^3/D^2)$, and $\mathcal{H}$ can be written in terms of (pseudo) spin $S = 1/2$

variables σ^z (where $S_i^z = 3\sigma_i^z$ in the low energy manifold) as:

$$\mathcal{H} = 9J \sum_{\langle ij \rangle} \sigma_i^z \sigma_j^z + \frac{9J^3}{32D^2} \sum_{\langle ij \rangle} (\sigma_i^+ \sigma_j^- + \sigma_i^- \sigma_j^+) - \frac{27J^3}{32D^2} \sum_{\langle ij \rangle} \frac{1 - 4\sigma_i^z \sigma_j^z}{2} (\sigma_i^z \tilde{H}_i + \sigma_j^z \tilde{H}_j) \quad (2.6)$$

where $\tilde{H}_i = \sum_j \Gamma_{ij} \sigma_j^z$. We do not, however, discuss this interesting case of $S = 3/2$ where the off-diagonal and diagonal terms that lift the degeneracy of the minimally frustrated states occur at the same order ($O(J^3/D^2)$).

2.2 Large-S expansion

We now analyze the problem using a large-S expansion procedure introduced by Hizi and Henley in Ref [6] and derive the effective Hamiltonian using this approach. In the large-S limit ($S \to \infty$), we had earlier seen that the ground state is collinear when $D > J$ for the kagome and when $D > 3J/2$ for the triangular case. A collinear state can be represented by associating an Ising variable σ_i with each site such that,

$$|\Psi\{\sigma_i\}\rangle = \prod_i |S_i^z = \sigma_i S\rangle \quad (2.7)$$

Since there is a large degeneracy of collinear ground states in the classical limit, it is useful to make the dependence of the Hamiltonian H (given in Eq 2.1) on the Ising pseudospins $\{\sigma_i\}$ explicit. This can be done by applying [6] the following unitary transformation:

$$U = \exp\left(i\pi \sum_i \frac{(1 - \sigma_i)}{2} S_i^x \right) \quad (2.8)$$

The operator effects a rotation about the x-axis in spin space only for the spins with $S_i^z = -S$. This interchanges the spin raising and lowering operators, and reverses the orientation of S_i^z on these sites. Thus, we get

$$|\Psi\{\sigma_i\}\rangle = U|\Psi_0\rangle \qquad \text{where} \qquad |\Psi_0\rangle = \prod_i |S_i^z = +S\rangle \quad (2.9)$$

To keep the physics invariant, we need to transform the Hamiltonian $H \rightarrow U^\dagger H U$. In the transformed basis, we get

$$\begin{aligned} H &= J\sum_{\langle ij\rangle}\sigma_i\sigma_j S_i^z S_j^z - D\sum_i (S_i^z)^2 \\ &+ \frac{J}{2}\sum_{\langle ij\rangle}\left(\frac{(1+\sigma_i\sigma_j)}{2}(S_i^+S_j^- + S_i^-S_j^+) + \frac{(1-\sigma_i\sigma_j)}{2}(S_i^+S_j^+ + S_i^-S_j^-)\right) \end{aligned} \quad (2.10)$$

To carry out the $1/S$ expansion, the spin variables are then represented in terms of Holstein-Primakoff bosons [7]:

$$\begin{aligned} S^+ &= (\sqrt{2S-n})b \\ S^- &= b^\dagger(\sqrt{2S-n}) \\ S^z &= S-n \end{aligned} \quad (2.11)$$

where $n = b^\dagger b$ and $[b, b^\dagger] = 1$. This representation is exact in the Hilbert subspace of $n \leq 2S$. The square-root function above can be expanded as a power series in $1/S$ if $\langle n\rangle \ll 2S$, where non-zero values of n represent spin fluctuations about the classical direction. At $1/S$, different classical ground states get different zero-point energies due to quantum fluctuations and states with lower zero-point energy are stabilized more.

We then write the transformed Hamiltonian (see Eq 2.10) in terms of the Holstein-Primakoff bosons. Carrying out this procedure to $O(S)$, we obtain

$$\begin{aligned} H &= -DS^2N + \frac{JS^2}{2}\sum_{ij}\Gamma_{ij}\sigma_i\sigma_j + 2DS\sum_i b_i^\dagger b_i - \frac{JS}{2}\sum_{ij}\Gamma_{ij}\sigma_i\sigma_j(b_i^\dagger b_i + b_j^\dagger b_j) \\ &+ \frac{JS}{2}\sum_{ij}\Gamma_{ij}\left(\frac{1+\sigma_i\sigma_j}{2}(b_i^\dagger b_j + b_i b_j^\dagger) + \frac{1-\sigma_i\sigma_j}{2}(b_i^\dagger b_j^\dagger + b_i b_j)\right) \end{aligned} \quad (2.12)$$

where $\Gamma_{ij} = 1$ if i, j are nearest neighbours on the lattice and zero otherwise. The $O(S^2)$ term enforces the minimum frustation condition on each triangle in the set of collinear states. Now let us calculate the zero-point energy due to quantum fluctuations which appear at $O(S)$. The $O(S)$ part of H is a quadratic and hermitian operator of bosonic variables, so it can be represented as decoupled harmonic oscillators in some "good" basis. Since there are N sites, there are N different decoupled oscillators and the collinear states where the sum of their zero-point energies ($\sum_i \frac{\omega_i}{2}$) is minimum are stabilized the most at $O(S)$ by quantum fluctuations.

For this calculation, we proceed in the following manner. We first evaluate the

equations of motion for b_k (in the Heisenberg representation). We use $\alpha = \frac{J}{2D}$ for notational convenience (the Einstein summation convention where repeated indices are summed over is used below).

$$\begin{aligned}\frac{db_k}{dt} &= -i[b_k, H] \\ &= -i(2SD)\left(\delta_{kl}b_l - \alpha\Gamma_{jl}\sigma_j\sigma_l\delta_{kl}b_l + \alpha\Gamma_{kl}\frac{1+\sigma_k\sigma_l}{2}b_l + \alpha\Gamma_{kl}\frac{1-\sigma_k\sigma_l}{2}b_l^\dagger\right) \quad (2.13)\end{aligned}$$

The hermitian conjugate of the above equation reads

$$\frac{db_k^\dagger}{dt} = i(2SD)\left(\delta_{kl}b_l^\dagger - \alpha\Gamma_{jl}\sigma_j\sigma_l\delta_{kl}b_l^\dagger + \alpha\Gamma_{kl}\frac{1+\sigma_k\sigma_l}{2}b_l^\dagger + \alpha\Gamma_{kl}\frac{1-\sigma_k\sigma_l}{2}b_l\right) \quad (2.14)$$

From the above two equations, we immediately see that

$$\begin{aligned}\frac{d}{dt}(b_i + b_i^\dagger) &= -i(2SD)(\delta_{ij} - \alpha\sigma_i H_i\delta_{ij} + \alpha\Gamma_{ij}\sigma_i\sigma_j)(b_j - b_j^\dagger) \\ \frac{d}{dt}(b_j - b_j^\dagger) &= -i(2SD)(\delta_{jk} - \alpha\sigma_j H_j\delta_{jk} + \alpha\Gamma_{jk})(b_k + b_k^\dagger) \quad (2.15)\end{aligned}$$

which gives

$$\begin{aligned}\frac{d^2}{dt^2}(b_i + b_i^\dagger) &= -(2SD)(\delta_{ik} - \alpha[2\sigma_i H_i\delta_{ik} - \Gamma_{ik} - \sigma_i\Gamma_{ik}\sigma_k] \\ &+ \alpha^2[H_i^2\delta_{ik} - \sigma_i H_i\Gamma_{ik} - \sigma_i\Gamma_{ik}H_k + \sigma_i\Gamma_{ij}\sigma_j\Gamma_{jk}])(b_k + b_k^\dagger) \quad (2.16)\end{aligned}$$

where $H_i = \Gamma_{ij}\sigma_j$ is the local field acting on the spin at site i. From this, we see that the zero-point energy $\mathcal{H}_{eff}(\{\sigma_i\})$ in a given collinear spin configuration $\{\sigma_i\}$ is given by

$$\mathcal{H}_{eff}(\{\sigma_i\}) = (2SD)\frac{1}{2}Tr\sqrt{M} \quad (2.17)$$

where the matrix M is defined as

$$M_{ik} = \delta_{ik} - \alpha[2\sigma_i H_i\delta_{ik} - \Gamma_{ik} - \sigma_i\Gamma_{ik}\sigma_k] + \alpha^2[H_i^2\delta_{ik} - \sigma_i H_i\Gamma_{ik} - \sigma_i\Gamma_{ik}H_k + \sigma_i\Gamma_{ij}\sigma_j\Gamma_{jk}] \quad (2.18)$$

The square root in Eq 2.17 can be Taylor series expanded in α and the effective Hamiltonian that encodes the dependence of the zero point energy on the spin configuration can be calculated perturbatively in α. The degeneracy of the minimally

frustrated collinear states is first lifted at $\mathcal{O}(\alpha^3)$. To see that, we expand the trace as

$$Tr(\sqrt{1-\alpha X_1+\alpha^2 X_2}) = Tr(1-\frac{1}{2}\alpha X_1+\frac{1}{2}\alpha^2 X_2-\frac{1}{8}\alpha^2 X_1^2+\frac{1}{4}\alpha^3 X_1X_2-\frac{1}{16}\alpha^3 X_1^3+\dots) \tag{2.19}$$

where

$$\begin{aligned}(X_1)_{ik} &= 2\sigma_i H_i\delta_{ik}-\Gamma_{ik}-\sigma_i\Gamma_{ik}\sigma_k \\ (X_2)_{ik} &= H_i^2\delta_{ik}-\sigma_i H_i\Gamma_{ik}-\sigma_i\Gamma_{ik}H_k+\sigma_i\Gamma_{ij}\sigma_j\Gamma_{jk}\end{aligned} \tag{2.20}$$

It is easy to see that terms in the trace till $\mathcal{O}(\alpha^2)$ do not lift the degeneracy of the minimally frustrated states. However, the situation is different at $\mathcal{O}(\alpha^3)$ and the degeneracy does get lifted at this order due to quantum fluctuations. At $\mathcal{O}(\alpha^3)$, there are two types of terms; from $\frac{1}{4}\alpha^3 X_1X_2$ and from $-\frac{1}{16}\alpha^3 X_1^3$.

$$\begin{aligned}Tr(\frac{1}{4}\alpha^3 X_1X_2) &= \frac{1}{2}\alpha^3\sigma_i H_i^3+\frac{3}{4}\alpha^3 H_i^2+\frac{1}{4}\alpha^3\sigma_i\Gamma_{ik}H_k \\ Tr(-\frac{1}{16}\alpha^3 X_1^3) &= -\frac{1}{2}\alpha^3\sigma_i H_i^3-\frac{1}{2}\alpha^3 H_i^2-\frac{1}{4}\alpha^3\sigma_i\Gamma_{ik}H_k\end{aligned} \tag{2.21}$$

Thus the zero-point energy $\mathcal{H}_{eff}$ comes out to be

$$\begin{aligned}\mathcal{H}_{eff} &= (2SD)\frac{1}{8}\alpha^3\sum_i H_i^2 \\ &= (2SD)\frac{1}{8}\alpha^3\sum_i(\sigma_i H_i)^2 \\ &= \frac{J^3S}{32D^2}\sum_i(\sigma_i H_i)^2\end{aligned} \tag{2.22}$$

This effective Hamiltonian obtained from large-S looks very different from the one that we obtained by doing perturbation in J/D. We will see in the next chapter that both the approaches do give identical results in the large S limit.

References

[1] S. Miyashita Magnetic properties of Ising-like Heisenberg antiferromagnets on the triangular lattice. *J. Phys. Soc. Jpn.* **55**, 3605 (1986).

[2] P. E. Melchy and M. E. Zhitomirsky. Interplay of anisotropy and frustration: triple transitions in a triangular-lattice antiferromagnet. *preprint* axXiv:0812.3574 (2008).

[3] H. Primas. Generalized perturbation theory in operator form. *Rev. Mod. Phys.* **35**, 710 (1963).

[4] R. Liebmann. Statistical mechanics of periodic frustrated Ising systems. *Springer*, Berlin (1986).

[5] A. Sen, F. Wang, K. Damle and R. Moessner. Triangular and kagome antiferromagnets with a strong easy-axis anisotropy. *Phys. Rev. Lett.* **102**, 227001 (2009).

[6] U. Hizi and C. L. Henley. Effective hamiltonian for the pyrochlore antiferromagnet: semiclassical derivation and degeneracy. *Phys. Rev. B* **73**, 054403 (2006).

[7] A. Auerbach. Interacting electrons and quantum magnetism. *Springer-Verlag*, New York (1994).

Chapter 3

Zero field results

In the previous chapter, we derived the effective Hamiltonian $\mathcal{H}$ that encodes the splitting of the degenerate Ising subspace of collinear spin states ($S_i^z = \sigma_i S$) that are picked by the leading easy axis anisotropy D when the anisotropy dominates over J (see Eq 2.1) for any $S > 3/2$ on the kagome and the triangular lattices:

$$\mathcal{H} = J_1(S) \sum_{\langle ij \rangle} \sigma_i \sigma_j - J_2(S) \sum_{\langle ij \rangle} \frac{1 - \sigma_i \sigma_j}{2} (\sigma_i H_i + \sigma_j H_j) \tag{3.1}$$

where $J_1(S) = JS^2$ and $J_2(S) = \frac{S^3 J^3}{4D^2(2S-1)^2}$.

From the derivation of the effective Hamiltonian in the earlier chapter, it is clear that (off-diagonal) pseudo-spin exchange terms, representing real transitions between different minimally frustrated states, dominate the low temperature physics for the case $S = 1$. However, such terms are sub-dominant compared to (diagonal) virtual quantum transitions for all $S > 3/2$ since the off-diagonal term is $O(J^{2S}/D^{2S-1})$. This makes the physics of the $S > 3/2$ magnets very different from the $S = 1$ case. From an earlier study [1], it is known that the $S = 1$ kagome antiferromagnet with strong easy axis anisotropy orderes into a spin nematic state with $\langle (S^+)^2 \rangle \neq 0$ (but $\langle \vec{S} \rangle = 0$) which breaks spin rotation symmetry. On the triangular lattice with $S = 1$, a nematic ordering which co-exists with a spin density wave ordering of S^z at the three sublattice wave-vector is predicted at low temperature.

In this chapter, we discuss how the $J_2(S)$ generated due to virtual quantum fluctuations change the physics at sufficiently low temperatures for the $S > 3/2$ case. A schematic phase diagram (Fig 3.1) is given for the kagome and triangular lattice magnets when $D \gg J$. Most of the results presented here have been previously published in Ref [2].

The results on the kagome lattice are expected to be of direct experimental rele-

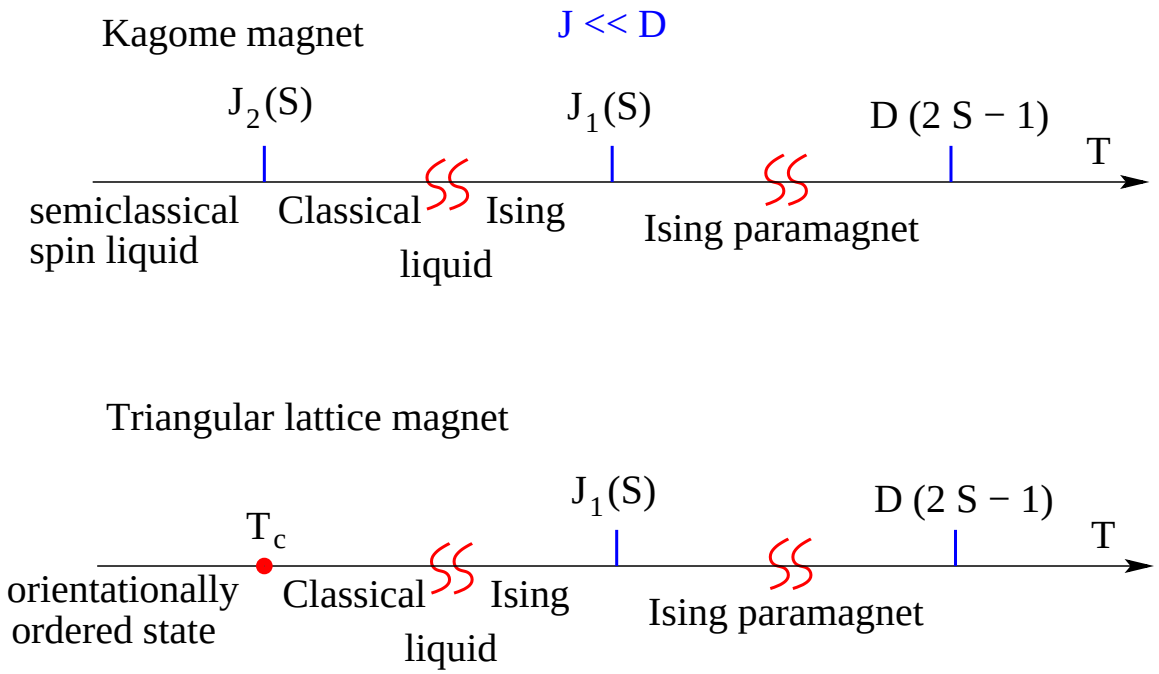

Figure 3.1: Schematic phase diagram of the kagome and triangular lattice antiferromagnets when $D \gg J$.

vance for the quasi two-dimensional kagome antiferromagnet Nd-langasite that does not exhibit any magnetic order down to 50 mK [3, 4], although the Nd^{3+} 'spins' (that carry a total angular momentum quantum number $\mathbf{J}_{\rm ion} = 9/2$) interact with nearest neighbours on the kagome lattice with an isotropic antiferromagnetic exchange coupling $J \sim 1.5K$ in the presence of a strong single-ion anisotropy term $D \sim 10K$ [5] that picks out the crytallographic c axis as the common easy axis of all the spins [6].

3.1 Classical Ising regime

For temperatures T well above the exchange energy scale $J_1(S)$ but lower than the anisotropy energy scale $D(2S-1)$, the behaviour of the system will be that of the high temperature paramagnetic regime of the classical Ising model on the respective lattices. As the temperature is lowered, the exchange begins to make itself felt, and the system crosses over to an intermediate temperature regime $J_2(S) \ll T \ll J_1(S)$ whose physics is controlled by the ground states of the classical Ising antiferromagnet on the kagome and the triangular lattices. In these ground states each triangle has exactly one frustrated bond connecting a pair of aligned spins. This ensemble of ground states has a macroscopic degeneracy on both the lattices. This macroscopic entropy ensemble of ground states can be conveniently represented by dimer configurations on

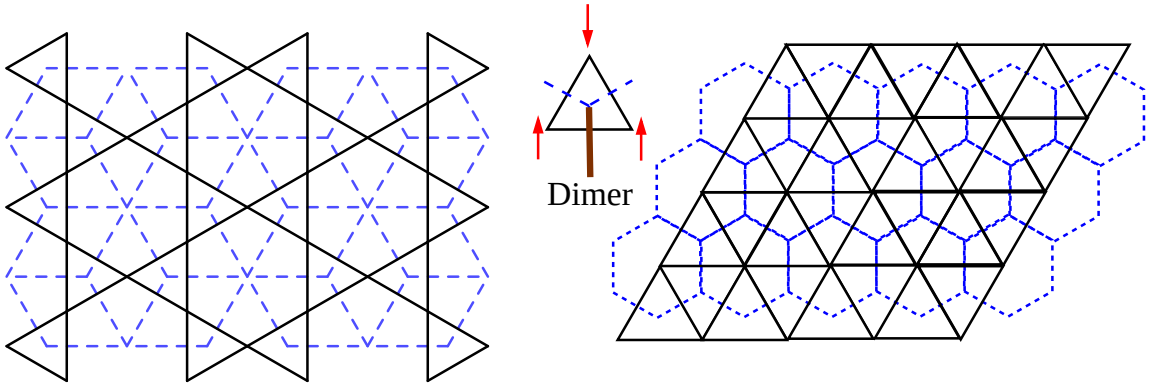

Figure 3.2: The dual lattices of the kagome lattice (dice lattice) and the triangular lattice (honeycomb lattice) shown in blue while the direct lattices are in black. The construction of a dimer on the dual lattice is also shown.

the respective dual lattices, and this dimer representation turns out to be useful for analyzing the $J_2(S)$ term. The dual lattice has a unique bond intersecting each bond of the direct lattice. The dual of the kagome lattice is the dice lattice and that of the triangular lattice is the honeycomb lattice (see Fig 3.2). If each frustrated bond is visualized by a dimer on the corresponding bond on the dual lattice (Fig 3.2), then every dimer covering determines a spin configuration upto a global spin flip. How does the local constraint of each triangle having only one frustrated bond translate in the dimer langauge? The dice lattice has two kinds of sites–three coordinated and six coordinated. Each three-coordinated site has one and only one dimer touching it because each triangle on the kagome lattice has only one frustrated bond. The six-coordinated sites have a soft constraint that an even number $(0, 2, 4, 6)$ of dimers touch them. This constraint comes because each such site is surrounded by a closed (hexagonal) loop of six sites on the direct kagome lattice. Going around the loop once gives the same spin as one started with, so the number of times the spin orientation changes must be even. This implies that the number of dimers touching the six-coordinated sites is even. The ground state constraint on the triangular lattice implies that each site on the honeycomb lattice has one and only one dimer touching it (this is an example of a *hard-core* dimer model).

The Ising antiferromagnet on both the kagome and the triangular lattices are examples of spin liquids where there is no spin order in the system [7] all the way down to $T = 0$. The spin correlations are extremely short-ranged on the kagome lattice. On the triangular lattice, spin correlations at the three-sublattice wave vector build up at low temperature, but there is no long range order. This intermediate temperature regime $J_2(S) \ll T \ll J_1(S)$ in both cases is thus a classical cooperative

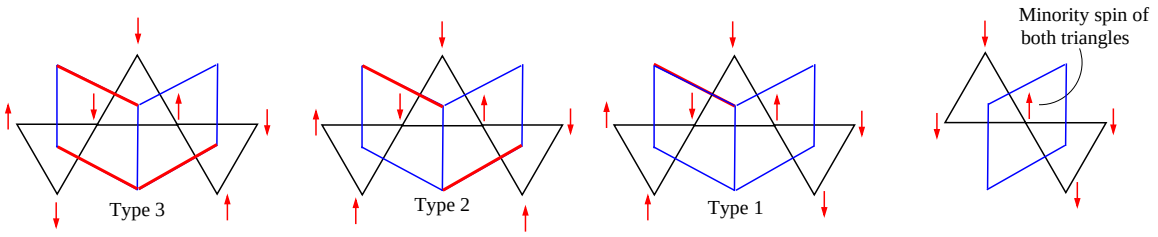

Figure 3.3: Double-plaquettes on the dice lattice corresponding to unfrustrated bonds can be of three types depending on the number of dimers on their perimeter. Also shown is a spin which is a minority spin of both the triangles to which it belongs.

Ising paramagnet.

To understand the behaviour at still lower temperatures, we need to focus on the effect of the $J_2(S)$ in the ground state manifold of minimally frustrated states on both the lattices.

3.2 Kagome lattice

When $D \gg J$, we also have $J_1(S) \gg J_2(S)$. We show below that the minimally frustrated spin configurations that also minimize the multi-spin interaction $J_2(S)$ satisfy the criterion that *no spin be the minority spin of both triangles to which it belongs*. From the definition, it is clear that the product $\sigma_i\sigma_j$ on a bond equals $2m-1$ where m is the dimer number ($m = 0, 1$) on the corresponding bond of the dual dice lattice. Now, consider any unfrustrated bond on the kagome lattice. Then, the quantity $\sigma_i H_i + \sigma_j H_j$ for an unfrustrated bond equals $2(n-z)$ where n is the number of dimers on the perimeter of the double plaquette where the common edge of the two plaquettes intersects that unfrustrated bond (Fig 3.3) (and z is the coordination number of the direct lattice). The number n of dimers on the perimeter can take values $1, 2, 3$. Then,

$$-J_2(S)\sum_{\langle ij\rangle}\left(\frac{1-\sigma_i\sigma_j}{2}\right)(\sigma_i H_i + \sigma_j H_j) = -J_2(S)N_{uf}\sum_{n=1}^{3}(2n-2z)f_n \qquad (3.2)$$

where N_{uf} denotes the number of unfrustrated bonds and f_n is the normalized fraction of unfrustrated bonds of the type n, or equivalently fraction of double plaquettes (with no dimer on the edge shared by the two plaquettes) having n dimers on their perimeter(Fig 3.3). Ignoring an unimportant constant, we need to simplify

$$-2J_2(S)N_{uf}\sum_{n=1}^{3} nf_n \tag{3.3}$$

$N_{uf}\sum_{n=1}^{3} nf_n$ just counts the total number of dimers on the perimeters of all double-plaquettes corresponding to unfrustrated bonds. Now, every single plaquette with n dimers is part of $4-n$ such double plaquettes corresponding to unfrustrated bonds, and these n dimers will therefore contribute with multiplicity $4-n$ to the total number of dimers on the perimeters of all such double plaquettes. Denoting the fraction of single plaquettes with n dimers on them to be $g_n(n=0,1,2)$ and the total number of such plaquettes on the dice lattice to be N_p, we get

$$N_{uf}\sum_{n=1}^{3} nf_n = N_p\sum_{n=0}^{2} n(4-n)g_n \tag{3.4}$$

Ignoring a constant, we thus find that the $J_2(S)$ term projected onto the ensemble of minimally frustrated states, can be written as (in dimer language)

$$H_D = 2J_2(S)\sum_{P} n^2|nP\rangle\langle nP| \tag{3.5}$$

where $|nP\rangle$ denotes elementary plaquettes with n dimers on their perimeter. Noting that each dimer is on the perimeter of two elementary plaquettes, we obtain $\sum_{n=0}^{2} ng_n = 4/3$. Using this, alongwith $\sum_{n=0}^{2} g_n = 1$, we immediately get that

$$\sum_{n=0}^{2} n^2 g_n = 2 + 2g_0 \tag{3.6}$$

which is minimized when $g_0 = 0$ (which fixes $g_1 = 2/3$ and $g_2 = 1/3$). Thus, the dimer coverings that minimize H_D (Eq 3.5) are the ones where $g_0 = 0$. This condition, when translated to spin language, implies that no spin be the minority spin of both triangles to which it belongs.

We have investigated the set of minimally frustrated configurations that satisfies this minority spin rule. It is possible to construct a large number of such states (i.e. with macroscopic degeneracy) satisfying this rule, and related to each other by local spin flips. One such subset is shown in Fig 3.4. This construction immediately provides a lower bound of $k_B\ln(2)/6$ per site on the entropy of the ground states of H_D. The question then arises whether the correlations at $T \to 0$ limit remain short-

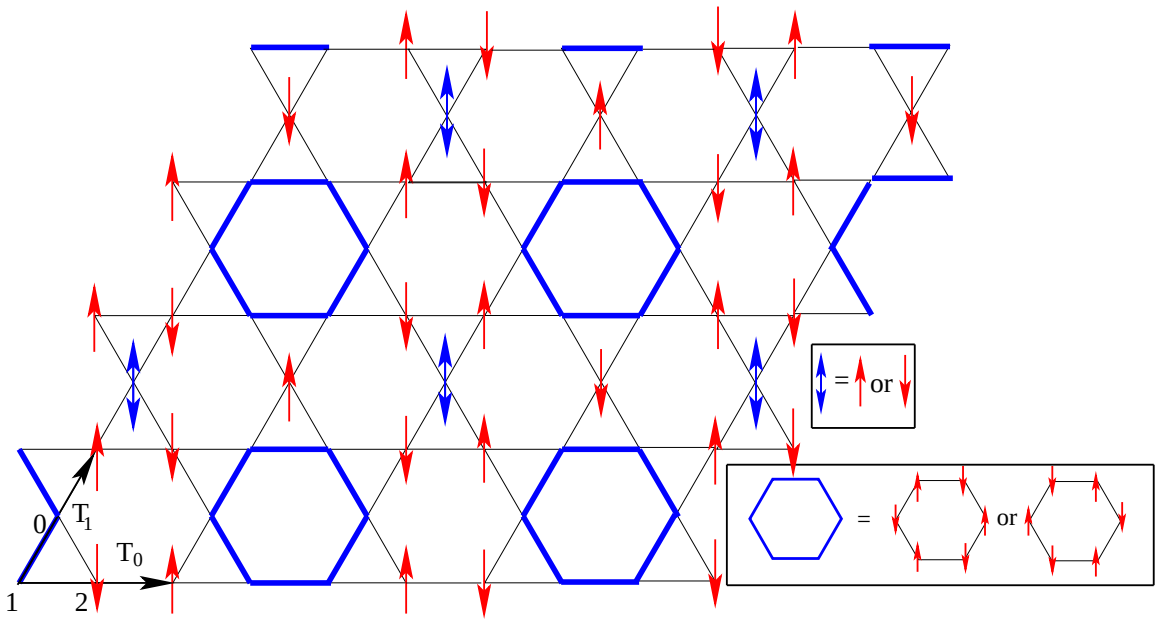

Figure 3.4: A class of partially ordered states with macroscopic entropy that simultaneously minimize $J_1(S)$ and $J_2(S)$.

ranged, or whether there at ordering at some low enough temperature, and below we address this question numerically. We take $J_1(S) \to \infty$ and measure temperature in units of $2J_2(S)$.

We developed a new loop algorithm [8] that can handle the non-trivial Boltzmann weights associated with the dimer potential H_D (Eq 3.5) as well as keep track of the different constraints on the three- and the six-coordinated sites of the dice lattice. This algorithm is a generalization of the usual hard-core dimer model loop algorithm [9, 10] and we describe it in Appendix A. Below, we discuss our findings from the numerics.

From numerical simulations on $L_x = L_y = L$ (where $3L^2$ is the number of sites on the kagome lattice) using this algorithm, where L ranges from 10 to 60, we see no evidence at all of any phase transition as we lower the temperature to access the $T \to 0$ limit. This is evident from the behaviour of the specific heat per site (Fig 3.5), which converges very quickly with system size, and does not show any singularity in the thermodynamic limit. Since the system is a spin liquid when $T \to \infty$, this indicates that the $T \to 0$ state is a spin liquid as well. Another quantity that is sensitive to the appearance of long-range spin order is the spin structure factor (that can be probed in neutron scattering experiments) $S(\vec{q}) = \frac{1}{N}|\sum_i \vec{S}_i \exp(i\vec{q}\cdot\vec{r})|^2$. If $S(\vec{q})$ is $O(1)$ for all wave-vectors $\vec{q}$, then this implies that the system has only short range magnetic order. However, if $S(\vec{q})$ is $O(N)$ for some $\vec{q}_0$, this means there is long range magnetic order in the system at the wave-vector $\vec{q}_0$. We monitor $S(\vec{q}) =$

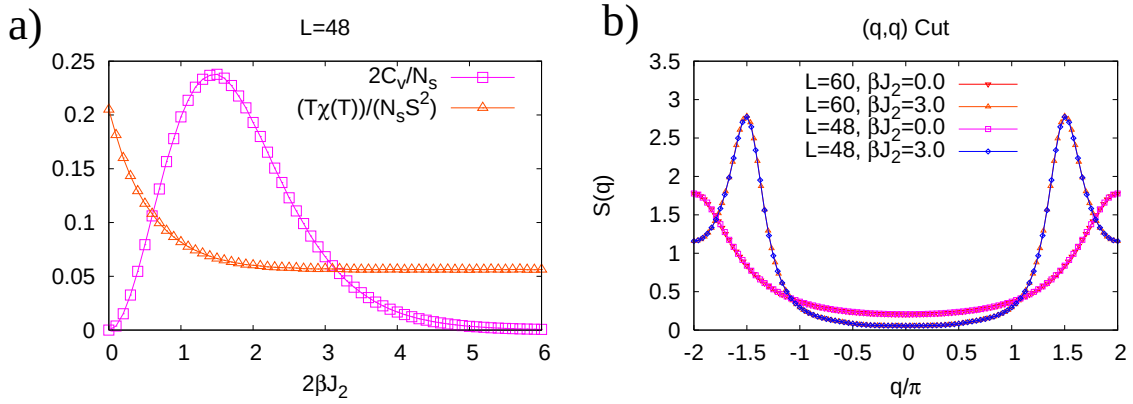

Figure 3.5: (a)Specific heat C_v and the uniform susceptibility χ in the crossover regime. (b) The $q_x = q_y$ cut for $S(\vec{q})$ is shown fir two different system sizes ($L = 48, 60$) at two different temperatures ($\beta J_2(S) = 0.0, 3.0$).

$|S_0(\vec{q})\exp(iq_y/2) + S_1(\vec{q}) + S_2(\vec{q})\exp(iq_x/2)|^2$ in our simulations where $S_\alpha(\vec{q})$ is the Fourier transform of the spin density on sublattice α of the kagome lattice and $q_x(q_y)$ refers to the projection of $\vec{q}$ on to lattice directions $T_0(T_1)$ (see Fig 3.4 for notation) measured in units of inverse Bravais lattice spacing. From Fig 3.5, we see that $S(\vec{q})$ converges with increasing system size for all $\vec{q}$ down to the lowest temperatures and does not show any $O(N)$ divergence at any wave-vector

Although there is no phase transition, the low temperature liquid is quite different from the classical cooperative Ising paramagnet. This crossover to a distinct semiclassical spin-liquid regime is evident in the temperature dependence of the specific heat per site, and the magnetization fluctuations $T\chi$ (Fig 3.5). The C_v versus T curve shows a distinct but non-singular peak at $T^* \approx 1.3J_2(S)$ that reflects the loss of entropy during this crossover from the cooperative Ising paramagnet to the low temperature limit in which the configurations sampled predominantly obey the minimum $J_2(S)$ constraint (The C_v/T data give an estimate of $0.32k_B$ per spin for the residual entropy of such states). In addition, this crossover is also characterized by a change in the magnetization fluctuations as reflected in the value of $T\chi$. Also, the spin structure factor evolves continuously (Fig 3.6) from being quite featureless in the classical cooperative Ising regime $T^* \ll T \ll J_1(S)$ to developing characteristic cresents of high intensity diffuse scattering in the low temperature semiclassical spin liquid regime $T \ll T^*$. The precursors of these features are already present at $T \sim 2T^*$.

Experiments on Nd-langasite: As mentioned earlier, recent experiments on the $J = 9/2$ easy axis Kagome antiferromagnet Nd-Langasite have seen a liquid-like state [3, 4] with fluctuating moments and no long range order down to $50mK$. From the

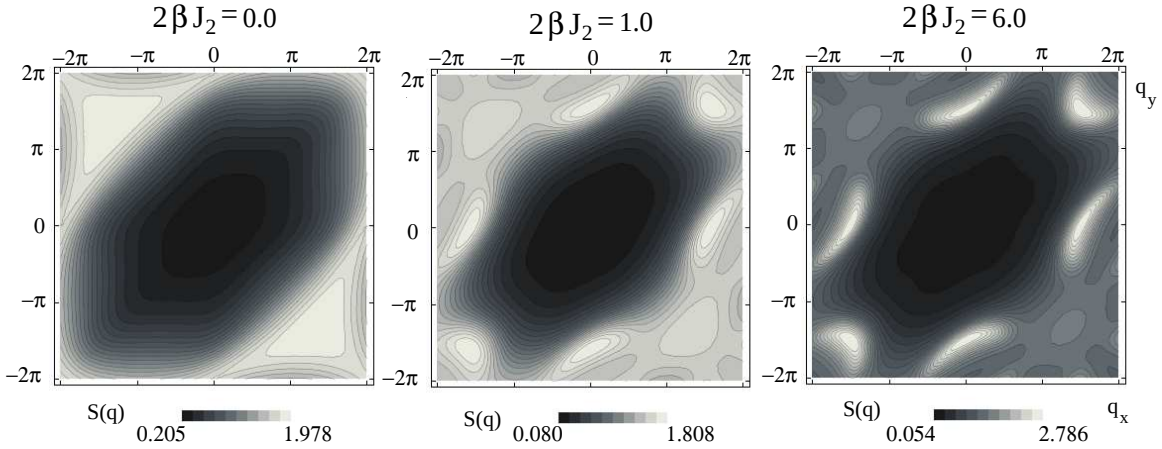

Figure 3.6: Spin structure factor $S(\vec{q})$ shown for three different temperatures, showing croosover to semiclassical spin liquid regime.

estimated values [5] of the exchange constant and the single-ion anisotropy ($J \sim 1.5K$, $D \sim 10K$), it is clear that the predicted crossover from a classical Ising spin liquid to a semiclassical spin liquid only occurs for temperatures significantly below $50mK$ (T^* can be estimated to be approximately $16mK$).

We therefore expect a simple classical Ising spin liquid description to work fairly well for the bulk of the temperature range studied in the recent low temperature experiments. Since correlations in the classical Ising spin liquid are extremely short-ranged and featureless, this is consistent with the fact that data from recent neutron scattering experiments (which probe the spin structure factor) show nearly featureless diffuse scattering that can be fit quite well to a model of spin correlations in which nearest neighbour spins are correlated, but there are no correlations of spins further away from each other. Thus still lower temperatures are needed to see this crossover. Another possible avenue for exploring this crossover in greater detail would involve identification of other easy axis Kagome antiferromagnets in which the separation of scales between J and D is not so large (or the overall scale of both J and D is somewhat larger) so that the crossover to the semiclassical spin liquid regime occurs at more easily accessible, higher temperatures.

3.3 Triangular lattice

We now analyze the effect of the $J_2(S)$ term on the low-temperature physics of easy axis triangular lattice antiferromagnets. As explained before, the minimally frustrated states of the triangular lattice (which become dominant when $T \ll J_1(S)$) can be represented as dimer coverings on the dual honeycomb lattice, where each site of the

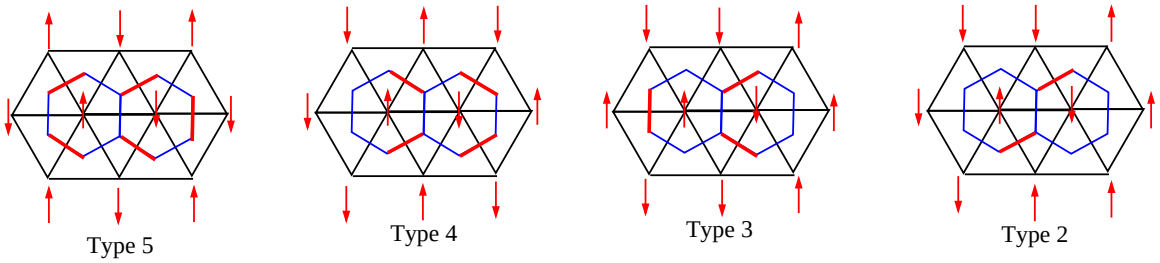

Figure 3.7: Double plaquettes on the honeycomb lattice corresponding to unfrustrated bonds can be of four types depending on the number of dimers on their perimeter.

honeycomb lattice has precisely one dimer touching it. The complicated multi-spin interaction $J_2(S)$ can again be simplified by using the dimer representation. As in the kagome lattice case, the $J_2(S)$ term, projected into the ensemble of minimally frustrated states (i.e., dimer coverings on the dual honeycomb lattice), can be written as (ignoring unimportant constants)

$$-2J_2(S)N_{uf}\sum_{n=2}^{5} nf_n \tag{3.7}$$

where N_{uf} denotes the number of unfrustrated bonds and f_n is the normalized fraction of unfrustrated bonds of the type n, or equivalently fraction of double plaquettes (with no dimer on the edge shared by the two plaquettes) having n dimers on their perimeter (Fig 3.7). $N_{uf}\sum_{n=2}^{5} nf_n$ just counts the total number of dimers on the perimeters of all double-plaquettes corresponding to unfrustrated bonds. Now, every single plaquette with n dimers is part of $6-n$ such double plaquettes corresponding to unfrustrated bonds, these n dimers therefore contribute with multiplicity $6-n$ to the total number of dimers on the perimeters of all such double plaquettes. Denoting the fraction of single plaquettes with n dimers on them to be $g_n(n=0,1,2,3)$ and the total number of such plaquettes on the honeycomb lattice to be N_p, we get

$$N_{uf}\sum_{n=1}^{5} nf_n = N_p\sum_{n=0}^{3} n(6-n)g_n \tag{3.8}$$

Ignoring a constant term, the $J_2(S)$ term can thus be written in the following manner in dimer langauge:

$$H_D = 2J_2(S)\sum_{P} n^2|nP\rangle\langle nP| \tag{3.9}$$

where $|nP\rangle$ denotes elementary plaquettes with n dimers on their perimeter. Noting that each dimer is on the perimeter of two elementary plaquettes, we get that $\sum_{n=0}^{3} n g_n = 2$. This means that the average number of dimers on the perimeter of a hexagon is 2. From this, it is clear that the minimum of H_D is achieved for all configurations with $g_2 = 1$, i.e. for configurations with all hexagons having precisely two dimers on their perimeter.

Dimer coverings with all hexagons having two dimers on their perimeter can be divided into three classes in the following manner. Any dimer on the honeycomb lattice is in one of three possible directions. Configuration with $g_2 = 1$ only includes dimers of at most two different orientations, and all bonds of one orientation are unoccupied. To prove this statement, we note that any dimer configuration can be obtained from a reference dimer state through dimer moves that involve *loops* of dimers and adjacent empty bonds [11], where the dimer move means that the dimers are shifted to the empty bonds. These loops can be simply constructed by placing the reference dimer state on the required dimer state and noting the loops where a dimer of the reference state is followed by an adjacent bond containing a dimer of the required state. Due to the hard-core constraint on dimers, no two loops can touch each other. Also, these loops are either closed or system spanning *open* loops for an infinite system. Take a reference state in which $g_2 = 1$ and all the dimers are placed in bonds of a single orientation and bonds in the remaining two directions are empty. Then it is easy to see that all the loops are system spanning loops (Fig 3.8). The loops can be categorized into two classes (see Fig 3.8): one in which only one of the remaining directions is used to construct the loop (call type I), and another in which both the remaining directions are used up in the loop construction (call type II). Whenever bonds of both the remaining directions are used to make a loop, the hexagon containing those two bonds and the adjacent hexagon which contains the dimer touching the two bonds no longer have exactly two dimers on their perimeter after the dimer move on the loop is made. Thus, these type II loop moves are not allowed when considering states with $g_2 = 1$ and only type I loops are permitted. Moreover, two type I loops which use up two different directions necessarily intersect each other which violates the dimer constraint. Thus, all type I loops need to be "parallel" to each other which implies that all bonds of one particular orientation stay unoccupied when $g_2 = 1$.

These states thus break rotational symmetry in real space. All dimer states where $g_2 = 1$ and bonds of one orientation necessarily have no dimers can be generated by placing dimers in one of the two possible ways in parallel rows (made by using the remaining two directions), where the dimer state on each row can be changed

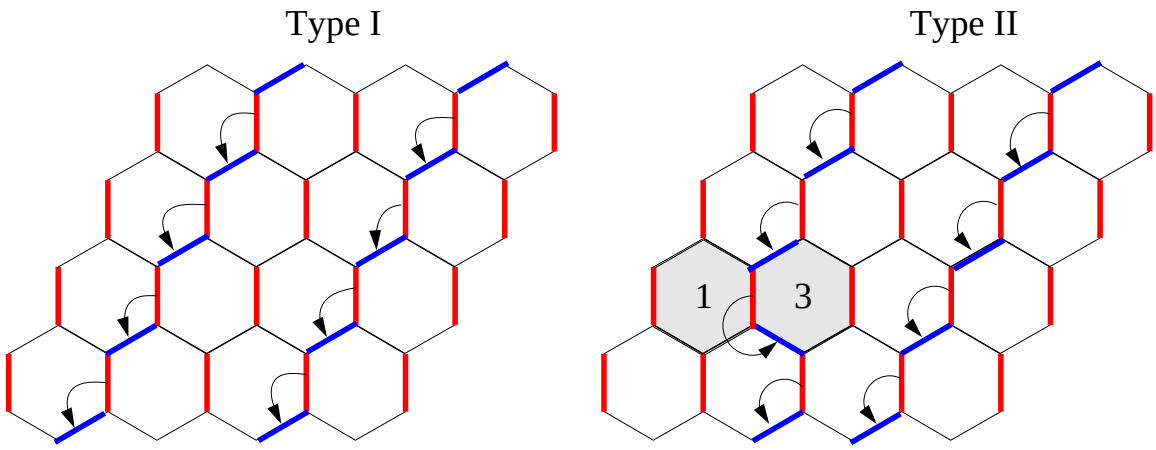

Figure 3.8: Loops containing dimers and adjacent empty bonds shown for a reference state with $g_2 = 1$ (the dimers are represented in red). All the loops are system spanning. The loops are of two types–Type I loops do not lead to any *defect* hexagons (where the perimeter does not have two dimers) while Type II loops necessarily lead to such defect hexagons.

independently (see Fig 3.9). In the spin langauge, the Ising pseudospins are antiferromagnetically arranged in parallel rows oriented along one of the three principle directions of the triangular lattice which is spontaneously chosen (Fig 3.10). The spin state of each antiferromagnetic row can be any one of the two possibilities (related by a spin flip). A Z_3 orientational order parameter to characterize this symmetry breaking can be defined in the following manner as

$$\Phi = \sum_p -B_p \exp(2p\pi i/3) \tag{3.10}$$

where B_p denotes the average of the Ising exchange energy $\sigma_i\sigma_j$ on all the links $\langle ij\rangle$ of the p^{th} orientation ($p = 0, 1, 2$) on the triangular lattice. Note the the $U(1)$ spin rotation symmetry of the Hamiltonian is unbroken for collinear states.

We explictly check this symmetry breaking by performing simulations of the corresponding interacting dimer model (H_D in Eq 3.9) using the loop update algorithm of hard-core dimer models in Refs [9, 10]. The simulations were done for $N = L^2$ systems where L ranged from 18 to 36. We find that below a critical temperature $T_c \approx 1.67 J_2(S)$ (Fig 3.11), the system orders into the orientationally ordered state described above, in which the mean Ising exchange energy on a link depends on its orientation, but not its position. From the double peak nature of the histogram of the order parameter at the transition (Fig 3.11), we see that the transition has a first order character. In such an orientationally ordered state, the Ising pseudospins are antiferromagnetically arranged in parallel rows oriented along one of the three

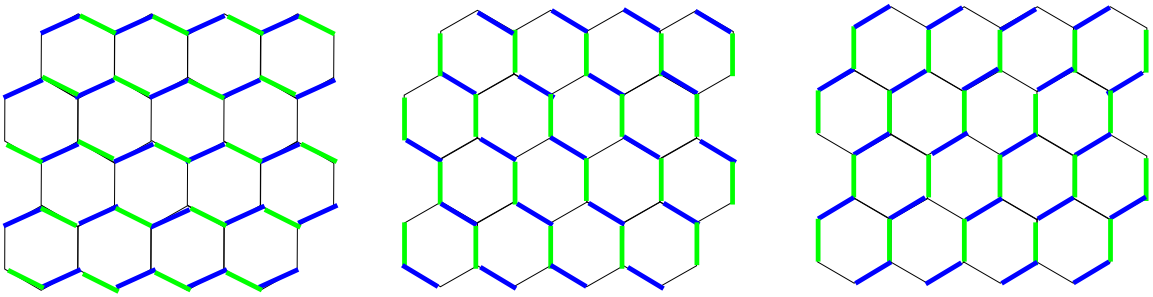

Figure 3.9: Dimer states with $g_2 = 1$ and bonds of one orientation having no dimers can be generated by choosing the dimer state in the rows made up using the remaining two orientations independently. Each row has two possibilities: either the dimers lie on the blue bonds or on the green ones.

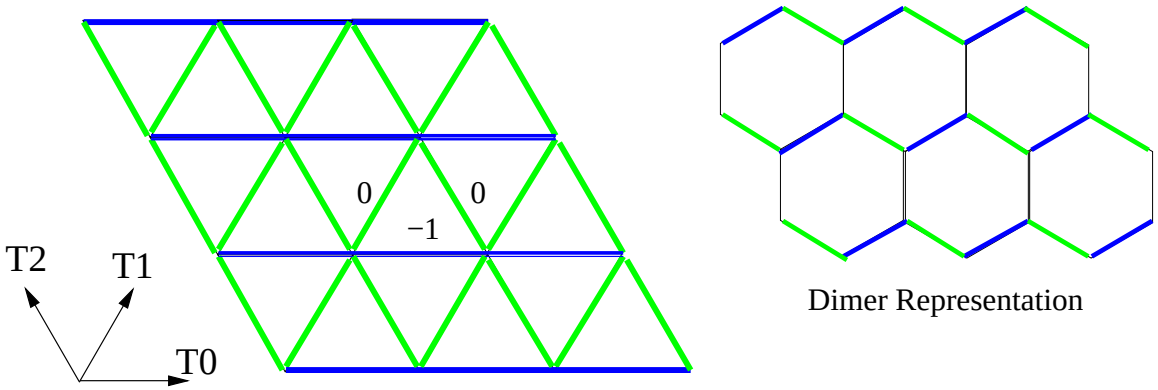

Figure 3.10: The orientationally ordered state on the triangular lattice. The Ising pseudospins are antiferromagnetically arranged on the parallel rows composed of blue bonds. The average Ising energy of the blue bonds is lower than that of the green bonds.

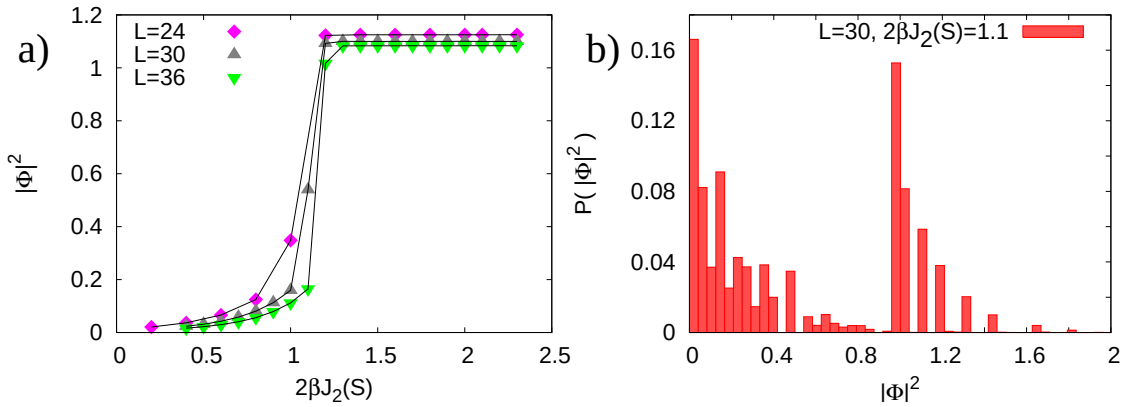

Figure 3.11: a) Temperature dependence of orientational order parameter Φ. b) The double peak in the histogram of Φ provides a clear signature of a first-order jump in Φ at the transition.

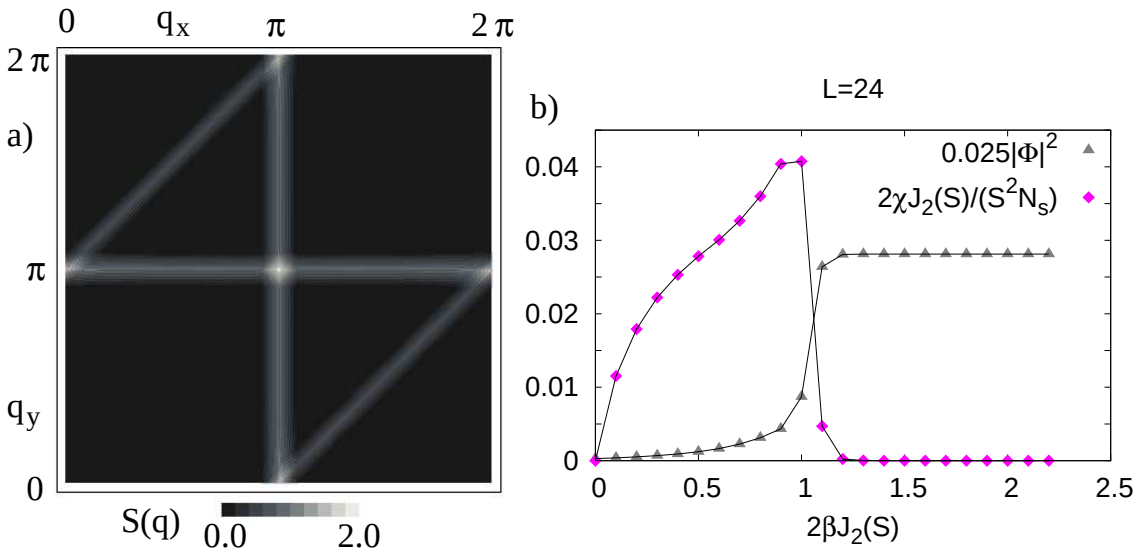

Figure 3.12: Shown here is the contour plot of the equal time spin structure factor $S(\vec{q})$ for size $L = 24$ at $2\beta J_2(S) = 2.2$. The Bragg lines with enhanced scattering are the signatures of the orientational order. Also shown is the magnetic susceptibility behaviour of a $N = 576$ system across the transition.

principle directions of the triangular lattice (Fig 3.10). Also each row fluctuates randomly between the two internal states corresponding to the two antiferromagnetic arrangements of σ on that row. One can easily calculate the spin structure factor in the orientationally ordered state when parallel rows fluctuate independently of each other. The structure factor $S(\vec{q})$ has Bragg lines with enhanced scattering ($\sim O(\sqrt{N})$) at (q_x, π), (π, q_y) and $q_x + q_y = \pi$ that correspond to the three possible directions of the antiferromagnetic rows (here $q_x(q_y)$ refers to the projection of $\vec{q}$ onto lattice directions $T_0(T_1)$ of the triangular lattice as shown in Fig 3.10 measured in units of inverse Bravais lattice spacing). This is the exactly the behaviour of $S(\vec{q})$ that is observed in the numerics deep in the orientationally ordered phase (Fig 3.12).

Another interesting aspect of this orientationally ordered state follows from the exponential suppression $[O(e^{-J_2(S)/T})]$ of the total easy axis magnetization and the corresponding magnetic susceptibility χ (Fig 3.12). This is because perfect orientational order implies zero magnetization for each antiferromagnetic row of spins. Defects cost energy of order $J_2(S)$. As long as the corresponding Zeeman energy gain due to magnetic field B is small compared to the multi-spin interaction $J_2(S)$, the orientationally ordered phase remains stable leading to a zero magnetization plateau. Since $J_2(S) \sim J^3 S/D^2$, this zero magnetization plateau extends for a range of magnetic fields $0 < |B| < B_c \sim J^3/D^2$.

Finally, as mentioned before, there is no long range order in the internal states

of the antiferromagnetic rows in the orientationally ordered phase. However, the different ground states (related by spin flip along an entire antiferromagnetic row) are not connected by local moves, and require moving an infinite number of spins in the thermodynamic limit to go from one configuration to another. In fully equilibrated simulations that employ efficient nonlocal multispin updates, we find that the antiferromagnetic rows fluctuate freely between their two allowed internal states. With realistic single-spin flip or spin-exchange dynamics, we see that the antiferromagnetic rows freeze into a random glassy pattern of internal states as we approach T_c. Similar glassy behaviour due to the formation of extended structures in the system has been discussed earlier [12] and we touch on this point some more in a later chapter.

To summarize, we have predicted that for $S > 3/2$, the kagome antiferromagnet with strong easy axis anisotropy goes into a semiclassical spin liquid state with distinctive and unusual short-ranged correlations below a crossover temperature $T^* \approx 0.08J^3S/D^2$ (for large S), while the triangular magnet undergoes a first order transition at $T_c \approx 0.1J^3S/D^2$ to an orientationally ordered collinear state that gives rise to a zero magnetization plateau for small magnetic fields along the easy axis.

References

[1] K. Damle and T. Senthil. Spin nematics and magnetization plateau transition in anisotropic kagome magnets. *Phys. Rev. Lett.* **97**, 067202 (2006).

[2] A. Sen, F. Wang, K. Damle and R. Moessner. Triangular and kagome antiferromagnets with a strong easy-axis anisotropy. *Phys. Rev. Lett.* **102**, 227001 (2009).

[3] J. Robert *et al.* Spin-Liquid correlations in the Nd-Langasite anisotropic kagome antiferromagnet. *Phys. Rev. Lett.* **96**, 197205 (2006).

[4] H. D. Zhou *et al.* Partial field-induced magnetic order in the spin-liquid kagome $Nd_3Ga_5SiO_{14}$. *Phys. Rev. Lett.* **99**, 236401 (2007).

[5] A. Zorko *et al.* Easy-axis kagome antiferromagnet: local-probe study of $Nd_3Ga_5SiO_{14}$. *Phys. Rev. Lett.* **100**, 147201 (2008).

[6] P. Bordet *et al.* Magnetic frustration on a Kagome lattice in $R_3Ga_5SiO_{14}$ langasites with R = Nd, Pr. *J. Phys. Condens. Matter* **18**, 5147 (2006).

[7] R. Liebmann. Statistical mechanics of periodic frustrated Ising systems. *Springer*, Berlin (1986).

[8] A. Sen, K. Damle and R. Moessner (unpublished).

[9] A. W. Sandvik and R. Moessner. Correlations and confinement in non-planar two-dimensional dimer models. *Phys. Rev. B* **73**, 144504 (2006).

[10] F. Alet *et al.* Interacting classical dimers on the square lattice. *Phys. Rev. Lett.* **94**, 235702 (2005).

[11] P. W. Kasteleyn. Dimer statistics and phase transitions. *J. Math. Phys. (N.Y.)* **4**, 287 (1963).

[12] D. Das, J. Kondev and B. Chakraborty. Activated dynamics at a non-disordered critical point. *Europhys. Lett.* **61**, 506 (2003).

Chapter 4

Effective Hamiltonian in Finite field

We now turn to the case where there is a magnetic field B applied along the easy axis, so that the spin Hamiltonian becomes

$$H = J \sum_{\langle ij \rangle} \vec{S}_i \cdot \vec{S}_j - D \sum_i (S_i^z)^2 - B \sum_i S_i^z \tag{4.1}$$

For the classical problem at $D = 0$, the ground state has a smoothly increasing magnetization with increasing field before the magnetization saturates to its maximum value. Thus, there is no magnetization plateau in the pure isotropic case ($D = 0$). On the triangular lattice, it is known that $1/S$ quantum corrections stabilize [1] a 1/3 magnetization plateau where $M = M_{sat}/3$. Exact diagonalization studies of low spin ($S = 1/2$) kagome antiferromagnet [2, 3] also give good evidence for the existence of a 1/3 plateau in the thermodynamic limit.

In the easy axis case on the kagome and triangular lattices, a 1/3 magnetization plateau exists even at the classical level when collinear states are prefered because of the anisotropy D. When $D \gg J$, a 1/3 plateau exists over a range of field $0 < B < 4JS$ in the kagome case. This $m = 1/3$ state is characterized by a $2:1$ constraint that requires two spins on each triangle to be maximally polarized along the field, and one *minority* spin to be maximally polarized anti-parallel to the field. States that satisfy this constraint are still macroscopically degenerate and hence quantum fluctuations can become important at low temperature. In this chapter, we derive the effective Hamiltonian $\mathcal{H}$ that encodes the effects of quantum fluctuations in a perturbative expansion in J/D and show that the degeneracy of this subspace is first lifted only at $O(J^6/D^5)$ for any $S \geq 3/2$. We also calculate the effective Hamiltonian

using a large-S approach. The 1/3 plateau on the triangular lattice is not considered here as a unique state (upto lattice symmetries) is obtained in the classical case.

4.1 Effective Hamiltonian for $m = 1/3$ on kagome

In the presence of a non-zero magnetic field, we split the Hamiltonian H in the following manner:

$$\begin{aligned} H &= H_0 + V \\ H_0 &= -D\sum_i (S_i^z)^2 \\ V &= V_d + V_o = (J\sum_{\langle ij\rangle} S_i^z S_j^z + B\sum_i S_i^z - \mathcal{E}_0) + \frac{\lambda J}{2}\sum_{\langle ij\rangle}(S_i^+ S_j^- + S_i^- S_j^+) \end{aligned} \quad (4.2)$$

The ground state of H_0 is all spin states in the Ising subspace in which $S_i^z = \sigma_i S$ where $\sigma_i = \pm 1$. Here $\mathcal{E}_0$ is the exchange energy ($J\sum_{\langle ij\rangle} S_i^z S_j^z$) of the collinear states which satisfy the $2:1$ constraint on each triangle of the kagome lattice. Let us now calculate the effective Hamiltonian $\mathcal{H}$ perturbatively in J/D. To first order, there is a potential term $J\sum_{\langle ij\rangle} S_i^z S_j^z + B\sum_i S_i^z - \mathcal{E}_0$. The magnetic field B is chosen here such that collinear states in which each triangle has two up spins and one down spin become ground states. These states are still massively degenerate. The degeneracy is further lifted only by terms at $O(J^6/D^5)$ and higher as we show below.

Firstly, the terms in the effective Hamiltonian terms *do not* depend explicitly on the magnetic field B since the total magnetization in the z direction is conserved by the Hamiltonian. The value of B, however, determines the total magnetization of the system.

Let us define an n bond process to be such that the perturbation V_o (off-diagonal term) acts on n different bonds of the system. The action of V_o depends purely on the spin states of the two sites of the bonds on which it acts. The diagonal term V_d also depends on the spin states of the sites which are directly connected to any of the sites belonging to the n bonds on which V_o acts in the subspace of states that satisfy the $2:1$ constraint (see Fig 4.2). This is because $V_d = J\sum_{\langle ij\rangle} S_i^z S_j^z - \mathcal{E}_0$ and $\mathcal{E}_0 = J\sum_{\langle ij\rangle} S_i^z S_j^z$ in any collinear state satisfying the $2:1$ constraint on each triangle. Hence V_d measures the exchange energy change on the bonds affected by V_o and the bonds that share a site with these bonds.

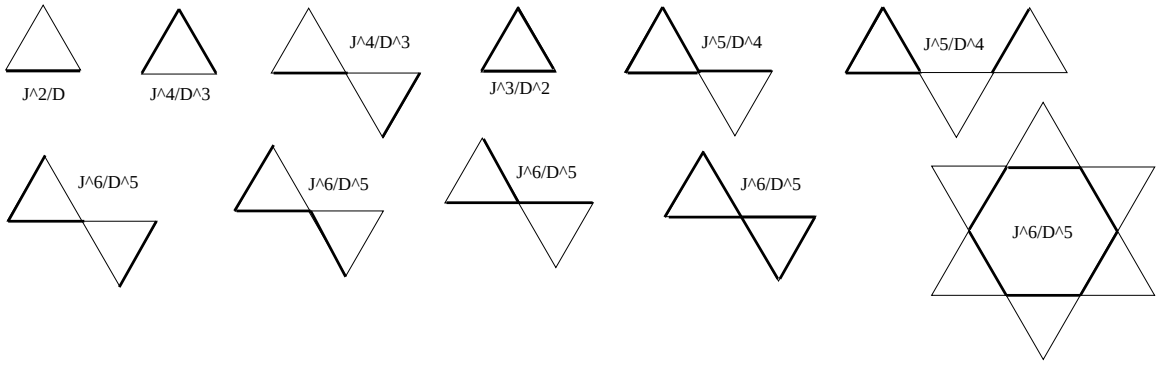

Figure 4.1: The n-bond patterns (bonds are indicated as thick black lines) which give contributions of $O(J^6/D^5)$ or lower in the perturbation series.

4.1.1 Diagonal terms

Here we prove that diagonal terms that lift the degeneracy of the ground state manifold satisfying the $2:1$ constraint occur only at $O(J^6/D^5)$. As stated earlier, V_o acts locally on a bond and just depends on the spin state on that bond. V_d is the excess energy measured with respect to the energy of the $2:1$ states and for this, one just needs to concentrate on the sites directly connected to the sites which are being changed due to V_o. The $2:1$ constraint implies that if a site has $\sigma = -1$, then its four nearest neighbors have $\sigma = +1$. Similarly, if a site has $\sigma = +1$, two of its neighbours have $\sigma = +1$ and two $\sigma = -1$, with the two spins belonging to the same triangle always anti-aligned. These strong constraints severely restricts the processes which can lift the degeneracy of the $2:1$ manifold as we will see below.

Since all the energy denominators are $O(D)$ and the matrix elements of the perturbation V are $O(J)$, a term generated at the p^{th} order in perturbation is $O(J^p/D^{p-1})$. For a n-bond process, it is simple to determine the lowest order in J/D where such a process can contribute in the perturbation expansion. This can be worked out by considering the minimum number of applications of V_o (and no application of V_d) needed to make a valid diagonal process involving all the n different bonds. For example, if the n bonds form a closed loop (say on a triangle), then the minimum order when these processes can contribute is $O(J^n/D^{n-1})$. Similarly, if the n bonds form a completely open pattern (i.e. no part of the pattern is a closed loop), then the minimum order is $O(J^{2n}/D^{2n-1})$. The different processes that we need to consider and the minimum order in J/D when they can appear are shown in Fig 4.1.

- Single-bond processes: Processes where the perturbation V_o acts on a single bond only cannot lift the degeneracy of the $2:1$ states. The spins on the bond have to be anti-aligned for generating non-zero terms. All such bonds have the

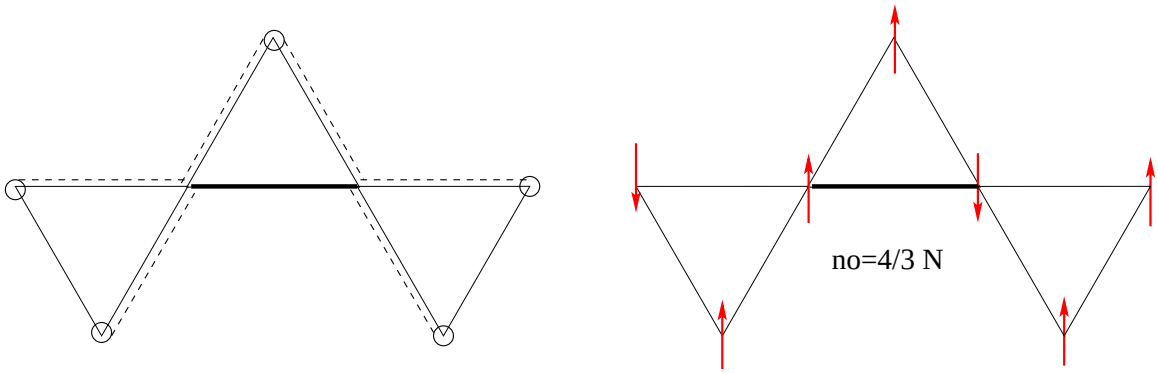

Figure 4.2: a) A change in the state of a bond changes the exchange energy on that bond and on bonds (shown as dotted lines) directly connected to one of the sites of that bond. b) Single bond processes do not lift the degeneracy of 2 : 1 states. The bond is indicated as a thick black line.

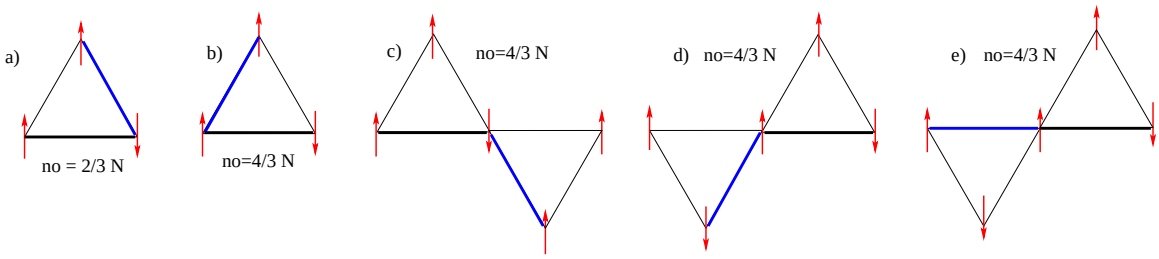

Figure 4.3: Two bond processes in which the two bonds share a common site The bonds are shown as thick dark lines (one in black and the other in blue).

same pattern of surrounding spins (see Fig 4.2): $+S$ is connected to two $+S$ and two $-S$ spins and $-S$ is connected to four $+S$ spins, and the number of such bonds is the same for all states satisfying the 2 : 1 constraint. Hence these single-bond processes cannot lift the degeneracy of these states at any order. The minimum order to which such processes appear in the perturbation is $O(J^2/D)$.

- Two-bond processes: Two bond processes, in which V_o acts on two different bonds, can be of different types. It can be shown that all such processes do not lift the degeneracy of the 2 : 1 processes at any order. The minimum order at which such processes appear in the perturbation is $O(J^4/D^3)$. First, let us consider processes in which the two bonds share a common site. Such processes can be divided into five different classes (see Fig 4.3) in which the spins on the involved bonds have identical nearest neighbour spin patterns and the number of occurences of each such two-bond pattern is the same for any minimally frustrated state satisfying the 2 : 1 constraint, proving that they do not lift the

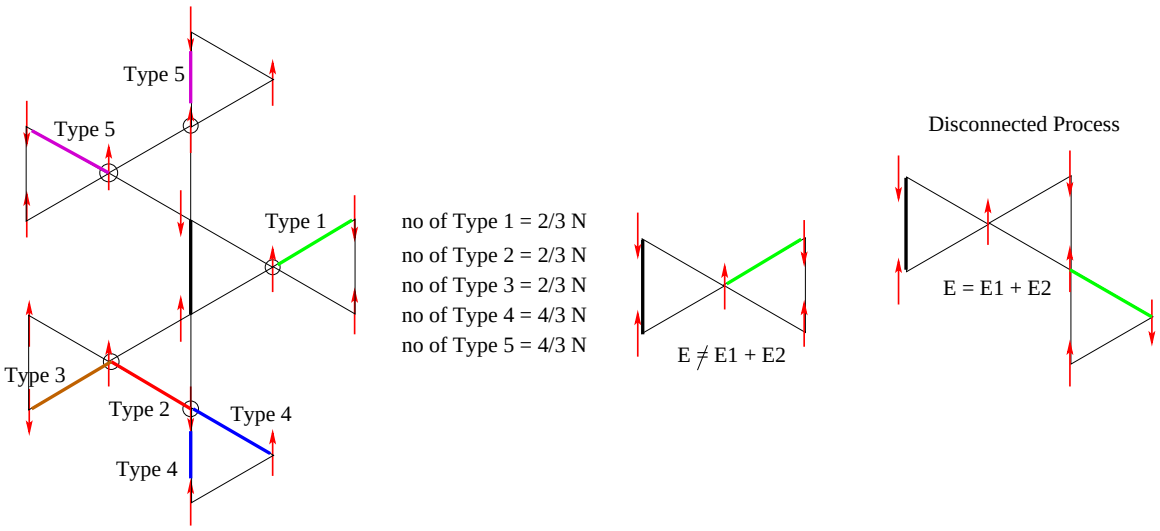

Figure 4.4: Two bond processes which do not share a common site. One bond is shown as a thick black line and other is indicated in different colors depending on its type. Also shown is an example of a "disconnected process" involving two bonds.

degeneracy.

Now we consider processes in which the two bonds do not share a common site. Firstly, both bonds should have anti-aligned spins to generate non-zero terms in the perturbation. If the two bonds are well seperated, any perturbation at a given order involving these bonds would be zero by to the linked cluster theorem, as the number of such processes scale as N^2 instead of N (where N is the number of sites in the system). For example, consider the "disconnected process" shown in Fig 4.4. Both the sites of the two bonds have the same set of nearest neighbours (whose spin states stay fixed) as two such bonds well seperated from each other. This is true for any two bonds with anti-aligned spins on them as long as the two bonds do not share a site and none of the sites of one bond are the nearest neighbour of any of the sites of the other bond. The contribution of all such perturbations at a given order must sum to zero by the linked cluster theorem.

What about the $+-$ bonds (i.e., the spins being anti-aligned) in which one or both the sites of a $+-$ bond is nearest neighbour to a site of the other $+-$ bond. These two bond processes are clearly different from the processes where the bonds are well seperated. However, such processes can again be divided into five different classes (see Fig 4.4), where the affected spins have identical surrounding neighbouring spins in each class. The number of patterns belonging to each class is the same irrespective of the state being considered in the $2:1$

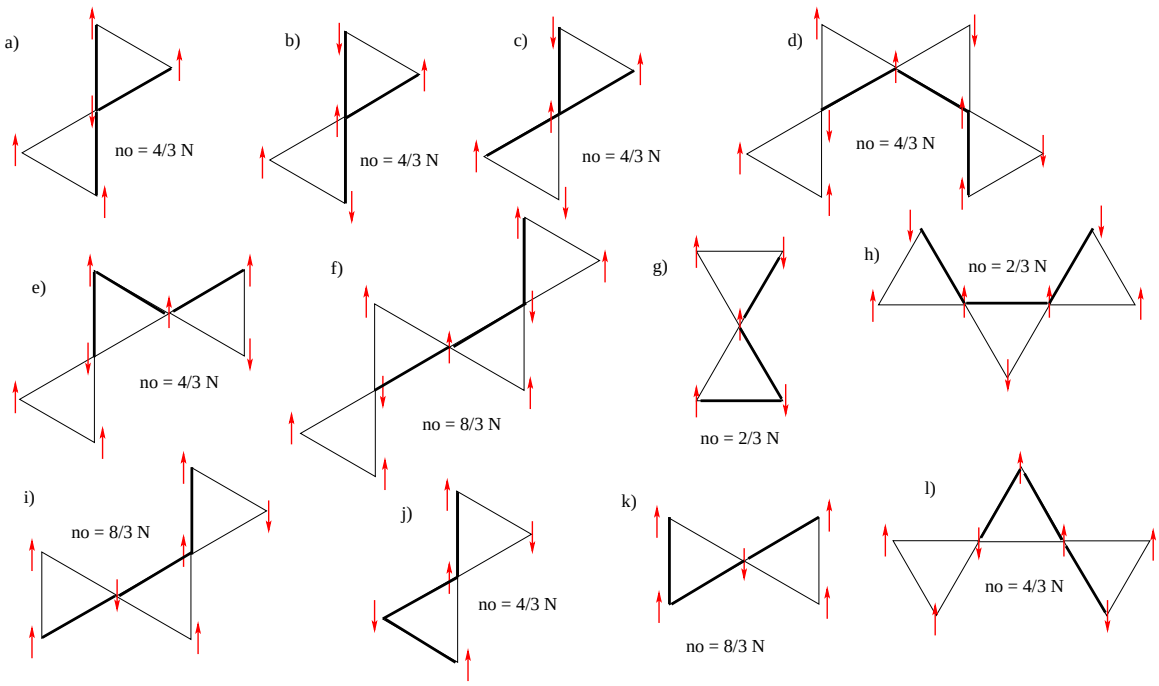

Figure 4.5: Three bond processes in which each bond is connected to at leat one of the other two bonds. The bonds are shown as thick black lines.

manifold. Thus, two bond process cannot lift the degeneracy of the ground state manifold either.

- Three bond processes: Three bond processes can be of many types. The first distinction is whether the three bonds lie on a closed loop (i.e., a single triangle on the lattice) or not. If the bonds lie on a single triangle, then the perturbation terms appear at $O(J^3/D^2)$ or higher. It can be easily seen that such processes do not lift the degeneracy to any order, since the number of such patterns and the surrounding spins are the same in any $2:1$ state. If the bonds do not lie on the same triangle, then the perturbation terms appear at $O(J^6/D^5)$ and higher.

  Now, let us consider the case when each bond is connected to at least one of the other two bonds. These processes can be divided into twelve different cases (see Fig 4.5), each of which have identical spin surroundings when considering the sites in the 3-bond process. Each of the 12 different cases have the same number of patterns in any $2:1$ state and hence the degeneracy is not lifted at any order by such processes.

  Now let us consider three bond processes in which two bonds share a common site but the third does not share a site with any of these two. When the third bond does not contain a site which is the nearest neighbour to any site of the

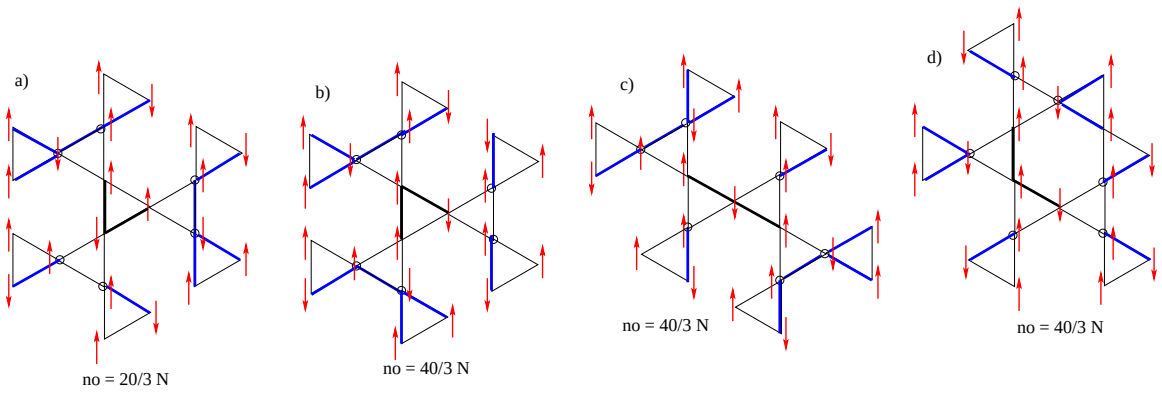

Figure 4.6: Three bond processes where two bonds share a common site and the third bond does not share a site with any of these bonds. The first two bonds are shown as thick black lines while the various positions of the third bond are indicated by thick blue lines.

other two bonds, then the sum of all such perturbation terms vanishes at each order by the linked cluster theorem. Let us now consider three bond processes where this argument cannot be used (Fig 4.6). Since such processes first appear at $O(J^6/D^5)$ where all applications of V are V_o (which just depends on the spin state at the bond and not on any neighbours), it is enough to show that the number of such processes is the same for any $2:1$ state to prove that no degeneracy is lifted at $O(J^6/D^5)$. This is indeed the case and can be proved by using the $2:1$ constraint on the ground state manifold. A similar argument can be used to show that three bond processes where none of the bonds touch each other do not lift the degeneracy at $O(J^6/D^5)$.

- Four bond processes: Four bond processes can be divided into two cases based on whether three bonds lie on the same triangle or not. When three of the bonds do not lie on the same triangle, the minimum order at which such terms can appear is $O(J^8/D^7)$, so we ignore such processes here. However, when three of the bonds do lie on a triangle, then the minimum order at which such terms can appear in the perturbation is $O(J^5/D^4)$. Such processes can be subdivided into two categories—Case I processes where the bond which is not part of the triangle has a site of the triangle as one of its sites and Case II processes where that bond does not touch any of the sites of the triangle. In both cases, it can be proven that such processes do not lift the degeneracy of the $2:1$ manifold to any order (see Fig 4.7). Case I can be divided into five cases and Case II into four different cases (see Fig 4.7) , where all the cases have identical spin surroundings and the same number of occurences in any $2:1$ state, to show

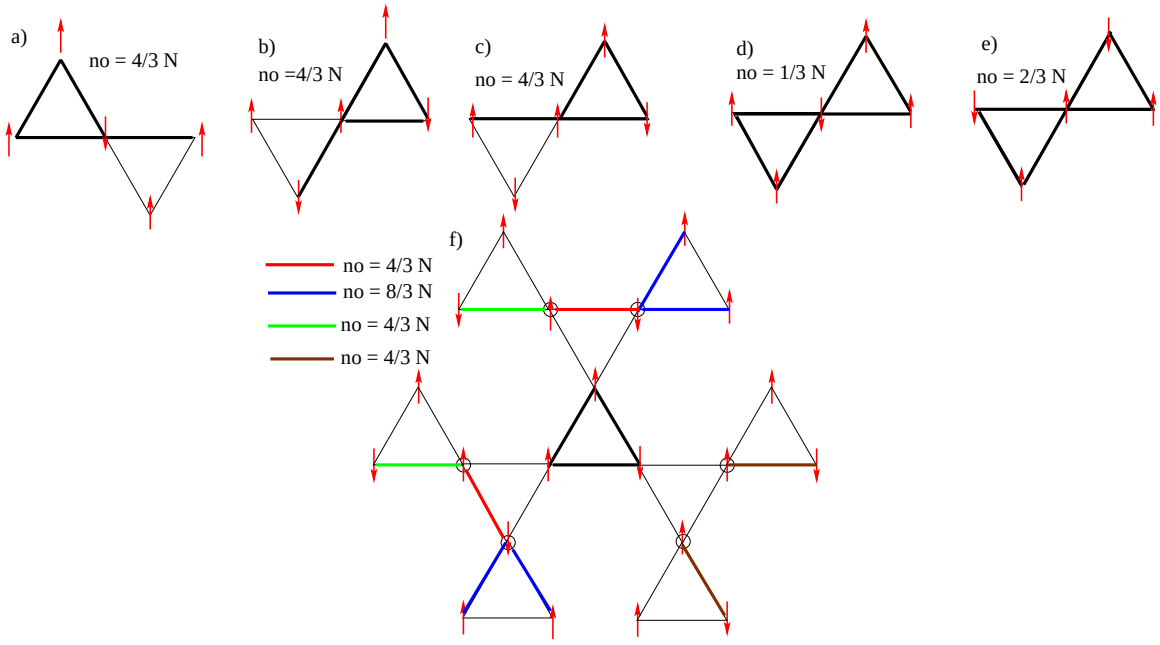

Figure 4.7: Four bond processes where three of the bonds are in the same triangle.From a)-e), the bonds are shown as thick black lines while in f), the three bonds on a triangle are shown as thick black lines and the various possibilities for the fourth bond are shown in different colors.

this.

- Five bond processes: Five bond processes can appear only at $O(J^7/D^6)$ or higher, so we do not consider such processes here.

- Six bond processes: Six bond processes which can contribute at $O(J^6/D^5)$ are the ones where all the six bonds lie on a closed loop. Two different patterns are possible in such a case: a bow-tie pattern or a hexagonal loop. It can be easily seen that the bow-tie patterns cannot lift the degeneracy of the $2:1$ states at any order in J/D. However, this is not true for the hexagonal loops as the number of different kinds of loops is not a constant for different members of the $2:1$ ground state manifold.

  At $O(J^6/D^5)$, the perturbative terms arise when V_o acts on each of the six bonds of the hexagonal loop once. The contribution of such processes have been calculated explictly and these can be written in terms of the following simple formula (see Appendix B):

$$H_{eff} = \sum_{\gamma_1,\gamma_2,\gamma_3,\gamma_4,\gamma_5 \neq g} \frac{\langle g|V_o|\gamma_1\rangle\langle\gamma_1|V|\gamma_2\rangle\cdots\langle\gamma_5|V|g\rangle}{(E_g - E_{\gamma_1})(E_g - E_{\gamma_2})\cdots(E_g - E_{\gamma_5})} \tag{4.3}$$

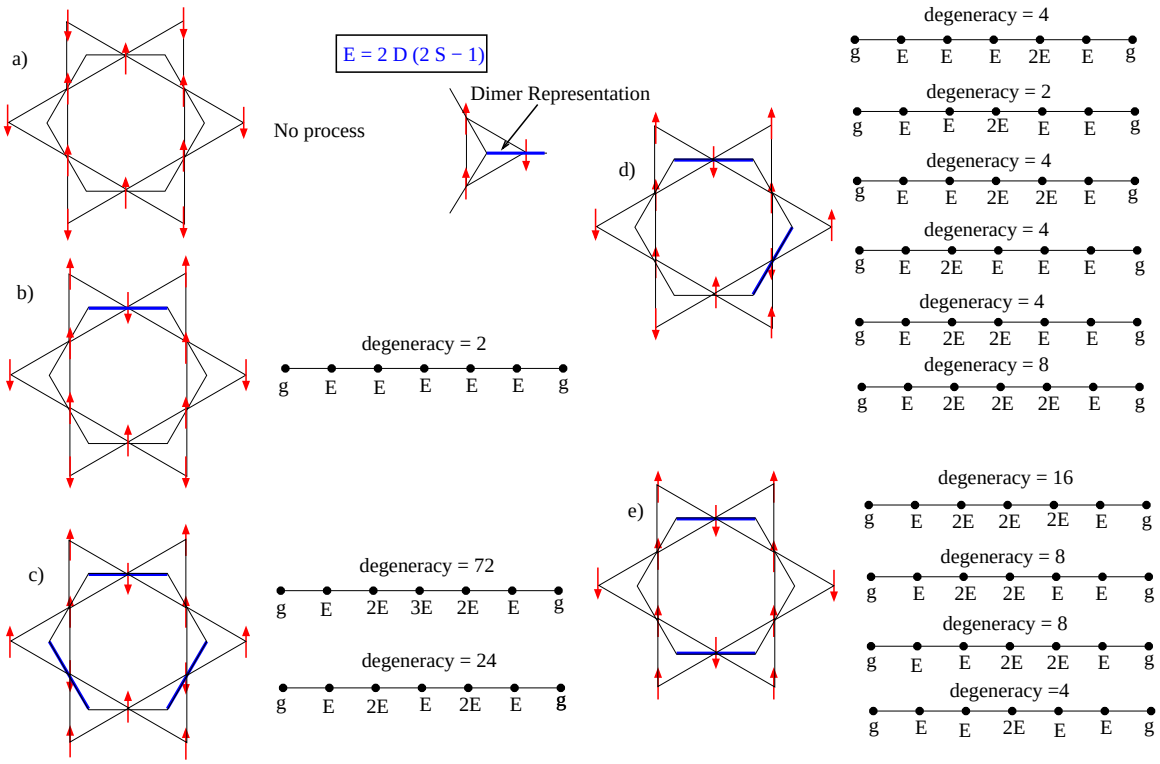

Figure 4.8: Six bond hexagonal processes which first lift the degeneracy at $O(J^6/D^5)$. The dimers on the corresponding honeycomb net are indicated by thick blue lines.

All the matrix elements for V_o in the above formula for these hexagonal processes equal λJS. Fig 4.8 gives the different choices of intermediate state energies for each type of hexagonal loop (there are five types) and the corresponding degeneracies of the processes. This information is enough to calculate the terms in the effective Hamiltonian using the above formula. For the effective Hamiltonian, we then get (this is written in dimer language here, see Fig 4.8)

$$H_{eff} = -\frac{\lambda^6 J^6 S^6}{32(2S-1)^5 D^5} \sum_{\hexagon} (0|\hexagon_0\rangle\langle\hexagon_0| + 2|\hexagon_1\rangle\langle\hexagon_1| + 8|\hexagon_2\rangle\langle\hexagon_2| + 12|\hexagon_3\rangle\langle\hexagon_3|) \quad (4.4)$$

where f_n is the fraction of elementary plaquettes on the honeycomb lattice which have n dimers on their perimeter. This can be simplified by using $f_0 + f_1 + 2f_2 + 3f_3 = 2$ since each dimer belongs to two hexagonal plaquettes. Then we have

$$H_{eff} = +\frac{\lambda^6 J^6 (2S)^6}{1024(2S-1)^5 D^5} \sum_{\hexagon} |\hexagon_1\rangle\langle\hexagon_1| \quad (4.5)$$

- Seven bond processes and higher: All such processes can appear in a perturba-

tive expansion only at orders higher than $O(J^6/D^5)$ so we do not analyze them here.

4.2 Large-S expansion

It is instructive to check the above result for the effective Hamiltonian independently using the semiclassical large-S expansion procedure of Hizi and Henley [4] (a similar calculation was performed in a previous chapter for the zero field case). Here we consider collinear states which satisfy the 2 : 1 constraint and calculate the zero-point energies of these states due to quantum fluctuations. Any collinear state can be represented in terms of Ising variables σ_i at each site. As before, the dependence of the spin Hamiltonian H on $\{\sigma_i\}$ is made explicit by applying the following unitary transformation:

$$U = \exp\left(i\pi \sum_i \frac{1-\sigma_i}{2} S_i^x\right) \tag{4.6}$$

To keep the physics invariant, we need to transform the Hamiltonian $H \rightarrow U^\dagger H U$ in Eq 4.1. Carrying out this transformation, we get

$$\begin{aligned} H &= J\sum_{\langle ij\rangle} \sigma_i\sigma_j S_i^z S_j^z - D\sum_i (S_i^z)^2 - B\sum_i \sigma_i S_i^z \\ &+ \frac{J}{2}\sum_{\langle ij\rangle}\left(\frac{1+\sigma_i\sigma_j}{2}(S_i^+S_j^- + S_i^-S_j^+) + \frac{1-\sigma_i\sigma_j}{2}(S_i^+S_j^+ + S_i^-S_j^-)\right) \end{aligned} \tag{4.7}$$

and then representing the spins by Holstein-Primakoff bosons, we get [till $O(S)$]

$$\begin{aligned} H &= \frac{JS^2}{2}\sum_{ij}\Gamma_{ij}\sigma_i\sigma_j - BS\sum_i \sigma_i + 2DS\sum_i b_i^\dagger b_i - \frac{JS}{2}\sum_{ij}\Gamma_{ij}\sigma_i\sigma_j(b_i^\dagger b_i + b_j^\dagger b_j) \\ &+ \frac{JS}{2}\sum_{ij}\Gamma_{ij}\left(\frac{1+\sigma_i\sigma_j}{2}(b_i^\dagger b_j + b_i b_j^\dagger) + \frac{1-\sigma_i\sigma_j}{2}(b_i^\dagger b_j^\dagger + b_i b_j)\right) \end{aligned} \tag{4.8}$$

where $\Gamma_{ij} = 1$ if i, j are nearest neighbours on the lattice and zero otherwise. H can be simplified further by using the 2 : 1 constraint on the collinear states. Firstly, $\sum_i \sigma_i$ is the same for all states satisfying the 2 : 1 constraint as each triangle has two $\sigma = 1$ and one $\sigma = -1$. Thus, it can be ignored. Secondly, on the 1/3 magnetization plateau, using the conservation of the z component of the magnetization, we have $\sum_i S_i^z = \frac{N}{3}S$. Doing the unitary transformation U, we get $\sum_i \sigma_i S_i^z = \frac{N}{3}S$ in the

"new" basis. Now, using the $2:1$ constraint, we immediately get

$$\sum_i \sigma_i n_i = 0 \tag{4.9}$$

Also, using the fact that each $\sigma = -1$ has $\sigma = 1$ on all its nearest neighbours and each $\sigma = +1$ has two $\sigma = +1$ and two $\sigma = -1$ as its neighbours, we get that

$$-JS \sum_{\langle ij \rangle} \sigma_i \sigma_j (n_i + n_j) = 4JS \sum_i n_i \tag{4.10}$$

Then, ignoring constants, we get that

$$\frac{H}{2SD} = (1+4\alpha) \sum_i n_i + \frac{\alpha}{2} \sum_{ij} \Gamma_{ij} \left(\frac{1+\sigma_i\sigma_j}{2} (b_i^\dagger b_j + b_i b_j^\dagger) + \frac{1-\sigma_i\sigma_j}{2} (b_i^\dagger b_j^\dagger + b_i b_j) \right) \tag{4.11}$$

where $\alpha = \frac{J}{2D}$. Then we calculate the equations of motion of b_k and $b_k^\dagger$ and use these to find the zero-point energy as before.

$$\mathcal{H}_{eff}(\{\sigma_i\}) = (1+4\alpha)(2SD) \frac{1}{2} Tr \sqrt{M} \tag{4.12}$$

where the matrix M is defined as

$$M_{ik} = \delta_{ik} + \eta(\Gamma_{ik} + \sigma_i \Gamma_{ik} \sigma_k) + \eta^2 \sigma_i \Gamma_{ij} \sigma_j \Gamma_{jk} \tag{4.13}$$

Here $\eta = \frac{\alpha}{1+4\alpha}$. The trace can be calculated perturbatively by expanding in powers of η. Using the properties of the $2:1$ manifold, it can be shown that no degeneracy is lifted till $O(\eta^5)$ and the large-S answer matches the large-S limit of the effective Hamiltonian result using a J/D perturbation.

The trace can be expanded in the following manner:

$$\begin{aligned} Tr(\sqrt{1+\eta X_1 + \eta^2 X_2}) = Tr \Bigg(1 + \frac{\eta}{2} X_1 + \eta^2 (\frac{X_2}{2} - \frac{X_1^2}{8}) + \frac{\eta^3}{16} (X_1^3 - 4X_1 X_2) \\ + \frac{\eta^4}{128} (-5X_1^4 + 24 X_1^2 X_2 - 16 X_2^2) + \frac{\eta^5}{256} (7X_1^5 - 40 X_1^3 X_2 + 48 X_1 X_2^2) \\ + \frac{\eta^6}{1024} (-21 X_1^6 + 140 X_1^4 X_2 - 240 X_1^2 X_2^2 + 64 X_2^3) + \cdots \Bigg) \end{aligned} \tag{4.14}$$

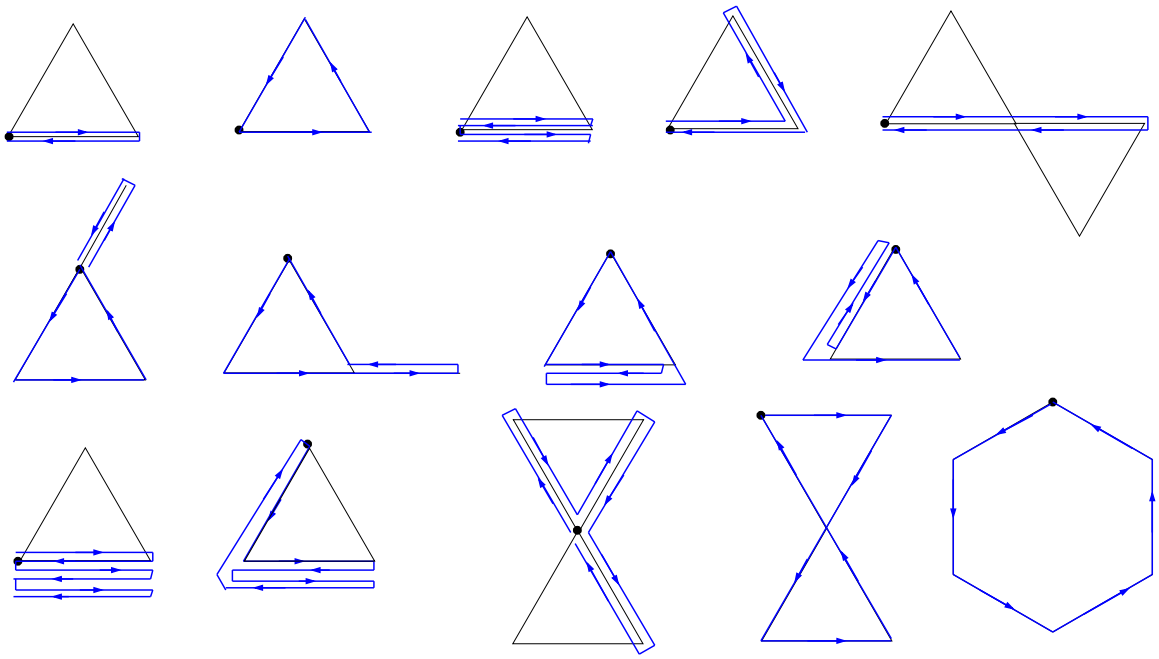

Figure 4.9: Closed loops which contribute to the perturbative calculation of the trace in Eq 4.14 till $O(\eta^6)$. Only the hexagonal loops break the degeneracy of the manifold of the states that satisfy the 2 : 1 constraint.

where the matrices X_1 and X_2 are the following :

$$\begin{aligned} (X_1)_{ik} &= \Gamma_{ik}(1+\sigma_i\sigma_k) \\ (X_2)_{ik} &= \sigma_i\Gamma_{ij}\sigma_j\Gamma_{jk} \end{aligned} \tag{4.15}$$

The trace operations in Eq 4.14 can be represented in a graphical manner. $(X_1)_{ik}$ can be represented as a line between two nearest neighbours i and k, while $(X_2)_{ik}$ can be represented by two lines, one between nearest neighbours i and j and another between nearest neighbours j and k, where k can be the same as i or different. All individual terms in the perturbative expansion of the trace have the following interpretation: We draw a closed loop where the end point is the same as the starting point i using m lines for a process at $O(\eta^m)$ (the same bond can have more than one line) and calculate $(X_1)_{ik}$ and $(X_2)_{ik}$ on the bonds of the loop knowing the spin configuration. Then the trace of the particular term being looked at is calculated by summing over the contributions obtained by taking the starting point to be any site in the lattice. For all processes till $O(\eta^5)$, it is easy to use the 2 : 1 constraint on each triangle to show that closed loops with some particular spin configuration on the sites of the loop will always occur the same number of times for any state satisfying the 2 : 1 constraint (using arguments similar to those of the previous section). For

example, a closed loop process that only uses the three bonds on a triangle (it can have any number of lines) cannot lift the degeneracy of the 2 : 1 states since each triangle has two $S_z = +S$ spins and one $S_z = -S$ spin. The degeneracy is first lifted at $O(\eta^6)$ due to hexagonal loop processes as the number of different kinds of hexagonal loops is not the same for different members of the 2 : 1 ground state manifold.

The trace on the hexagonal loops can be most easily done by explictly calculating $(X_1)_{ik}$ and $(X_2)_{ik}$ on the bonds of a given type of hexagonal loop. To illustrate this, we take the following two examples. Consider the hexagonal loop that has all $+S$. Then $(X_1)_{ik} = 2$ and $(X_2)_{ik} = 1$ for all the bonds (note that in $(X_2)_{ik}$ here, site i is different from site k, otherwise the loop cannot be closed in six lines). From this, we see that the sixth order contribution $-21X_1^6+140X_1^4X_2-240X_1^2X_2^2+64X_2^3 = 0$. Similarly, consider a hexagonal loop where $+S$ and $-S$ spins are arranged on alternating sites. Then, we get that $(X_1)_{ik} = 0$ and $(X_2)_{ik} = -1$, using which the sixth order contribution $-21X_1^6 + 140X_1^4X_2 - 240X_1^2X_2^2 + 64X_2^3 = -64$. Also, there are 12 ways to construct the loop here because of 6 choices of the initial point and 2 choices of the orientation of the loop. We calculate the other contributions similarly, and the effective Hamiltonian at $O(S)$ (at leading order in α) is:

$$H_{eff} = -\frac{J^6 S}{1024 D^5} \sum_{\hexagon} (0|\hexagon_0\rangle\langle\hexagon_0| + 2|\hexagon_1\rangle\langle\hexagon_1| + 8|\hexagon_2\rangle\langle\hexagon_2| + 12|\hexagon_3\rangle\langle\hexagon_3|) \quad (4.16)$$

where the result is written in dimer langauge for notational clarity. This large-S result precisely matches the large S limit of the effective Hamiltonian obtained earlier using perturbation in J/D (Eq 4.4).

References

[1] A. V. Chubukov and D. I. Golosov. Quantum theory of an antiferromagnet on a triangular lattice in a magnetic field. *J. Phys. Condens. Matt.* **3**, 69 (1991).

[2] K. Hida. Magnetization process of the $S = 1$ and $1/2$ uniform and distorted kagome Heisenberg antiferromagnets. *J. Phys. Soc. Jpn.* **70**, 3673 (2001).

[3] D. C. Cabra, M. D. Grynberg, P. C. W. Holdsworth and P. Pujol. From classical to quantum kagome antiferromagnet in a magnetic field. *Phys. Rev. B* **65**, 094418 (2002).

[4] U. Hizi and C. L. Henley. Effective hamiltonian for the pyrochlore antiferromagnet: semiclassical derivation and degeneracy. *Phys. Rev. B* **73**, 054403 (2006).

Chapter 5

Kagome in finite field

In this chapter, we consider the easy axis kagome antiferromagnet for values of fields B along the easy axis such that the ground state has magnetization $m = 1/3$ and is characterized by a $2:1$ constraint that requires two spins in each triangle to be maximally polarized along the field, and one, minority, spin to be maximally polarized antiparallel to the field. The Zeeman energy gap that drives the formation of this magnetization plateau is largest for $B \sim 2JS$. The plateau however, extends down to a relatively small onset field that scales as $B_{onset} \sim J^3/D^2$ as we will see later. These states (satisfying the $2:1$ constraint) have an extensive degeneracy and a convenient way to represent them [1] is to encode the presence of a minority spin by placing a dimer on the corresponding bond on the underlying honeycomb lattice (see Fig 5.1) . The low temperature physics on the plateau in then determined by the leading order effective Hamiltonian that acts within this dimer subspace. Most of the results presented in this chapter have been published earlier in Ref [2]. Reference [3] employed a closely related procedure for collinear states on the pyrochlore antiferromagnet in a field, but without anisotropy.

Because of the $2:1$ constraint, the first term (for any $S \geq 3/2$) that breaks degeneracy of states in the dimer subspace is a diagonal (potential energy) term that occurs at $O(J^6/D^5)$ [2] and which can be written as

$$\mathcal{H} = V(S) \sum_{\hexagon} |\hexagon_1\rangle\langle\hexagon_1| \tag{5.1}$$

where $V(S) = \frac{(2S)^6 J^6}{1024(2S-1)^5 D^5}$ and $\hexagon_1$ denote hexagonal plaquettes with 1 dimer on their perimeter (we also use f_n to denote the fraction of hexagons having n dimers on the perimeter later in the chapter). In contrast, the leading off-diagonal term, that corresponds to changing the state of a flippable hexagon (with alternating $\pm S$ values

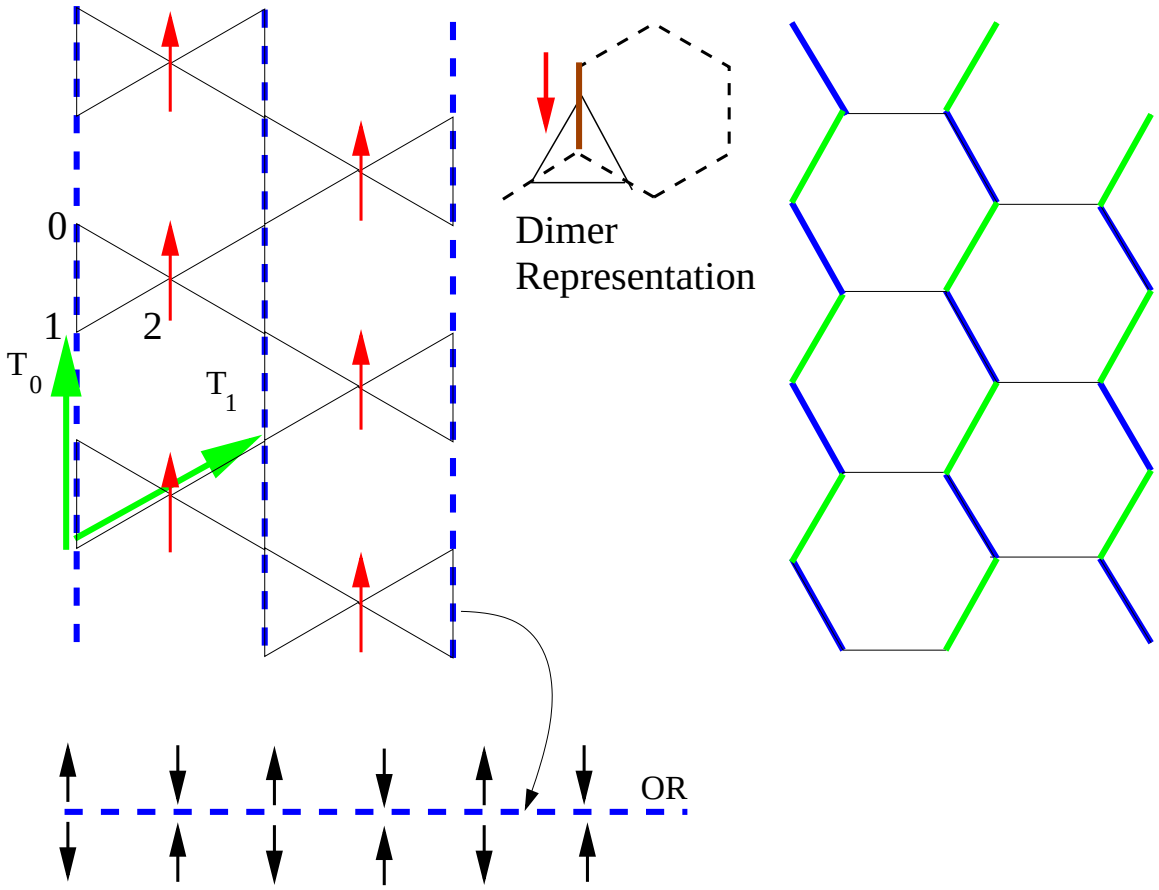

Figure 5.1: Sublattice rotation symmetry breaking on the $m = 1/3$ plateau: Dotted lines denote alternating arrangement of spins with average moment zero; up arrows correspond to $S_z = +S$. The dimer representation of the $m = 1/3$ configurations is also shown. The low temperature state is also shown in dimer langauge where the dimers can be either on the green or the blue bonds in each row independently and the horizontal bonds have no dimers.

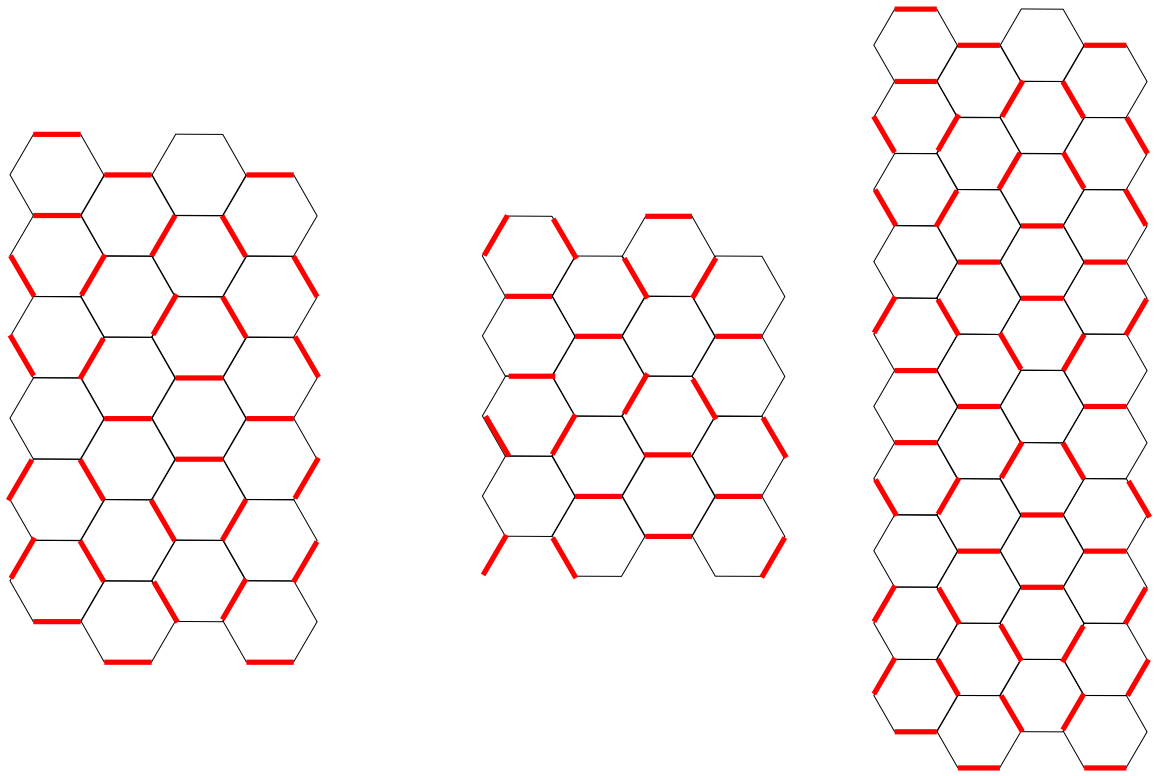

Figure 5.2: Some dimer configurations which satisfy the no plaquette with one dimer constraint which do not belong to the class of $f_2 = 1$ configurations.

of S_z around the hexagon) by reversing all spins on it, arise at order J^{6S-2}/D^{6S-3} [2]. This immediately implies the the low temperature physics is very different for the $S = 1$ case when compared to $S \geq 3/2$ since the off-diagonal term is dominant (sub-dominant) in the former (latter) case. For $S = 1$, quantum transitions between different ground states dominate the splitting of degeneracy. There, a 1/3 magnetization plateau with $\sqrt{3} \times \sqrt{3}$ collinear order was obtained in the presence of a magnetic field along the easy axis [4].

5.1 Dimer configurations with $f_1 = 0$

At low temperatures, the effective Hamiltonian $\mathcal{H}$ penalizes any dimer configuration with hexagonal plaquettes with one dimer on their perimeter. What the are dimer states that have no plaquettes with one dimer on their perimeter? Any dimer configuration with all plaquettes having 2 dimers on them satisfy this constraint and minimize $\mathcal{H}$. There are,however, other dimer configurations (see Fig 5.2) that satisfy this constraint but we have not been able to identify such states fully.

Furthermore, dimer configurations on the honeycomb lattice with $f_1 = 0$ have

the interesting property that there are no *independent* loop moves of dimers on closed loops (which are otherwise arbitrary) which result in another valid dimer configuration with $f_1 = 0$ on the (infinite) honeycomb lattice. As before, a loop on the honeycomb lattice is made up of links with dimers followed by adjacent empty links, and the move consists of shifting the dimers to the empty links along the loop generating another dimer configuration. Here we indicate the proof of this statement. Consider the closed path shown in Fig 5.3(a), defined as the perimeter of the polygons enclosed by the path. An arbitrary closed loop that lies within this basic closed path can be generated by deleting some hexagons and considering the perimeter of the resulting polygon (see Fig 5.3(c)). We scan the basic polygon from left to right along rows of hexagons (lines) not along the direction of scan (as shown in Fig) and define the corner row of a polygon as C_n (Fig 5.3(a)) if any hexagon of the polygon is not encountered till the $(n-1)^{th}$ row. Clearly, the basic polygon can be made bigger to enclose all closed paths of a certain size on the honeycomb lattice. Now, there are two basic segments (we call them Type 1 and Type 2, see Fig 5.3(b)) which if present in a closed path are enough to show that the dimer loop move on that path would generate a configuration with at least one hexagon with one dimer on its perimeter if starting from a configuration with no such hexagons. In the Type 1 case, a segment of the path covers at least four bonds of a single hexagon and the other hexagons sharing those bonds lie outside the closed path. In the Type 2 case, the segment is composed of elementary plaquettes which lie in a single row and there can be an arbitrary number of such hexagons. The other hexagons which share the bonds used up in the path segment again lie outside the closed path. Now, if the corner row of the closed path we are considering is C_n, then it is necessarily made by deleting one or more hexagons from that row. Then this row always contains path segments which are Type 1 or Type 2 or both (Fig 5.3(c)), which immediately proves that the closed path cannot be used to define a dimer loop move that gives a $f_1 = 0$ configuration starting from another.

5.2 Broken sublattice rotation symmetry

To study this interesting dimer model further and get the low temperature phase, we employ the procedure of Refs [5, 6] to efficiently simulate an interacting classical dimer model with the given potential energy term–our algorithm employs nonlocal loop updates but preserves detailed balance in order to generate the correct equilibrium Gibbs distribution at temperature T. The simulations were done on systems with L ranging from 18 to 30, where the number of sites in the system is $3L^2$. As the

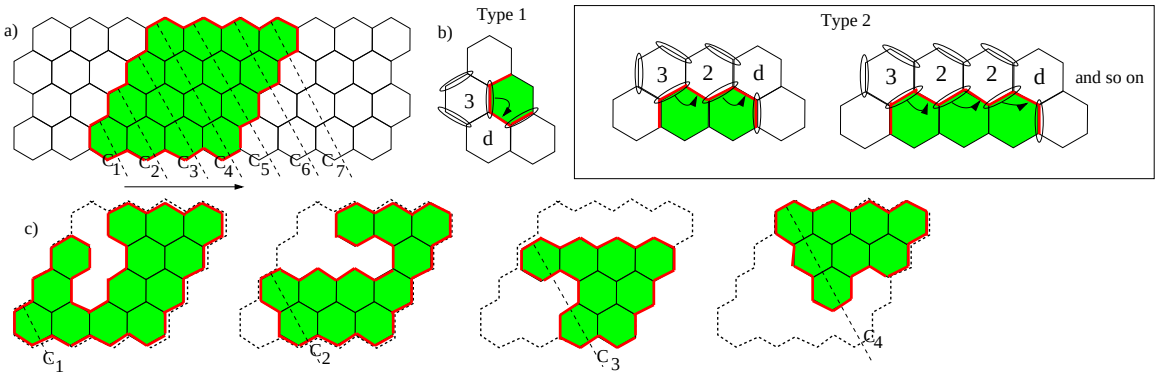

Figure 5.3: (a) Shown here is a basic closed path which is the perimeter of a polygon made of 16 hexagons. Any other closed path that can be contained inside this can be generated by deleting some hexagons and considering the perimeter of the resulting polygon. The convention for defining the corner rows is also shown. (b) Type 1 or Type 2 segments in a closed path imply that starting from a state with $f_1 = 0$, a configuration with defect hexagons (marked as d) where the number of dimers is 1 is produced, if a dimer loop move is done using that path. (c) Four examples of polygons derived from the basic polygon in (a). The corner row of each path contains segment of Type 1 or Type 2.

temperature is lowered to below $T_c \approx 0.23V(S)$, we find that the system undergoes a transition (Fig 5.4) to a state with sublattice rotation symmetry breaking as shown in Fig 5.1. In this schematic of the ordered state, one spontaneously chosen sublattice of spins aquires the maximum polarization $+S$ along the field. In order to then satisfy the 2 : 1 constraint on each triangle, the spin moments on the other two sublattice sites then alternate $+S, -S, \cdots$ in one of the two possible alternating arrangements along a stripe. This ordering can be conveniently characterized by using the sublattice order parameter

$$\Phi = \sum_p m_p \exp(2p\pi i/3) \tag{5.2}$$

where m_p denotes the sublattice magnetization of the p^{th} sublattice on the kagome lattice (see Fig 5.4 for the behaviour of $|\Phi|^2$ as a funtion of temperature). The two peak structure in the hoistogram of $|\Phi|^2$ near T_c (Fig 5.4) provides good evidence for the first order nature of this transition.

Each stripe can be in one of two possible alternating states and its internal state can be represented by an (Ising) pseudospin variable σ. From our numerics, we find very good evidence that these σ fluctuate independently in each stripe and do not show any ordering. Note that this state has the same dimer representation on the honeycomb lattice as the triangular lattice ground state at zero field on its dual lattice.

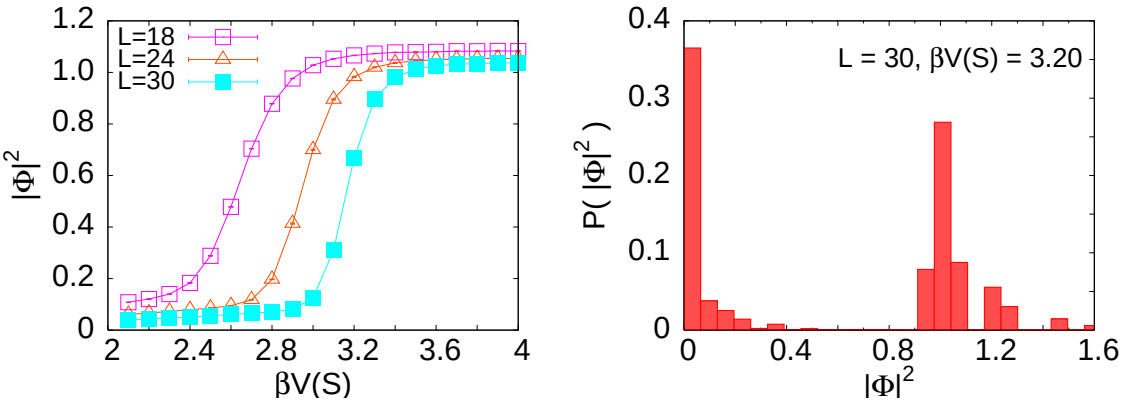

Figure 5.4: First order transition to the ordered state that breaks sublattice rotation symmetry upon lowering temperature.

The sublattice symmetry breaking corresponds to the three possible ways of choosing bonds of a certain orientation which have no dimers on them in a state with $f_2 = 1$ (all elementary plaquettes having two dimers on them). This low temperature state does not break any translational symmetry nor the $U(1)$ spin rotation symmetry of the Hamiltonian.

5.2.1 Glassy dynamics

Even though the fully equilibrated system consists of independently fluctuating stripes that have two possible internal states, this equilibration is achieved in our numerics because the algorithm incorporates nonlocal loopupdates that can flip a macroscopic number of spins in one move. However, the dynamics is local in the experimental system. Such local spin flips cost significant potential energy, and the system needs to change the internal state of an entire stripe to avoid the potential energy penalty. Systems with very similar potential energy landscapes have been the subject of earlier studies [7] which demonstrate glassy behaviour due to the formation of extended structures in the system. It is thus clear that the low temperature phase of our system would display glassy freezing of the stripes.

We further investigate the glassy behaviour of the system numerically by imploying a local algorithm. We consider the following Hamiltonian with Ising spins on the sites of the kagome lattice:

$$H = JS^2 \sum_{\langle ij \rangle} \sigma_i \sigma_j - BS \sum_i \sigma_i + V(S) f_1 \tag{5.3}$$

This is identical to our effective dimer model (see Eq 5.1) when $JS^2 \to \infty$. However,

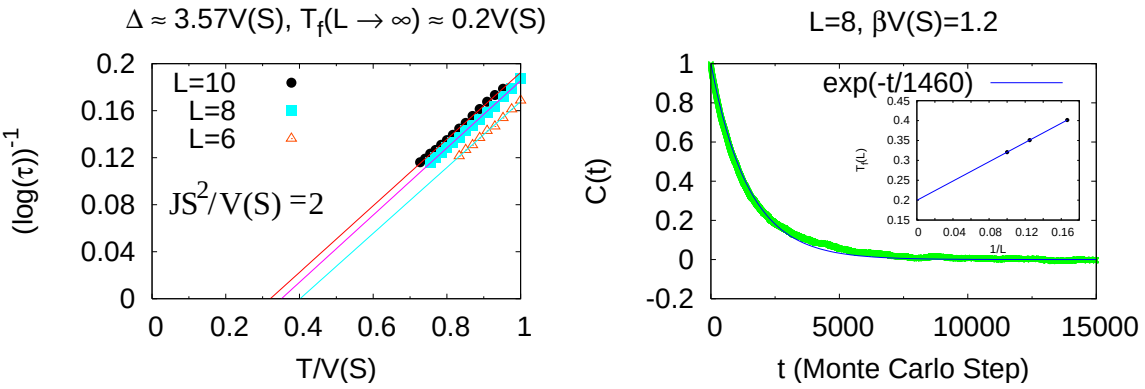

Figure 5.5: Data for single-spin autocorrelation time τ fit to the Vogel-Fulcher form $(\log(\tau))^{-1} = (T - T_f)/\Delta$; the intercept on the x axis yields T_f, while the slope gives Δ^{-1}. The extrapolation of $T_f(L)$ to $L \to \infty$ is shown in the inset.

here we keep the ratio $JS^2/V(S)$ finite as we wish to explore the higher temperature dynamics, and configurations outside the 'dimer subspace' are *allowed* but *exponentially unlikely* (as opposed to forbidden). A dimer is still defined by the presence of $\sigma_i = -1$ when determining the $V(S)f_1$ term. We use purely local two spin exchange dynamics satisfying detailed balance (with energies calculated according to the above Hamiltonian) and monitor the temperature dependence of the single-spin autocorrelation function for a range of moderately large values for the ratio $JS^2/V(S)$. In these simulations, the magnetic field B is fixed to its nominally optimal value $B = 2JS$ which places the system close to the center of the $m = 1/3$ plateau. We find that the single spin autocorrelation time τ increases very rapidly as we lower the temperature. Indeed, $\tau(T)$ can be fit well by an activated functional form of the Vogel-Fulcher type $\tau(T) = \exp(\Delta/(T - T_f(L))$ (Fig 5.5), thus extending further the analogy to other models of glass-formers. Vogel Fulcher law describes the slowing down of relaxation processes associated with many glasses. In our fits, the freezing temperature $T_f(L)$ drifts somewhat with linear size L, but its extrapolated $L \to \infty$ value (Fig 5.5) is within 10% of the equilibrium T_c obtained earlier, while the barrier energy scale Δ shows no appreciable L dependence. We thus conclude that while the fully equilibriated system only breaks sublattice rotation symmetry but not lattice translation symmetry, slow glassy dynamics that sets in as the temperature is lowered through T_c forces the system into a glassy state in which the stripe pseudospins also freeze in a random pattern.

5.2.2 Onset field for $m = 1/3$ plateau

Let us now understand how the onset field of the $m = 1/3$ plateau scales with J/D and S. We saw earlier that quantum fluctuations generate an $O(J^3S/D^2)$ multi-spin interaction at zero field on the kagome lattice and the collinear states that minimize this energy have the constraint that no spin is the minority spin of both triangles to which it belongs. This zero field ensemble is stable to small magnetic fields since the defining constraint on minority spins does not fix the average magnetization. When the field is increased further beyond $B \sim J^3/D^2$, the $O(BS)$ Zeeman energy gain of the $m = 1/3$ ensemble will begin to dominate over the $O(J^3S/D^2)$ potential energy gain of the zero field ensemble, and this will trigger the onset of the $m = 1/3$ plateau. Thus the onset field scales as $B_{onset} \sim J^3/D^2$.

To summarize, we have predicted an unusual sublattice ordered $m = 1/3$ magnetization plateau at low temperature in $S \geq 3/2$ kagome antiferromagnets with strong easy axis anisotropy that breaks sublattice rotation symmetry but not translational symmetry. This is also an interesting example of slow glassy dynamics in a spin system without any disorder.

References

[1] R. Moessner and S. L. Sondhi. Theory of the [111] magnetization plateau in spin ice. *Phys. Rev. B* **68**, 064411 (2003).

[2] A. Sen, K. Damle and A. Vishwanath. Magnetization plateaus and sublattice ordering in easy-axis kagome lattice antiferromagnets. *Phys. Rev. Lett.* **100**, 097202 (2008).

[3] D. Bergman, R. Shindou, G. Fiete and L. Balents. Degenerate perturbation theory of quantum fluctuations in a pyrochlore antiferromagnet. *Phys. Rev. B* **75**, 094403 (2007).

[4] K. Damle and T. Senthil. Spin nematics and magnetization plateau transition in anisotropic kagome magnets. *Phys. Rev. Lett.* **97**, 067202 (2006).

[5] A. W. Sandvik and R. Moessner. Correlations and confinement in non-planar two-dimensional dimer models. *Phys. Rev. B* **73**, 144504 (2006).

[6] F. Alet *et al.* Interacting classical dimers on the square lattice. *Phys. Rev. Lett.* **94**, 235702 (2005).

[7] D. Das, J. Kondev and B. Chakraborty. Activated dynamics at a non-disordered critical point. *Europhys. Lett.* **61**, 506 (2003).

Chapter 6

Conclusions

In this thesis, we have studied kagome and triangular lattice antiferromagnets with isotropic nearest neighbour Heisenberg interactions J and a single-ion anisotropy D of the easy axis type. It can be shown that moderately large values of D are sufficient to make collinear spin states dominate the low temperature physics on both the lattices. Such kind of a magnetic anisotropy is relevant in certain rare earth magnets. In this collinear regime, we expect an analysis based on the smallness of J/D to give reliable results. We use J/D as the small parameter in a systematic perturbative approach that allows us to calculate the effective low-energy Hamiltonian and the resulting low-temperature phases.

In the zero field problem, we find that the physics of all $S > 3/2$ moments is very different from the previously studied $S = 1$ case on both the lattices. When $D \gg J$, the low energy states selected by the anisotropy map onto configurations of the corresponding classical Ising antiferromagnet. Subleading $O(J^3S/D^2)$ multi-spin interaction arising from the tranverse quantum dynamics makes the low-temperature behaviour very different from the well known classical case. The kagome magnet goes into a semiclassical spin liquid state with distinctive and unusual short-range correlations below a crossover temperature $T^* \approx 0.08J^3S/D^2$, while the triangular magnet undergoes a first-order transition at $T_c \approx 0.1J^3S/D^2$ to an orientationally ordered collinear state that gives rise to a novel zero-magnetization plateau along the easy axis.

We also study the kagome lattice antiferromagnet in the presence of a magnetic field along the easy axis. For $S \geq 3/2$, virtual quantum fluctuations at $O(J^6S/D^5)$ help lift the classical degeneracy. We demonstrate the presence of a one-third magnetization plateau for a broad range of magnetic fields $J^3/D^2 \lesssim B \lesssim JS$ along the easy axis. The system develops an unusual order that breaks sublaltice rotation symmetry but not translation symmetry on this plateau due to the virtual quantum fluctua-

tions. This also provides an example of a spin system which shows glassy behaviour in the absence of any disorder.

Appendix A

Directed-loop algorithm for Dimer models

In this appendix, we first briefly discuss the directed-loop algorithm for a hard-core dimer model (see Refs [1, 2]) on the honeycomb lattice. We then generalize the algorithm to the case of dimer models on the dice lattice where the hard-core constraint is applicable only on the three-coordinated sites.

A.1 Dimer model on the honeycomb lattice

Consider the dimer model on the honeycomb lattice (finite with periodic boundary conditions) where each site on the lattice has precisely one dimer touching it. The algorithm starts by creating two defect sites in a valid dimer configuration where a defect site is any site that violates the constraint of one dimer touching it. One of the defect sites stays stationary, while the other keeps moving stochastically in a way that satisfies detailed balance. In the final step, this defect meets the immobile defect and they annihilate to give another valid dimer configuration. The motion of the defects can be visualized as a directed closed loop.

The construction of the directed loop proceeds in the following manner: An entry site en_0 is randomly selected on the honeyconb lattice. The site has a dimer touching it. The path then starts from en_0 and reaches a site p_0 through the connecting dimer. At the pivot site p_0, the dimer through which the site is entered is pivoted according to detailed balance equations (which we come to later) keeping one end at p_0. The dimer then touches the site ex_0 alongwith p_0. The site ex_0 becomes the new entry site en_1 for the directed path and then a new pivot p_1 is obtained by using the dimer that was present on en_1 before the pivoting at p_0. The path proceeds in such a manner

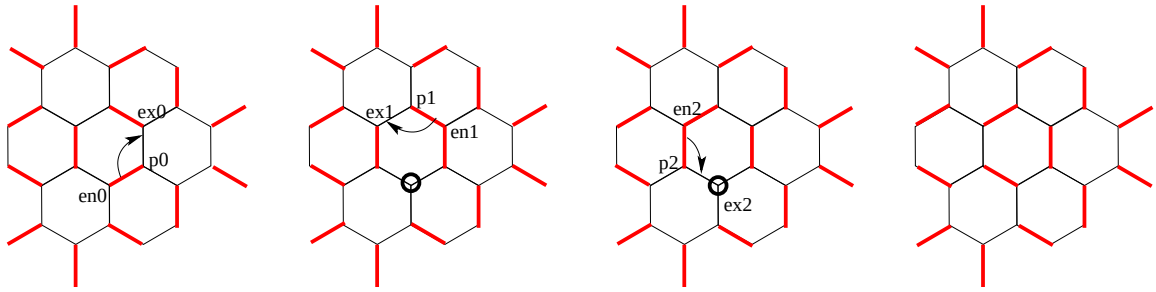

Figure A.1: A simple example of a directed loop which gives a valid dimer configuration starting from another one is shown here.

till an exit site ex_n gets chosen which is precisely the starting site en_0. Then the pivoting at p_n annihilates the two defect sites, en_0 which was stationary and ex_n which was moving stochastically, and another valid dimer configuration is obtained. A very simple example of such a directed loop is given in Fig A.1.

Given an entry and a pivot, how is the exit site chosen stochastically? Consider a dimer model where the potential energy can be expressed as a sum of single-plaquette terms (say $V = \sum_{\hexagon} |\hexagon_1\rangle\langle\hexagon_1|$). For detailed balance to be satisfied for the entire directed loop, it is sufficient to impose it at every step. Thus, we need

$$W_i P_\nu(i \to j) = W_j P_\nu(j \to i) \tag{A.1}$$

where i represents the entry site and j the exit site, and $P_\nu(i \to j)$ is the probability of choosing j as the exit site given that i is the entry and ν the pivot site. The weights are $\exp(-\beta V)$ where V is calculated for the two dimer configurations (before and after the pivot move). For a single plaquette potential, the weights would just depend on the dimer states of the three hexagons that share the pivot site ν, before and after the move. Denoting the sites connected to the pivot site ν as $1, 2, 3$ and $a_{ij} = W_i P_\nu(i \to j)$, the detailed balance condition can be written as (Ref [3]):

$$\begin{pmatrix} a_{11} & a_{12} & a_{13} \\ a_{21} & a_{22} & a_{23} \\ a_{31} & a_{32} & a_{33} \end{pmatrix} \begin{pmatrix} 1 \\ 1 \\ 1 \end{pmatrix} = \begin{pmatrix} W_1 \\ W_2 \\ W_2 \end{pmatrix} \tag{A.2}$$

where $a_{ij} = a_{ji}$ (detailed balance condition) and all a_{ij} are non-negative to avoid negative probabilities. Also, we order the matrix so that $W_1 \geq W_2 \geq W_3$. The equations for a_{ij} are underdetermined and thus there may be more than one possible solution. The solutions can be selected such that preferably all $a_{ii} = 0$ so that the path does not backtrack which is *a priori* wasteful. Such solutions are called no-bounce

solutions, and we have

$$\begin{aligned} a_{12} &= \frac{W_1 + W_2 + W_3}{2} - W_3 \\ a_{13} &= \frac{W_1 + W_2 + W_3}{2} - W_2 \\ a_{23} &= \frac{W_1 + W_2 + W_3}{2} - W_1 \end{aligned} \tag{A.3}$$

This solution does not remain valid when $W_1 > (W_2 + W_3)$ and then some bounces become necessary to solve the detailed balance equations. One possible solution in such a case is given below:

$$\begin{aligned} a_{11} &= W_1 - (W_2 + W_3), \quad a_{12} = W_2, \quad a_{13} = W_3 \\ a_{21} &= W_2, \quad a_{22} = 0, \quad a_{23} = 0 \\ a_{31} &= W_3, \quad a_{32} = 0, \quad a_{33} = 0 \end{aligned} \tag{A.4}$$

Knowing how the exit probabilities are chosen from the above solutions, the directed loops can now be constructed to give valid dimer configurations. The detailed balance property ensures that the correct equilibrium Gibbs distribution is generated at the given temperature T for the given single-plaquette potential term.

A.2 Dice lattice algorithm

The dice lattice (dual lattice of the kagome lattice) has two kinds of sites—three coordinated and six coordinated. The three coordinated sites have the constraint that exactly one dimer touches each such site. The six coordinated site only have the soft constraint that an even number of dimers ($0, 2, 4$ or 6) touches them. However, the directed loop algorithm of the previous section can be generalized to these kinds of dimers models as well. We again restrict to the case where the potential energy of a dimer configuration can be written in terms of single elementary plaquette terms.

In the directed loop construction for the dice lattice dimer model, the entry and exit sites are always six-coordinated while the pivot sites are three-coordinated. At the first step, two defect six-coordinated sites are produced (i.e., they violate the soft constraint of an even number of dimers touching them). Subsequently, one of the defects moves around stochastically until it meets the first defect. At this point, they annihilate and a new dimer configuration is obtained. Here the basic moves are of two types (see Fig A.2). Let us denote the six-coordinated entry site by ν and the three-coordinated pivot site by i. Then, if there is a dimer on the link between the

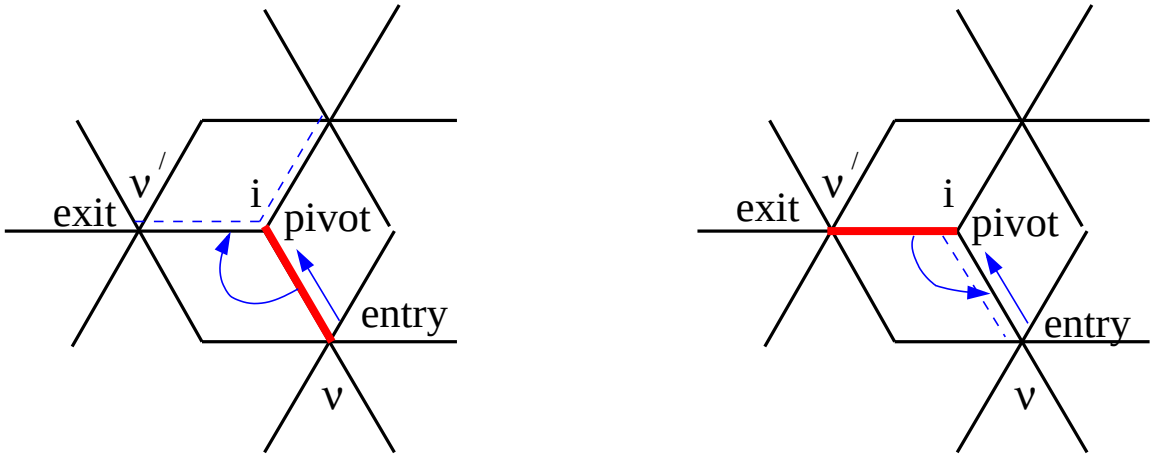

Figure A.2: The two different kinds of dimer moves shown here: in the first, the dimer is pivoted using the three coordinated site i to any of the two empty links connected to that site or left at the original link with certain probabilities. In the second, the bond connecting the six-coordinated entry site ν and pivot site i is empty, and the dimer attached to i moves to that empty link with a certain probability or stays at the original link. The dimer is represented as a thick red line.

two sites, it is rotated to one of the other two links emerging from site i or left where it is (bounce process) with probabilities $P^i_{\nu\nu'}$ where ν' denotes the new six-coordinated site that the dimer touches after pivoting. On the other hand, if there is no dimer on the link between i and ν, then with site i as pivot, we try to rotate the dimer touching it to touch ν instead of the original site ν' and denote this probability by $Q^i_{\nu\nu'}$. These probabilities can be chosen so that detailed balance is satisfied (as in the case of a hard-core dimer model). The weights are $\exp(-\beta V)$ where V is the single-plaquette potential calculated for the two dimer configurations (before and after the pivot move). For such a potential, the weights would just depend on the dimer states of the three elementary plaquettes that share the pivot site i, before and after the move. We can use the solutions given in the previous section for the 3×3 set of $P^i_{\nu\nu'}$. For the 2×2 set of $Q^i_{\nu\nu'}$, we take the standard metropolis solution [4]:

$$\begin{aligned} P(C_1 \to C_2) &= 1 && \text{if} \quad W(C_2) > W(C_1) \\ &= \frac{W(C_2)}{W(C_1)} && \text{else} \end{aligned} \tag{A.5}$$

where $W(C_1)$ and $W(C_2)$ denote the weight of the configurations.

Below we give a summary of the algorithm.

S1: A random six-coordinated site μ_0 is chosen with uniform probability for

choosing any such site (all 6-coordinates sites are denoted by greek letters and all 3-coordinates sites by roman letters). Then, a random three-coordinated site connected to μ_0 (call it i) is picked with a probability 1/6.
S2: There is always one dimer touching the site i. If this dimer connects i to the site μ_0, then with site i as pivot, we rotate this dimer to one of the other two links emerging from this site, or leave it where it is. Those probabilities are denoted as $P^i_{\mu_0\nu}$. If the dimer is left where it was, the loop closes without doing anything and we return to step *S1*. Else we proceed.

OR

S2′: On the other hand, if this dimer does not connect i to μ_0, then with site i as pivot, we try to rotate it to touch μ_0 instead of the original site μ it touched. The probability of doing this is $Q^i_{\mu_0\nu}$, and with probability $Q^i_{\mu_0\mu_0}$ we do not move the dimer—here again, the index μ_0 denotes the fact that we entered site i from site μ_0, but this time along an empty link.

The two different cases explained above can be summarized in a unified way by stating that each 3-coordinated site j has a matrix of probabilities for changing the orientation of the dimer connected to it. This matrix is denoted by $R^j_{\nu\nu'}$, where ν denotes the site from which we entered the site j. If the link is covered by a dimer, then $R^j_{\nu\nu'} = P^j_{\nu\nu'}$. If it is empty, then $R^j_{\nu\nu'} = Q^j_{\nu\nu'}$.

S3: As a result of *S2* or *S2′*, one additional six-coordinated site ν violates the (soft) constraint that the total number of dimers touching this site is even in addition to the site μ_0. We therefore *enter* this 6-coordinated site ν *from* the 3-coordinated site i.

S4: To proceed further, we need to leave ν via one of the six 3-coordinated sites it is connected to, and in the process heal this defect on site ν. To do this, we enter one of these sites, say site j, with probabilities T^ν_{ij}, where the first index i refers to the fact that this is the probability of entering j from ν given taht we arrived at ν from i in the previous step. Thus T^ν_{ij} is a 6×6 matrix of these probabilities. We only require that the matrix is symmetric, that each entry be positive, and that the sum of each row is 1.

S5: We have now entered site j from the 6-coordinated site ν. If there is a dimer connecting j to ν, then we go to *S2* and use j as a pivot with probabilities $P^j_{\nu\nu'}$.

OR

S5′: If there is no dimer connecting j to ν, then j is connected by a dimer to some other 6-coordinated site ν'. In this case we follow the procedure of *S2′*, with j as

the pivot and probability $Q^j_{\nu\nu'}$ of rotating the dimer to touch ν instead of ν', and probability $Q^j_{\nu\nu}$ to leave it unchanged (bounce event).

S6: By carrying out *S5* or *S5'*, we have either healed the defect at ν and entered ν' or bounced back to ν. Let the new 6-coordinated site we have entered thus from j be denoted by ν_1; thus ν_1 can be either ν or ν'. We now repeat *S4* using the probabilities $T^{\nu_1}_{jj'}$.

S7: Continue this till eventually, the two defects ν_1 and μ_0 will meet and annihilate each other.

Proof of detailed balance: As stated earlier, we choose the probabilities $R^j_{\nu\nu'}$ to satisfy detailed balance at each step, i.e. $B_\nu R^j_{\nu\nu'} = B_{\nu'} R^j_{\nu'\nu}$, where B_ν and $B_{\nu'}$ are the respective Boltzmann weights of the two configurations connected by the transition probability. With these choices for the probability matrices, the probability for the forward process is

$$P(i \to f) = \frac{1}{N_6}\frac{1}{6} R^i_{\mu_0\nu}(T^\nu_{ij} R^j_{\nu\nu_1}) \times (T^{\nu_1}_{jj_1} R^{j_1}_{\nu_1\nu_2}) \cdots (T^{\nu_k}_{j_{k-1}j_k} R^{j_k}_{\nu_k\mu_0}) \tag{A.6}$$

Here, the factor $1/N_6$ refers to the uniform probability with which the initial 6-coordinated site is picked from a total of N_6 such sites, and the factor $1/6$ refers to the uniform probability with which one of the 3-coordinated sites connected to it is entered in the first step of the move.

Similarly, the probability for the reverse process retracting all steps is

$$P(f \to i) = \frac{1}{N_6}\frac{1}{6} R^{j_k}_{\mu_0\nu_k}(T^{\nu_k}_{j_k j_{k-1}} R^{j_{k-1}}_{\nu_k\nu_{k-1}}) \times (T^{\nu_{k-1}}_{j_{k-1}j_{k-2}} R^{j_{k-2}}_{\nu_{k-1}\nu_{k-2}}) \cdots (T^{\nu}_{ji} R^{i}_{\nu\mu_0}) \tag{A.7}$$

Detailed balance requires that $B_i P(i \to f) = B_f P(f \to i)$. To prove this, multiply both sides by the product of the Boltzmann weights of all intermediate configurations that appear during the process of making the loop, i.e. multiply both sides by the product $B_\nu B_{\nu_1} B_{\nu_2} \cdots B_{\nu_k}$. Rearranging the factors, we write

$$B_i B_\nu B_{\nu_1} B_{\nu_2} \cdots B_{\nu_k} P(i \to f) =$$
$$\frac{1}{N_6}\frac{1}{6}(B_i R^i_{\mu_0\nu})(T^\nu_{ij} B_\nu R^j_{\nu\nu_1}) \times (T^{\nu_1}_{jj_1} B_{\nu_1} R^{j_1}_{\nu_1\nu_2}) \cdots (T^{\nu_k}_{j_{k-1}j_k} B_{\nu_k} R^{j_k}_{\nu_k\mu_0}) \tag{A.8}$$

Now we can use the symmetric nature of the $\mathbf{T}$ matrices, and detailed balance conditions on the $\mathbf{R}$: $B_{\nu_l} R^{j_l}_{\nu_l\nu_{l+1}} = B_{\nu_{l+1}} R^{j_l}_{\nu_{l+1}\nu_l}$, $B_i R^i_{\mu_0\nu} = B_\nu R^i_{\nu\mu_0}$ and $B_{\nu_k} R^{j_k}_{\nu_k\mu_0} = B_f R^{j_k}_{\mu_0\nu_k}$,

and rearrange the factors in the above equation to give

$$B_i B_\nu B_{\nu_1} B_{\nu_2} \cdots B_{\nu_k} P(i \to f) = \\ (T^{\nu}_{ji} B_\nu R^{i}_{\nu\mu_0}) \times (T^{\nu_1}_{j_1 j} B_{\nu_1} R^{j}_{\nu_1 \nu}) \times (T^{\nu_2}_{j_2 j_1} B_{\nu_2} R^{j_1}_{\nu_2 \nu_1}) \cdots (\frac{1}{N_6}\frac{1}{6} B_f R^{j_k}_{\mu_0 \nu_k}) \tag{A.9}$$

which is equal to $(B_f B_\nu B_{\nu_1} B_{\nu_2} \cdots B_{\nu_k}) P(f \to i)$ which proves the detailed balance condition: $B_i P(i \to f) = B_f P(f \to i)$.

References

[1] A. W. Sandvik and R. Moessner. Correlations and confinement in non-planar two-dimensional dimer models. *Phys. Rev. B* **73**, 144504 (2006).

[2] F. Alet *et al.* Interacting classical dimers on the square lattice. *Phys. Rev. Lett.* **94**, 235702 (2005).

[3] O. Syljuasen and A. W. Sandvik. Quantum Monte Carlo with directed loops. *Phys. Rev. E* **66**, 046701 (2002).

[4] N. Metropolis *et al.* Equations of state calculations by fast computing machines. *J. Chem. Phys.* **21**, 1087 (1953).

Appendix B

Calculation details for 6^{th} order term

Below we briefly describe the Van Vleck method of unitary transformations to get an effective Hamiltonian in a reduced Hilbert space.

B.1 Effective Hamiltonian method

Let the given Hamiltonian H be written as

$$H = H_0 + \lambda V \tag{B.1}$$

where the Hamiltonian H_0 can be *solved* and V acts as a perturbation on it. λ is some small parameter which allows the perturbation to be performed order by order. Consider the energy levels of H_0 first. Let us assume that they are bunched in manifolds $|i,\alpha\rangle, |j,\beta\rangle$ etc which are well seperated from each other in energy, where $\alpha, \beta \ldots$ denote the manifolds and $i, j \ldots$ denote the states inside a given manifold. For this identification to be valid, we require

$$|E_{j,\beta} - E_{i,\alpha}| \gg |E_{j,\alpha} - E_{i,\alpha}|, \quad \alpha \neq \beta \tag{B.2}$$

Also, to consider λV as a perturbation on H_0, we need that

$$\lambda |\langle i,\alpha|V|j,\beta\rangle| \ll |E_{i,\alpha} - E_{j,\beta}|, \quad \alpha \neq \beta \tag{B.3}$$

Then the spectrum of $H = H_0 + \lambda V$ is also formed of well seperated energy manifolds. A convenient description of the low temperature physics can then be achieved by

formulating an "effective Hamiltonian" in the ground state manifold of H_0. We want to derive a Hamiltonian H^{α}_{eff} which acts only inside $\mathcal{E}^0_\alpha$ (the manifold of H_0) and such that its eigenvalues coincide with the corresponding eigenvalues of $H = H_0 + \lambda V$ to a given order in λ. Since H^{α}_{eff} only acts inside $\mathcal{E}^0_\alpha$, its eigenstates are different from the true eigenstates of H. How does one construct such an effective Hamiltonian?

For this, we need to apply a unitary transformation $\exp(iS)$ on the Hamiltonian H,

$$H_{eff} = \exp(iS) H \exp(-iS) \tag{B.4}$$

where S is a hermitian operator which is suitably chosen. Let us expand S as a power series of the form

$$S = \lambda S_1 + \lambda^2 S_2 + \lambda^3 S_3 + \cdots \tag{B.5}$$

Then the following two conditions fix the $S_n, (n = 1, 2, \cdots)$ uniquely and thus determine the effective Hamiltonian H_{eff}.
(I) The effective Hamiltonian is constructed to be purely diagonal in the energy manifold of H_0. To satisfy this condition, we demand that

$$\langle i, \alpha | H_{eff} | j, \beta \rangle = 0, \quad \alpha \neq \beta \tag{B.6}$$

order by order in λ.
(II) Condition I does not uniquely fix S because for any $\exp(iS)$ which satisfies the above condition, it is also satisfied by $\exp(iS)\exp(iT)$ where T does not connect states in different energy manifolds. This is fixed by imposing the condition that S be purely off-diagonal,i.e.,

$$\langle i, \alpha | S | j, \alpha \rangle = 0 \tag{B.7}$$

order by order in λ. The effective Hamiltonian H_{eff} can be derived to all orders by implementing the above two conditions,

$$\begin{aligned} \langle i, \alpha | H_{eff} | j, \alpha \rangle &= \langle i, \alpha | H_0 | j, \alpha \rangle + \lambda \langle i, \alpha | V | j, \alpha \rangle \\ &+ \frac{\lambda^2}{2} \sum_{\gamma \neq \alpha} \sum_k \langle i, \alpha | V | k, \gamma \rangle \langle k, \gamma | V | j, \alpha \rangle \left(\frac{1}{E_{i,\alpha} - E_{k,\gamma}} + \frac{1}{E_{j,\alpha} - E_{k,\gamma}} \right) + \cdots \end{aligned} \tag{B.8}$$

Similarly, the expressions for all S_n can be derived from the above two conditions. Here, we give the expressions for the first two:

$$\begin{aligned}
\langle i\alpha|S_1|j\beta\rangle &= \frac{-i}{E_{i\alpha}-E_{j\beta}}\langle i\alpha|V|j\beta\rangle \\
\langle i\alpha|S_2|j\beta\rangle &= \frac{-i}{E_{i\alpha}-E_{j\beta}}\left(\sum_{\gamma_1\neq\alpha}\frac{\langle i\alpha|V|k_1\gamma_1\rangle\langle k_1\gamma_1|V|j\beta\rangle}{E_{i\alpha}-E_{k_1\gamma_1}}+\sum_{\gamma_1\neq\beta}\frac{\langle i\alpha|V|k_1\gamma_1\rangle\langle k_1\gamma_1|V|j\beta\rangle}{E_{j\beta}-E_{k_1\gamma_1}}\right. \\
&- \left.\frac{1}{2}\sum_{\gamma_1\neq\alpha,\gamma_1\neq\beta}\langle i\alpha|V|k_1\gamma_1\rangle\langle k_1\gamma_1|V|j\beta\rangle(\frac{1}{E_{i\alpha}-E_{k_1\gamma_1}}+\frac{1}{E_{j\beta}-E_{k_1\gamma_1}})\right) \qquad \text{(B.9)}
\end{aligned}$$

To find out the eigenstates of H, we need to simply apply $\exp(-iS)$ to the eigenstates of H_{eff}.

B.2 6^{th} order term

We now summarize the procedure we used to calculate the 6^{th} order term in J/D in the effective Hamiltonian for the kagome antiferromagnet in field. Even though, the calculation looks very tedious, it can be simplified in the following manner. First, the general expression for H_6 can be simplified by using the exact degeneracy of the ground state manifold of H_0 and we give the simplified expression below.

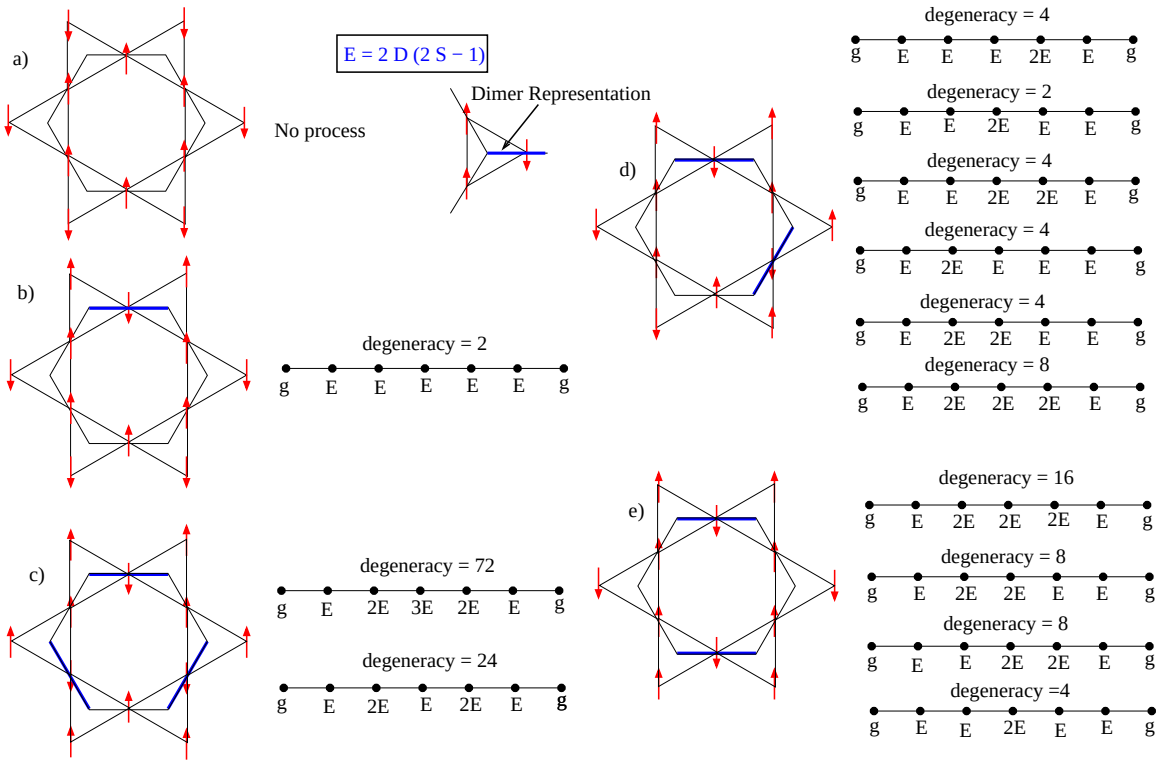

Figure B.1: Six bond hexagonal processes which first lift the degeneracy at $O(J^6/D^5)$. The dimers on the corresponding honeycomb net are indicated by thick blue lines.

$$
\begin{aligned}
\langle \quad & i,\alpha|H_6|j,\alpha\rangle = \langle i,\alpha| \left(\frac{i^2}{2!}[S_1,[S_4,V]] - \frac{i^3}{12}([S_4,[S_1,[S_1,H_0]]] + [S_2,[S_3,[S_1,H_0]]] \right. \\
+ \quad & [S_2,[S_1,[S_3,H_0]]] + [S_2,[S_2,[S_2,H_0]]] + [S_3,[S_1,[S_2,H_0]]] + [S_3,[S_2,[S_1,H_0]]]) \\
- \quad & \frac{i^3}{12}([S_2,[S_1,[S_2,V]]] + [S_2,[S_2,[S_1,V]]] + [S_3,[S_1,[S_1,V]]]) + \frac{i^3}{3!}([S_1,[S_4,[S_1,H_0]]] \\
+ \quad & [S_1,[S_1,[S_4,H_0]]] + [S_1,[S_2,[S_3,H_0]]] + [S_1,[S_3,[S_2,H_0]]]) \\
+ \quad & \frac{i^3}{3!}([S_1,[S_1,[S_3,V]]] + [S_1,[S_3,[S_1,V]]] + [S_1,[S_2,[S_2,V]]]) \\
- \quad & \frac{i^4}{4!}([S_2,[S_1,[S_1,[S_2,H_0]]]] + [S_2,[S_1,[S_2,[S_1,H_0]]]] + [S_2,[S_2,[S_1,[S_1,H_0]]]] \\
+ \quad & [S_3,[S_1,[S_1,[S_1,H_0]]]] + [S_2,[S_1,[S_1,[S_1,V]]]]) \\
+ \quad & \frac{i^4}{4!}([S_1,[S_1,[S_3,[S_1,H_0]]]] + [S_1,[S_1,[S_1,[S_3,H_0]]]] + [S_1,[S_1,[S_2,[S_2,H_0]]]] \\
+ \quad & [S_1,[S_2,[S_1,[S_2,H_0]]]] + [S_1,[S_2,[S_2,[S_1,H_0]]]] + [S_1,[S_3,[S_1,[S_1,H_0]]]]) \\
+ \quad & \frac{i^4}{4!}([S_1,[S_1,[S_2,[S_1,V]]]] + [S_1,[S_1,[S_1,[S_2,V]]]] + [S_1,[S_2,[S_1,[S_1,V]]]]) \\
- \quad & \frac{3}{10}\frac{i^5}{4!}([S_2,[S_1,[S_1,[S_1,[S_1,H_0]]]]]) + \frac{i^5}{5!}([S_1,[S_2,[S_1,[S_1,[S_1,H_0]]]]] \\
+ \quad & [S_1,[S_1,[S_2,[S_1,[S_1,H_0]]]]] + [S_1,[S_1,[S_1,[S_2,[S_1,H_0]]]]] + [S_1,[S_1,[S_1,[S_1,[S_2,H_0]]]]]) \\
+ \quad & \left. \frac{i^5}{5!}([S_1,[S_1,[S_1,[S_1,[S_1,V]]]]]) + \frac{i^6}{6!}([S_1,[S_1,[S_1,[S_1,[S_1,[S_1,H_0]]]]]]) \right) |j,\alpha\rangle \qquad \text{(B.10)}
\end{aligned}
$$

Now, given a sixth-order process on a hexagonal plaquette, it is useful to first calculate S_1, S_2, S_3, S_4 between any two states that occur in the process. For these 6^{th} order processes on hexagonal loops, it is easy to verify that

$$\begin{aligned}\langle g|V|k_5,\gamma_5\rangle &= \langle k_5,\gamma_5|V|k_4,\gamma_4\rangle = \langle k_4,\gamma_4|V|k_3,\gamma_3\rangle = \langle k_3,\gamma_3|V|k_2,\gamma_2\rangle \\ &= \langle k_2,\gamma_2|V|k_1,\gamma_1\rangle = \langle k_1,\gamma_1|V|g\rangle = JS \end{aligned} \tag{B.11}$$

To calculate S_1, S_2, S_3, S_4, all the S_1 values should be calculated for a given process first, followed by the values of S_2 in terms of S_1, then the values of S_3 in terms of S_1 and S_2 and finally the values of S_4 in terms of the already calculated S_1,S_2 and S_3 (see Eq B.12).

$$\begin{aligned}\langle i,\alpha|S_1|j,\beta\rangle &= -i\frac{\langle i,\alpha|V|j,\beta\rangle}{(E_{i,\alpha}-E_{j,\beta})} \\ \langle i,\alpha|i[S_2,H_0]|j,\beta\rangle &= -\langle i,\alpha|i[S_1,V]+\frac{i^2}{2!}[S_1,[S_1,H_0]]|j,\beta\rangle \\ \langle i,\alpha|i[S_3,H_0]|j,\beta\rangle &= -\langle i,\alpha|i[S_2,V]+\frac{i^2}{2!}([S_1,[S_2,H_0]]+[S_2,[S_1,H_0]]+[S_1,[S_1,V]]) \\ &+ \frac{i^3}{3!}[S_1,[S_1,[S_1,H_0]]]|j,\beta\rangle \\ \langle i,\alpha|i[S_4,H_0]|j,\beta\rangle &= -\langle i,\alpha|i[S_3,V]+\frac{i^2}{2!}([S_2,[S_2,H_0]]+[S_1,[S_3,H_0]]+[S_3,[S_1,H_0]] \\ &+ [S_1,[S_2,V]]+[S_2,[S_1,V]])+\frac{i^3}{3!}([S_1,[S_1,[S_2,H_0]]] \\ &+ [S_1,[S_2,[S_1,H_0]]]+[S_2,[S_1,[S_1,H_0]]]+[S_1,[S_1,[S_1,V]]]) \\ &+ \frac{i^4}{4!}[S_1,[S_1,[S_1,[S_1,H_0]]]]|j,\beta\rangle \end{aligned} \tag{B.12}$$

These can be calculated by knowing the energies of the intermediate states that arise in the processes on elementary hexagonal loops (see Fig B.1). Knowing these, it is straightforward to calculate the contribution of a process to H_6 using Eq B.10. Doing this calculation, we get the following remarkably simple result for the sixth order perturbation result of such processes:

$$H_6 = \frac{\langle g|V|k_5,\gamma_5\rangle\langle k_5,\gamma_5|V|k_4,\gamma_4\rangle\ldots\langle k_1,\gamma_1|V|g\rangle}{(E_g-E_{k_5,\gamma_5})(E_g-E_{k_4,\gamma_4})\ldots(E_g-E_{k_1,\gamma_1})} \tag{B.13}$$